THREE-DIMENSIONAL SHORT-TERM STABILITY ANALYSIS OF CLAYEY SLOPES STABILIZED WITH PILES

by

Yılmaz Emre Tekdemir

B.S., Civil Engineering, Istanbul Technical University, 2020

Submitted to the Institute for Graduate Studies in
Science and Engineering in partial fulfillment of
the requirements for the degree of
Master of Science

Graduate Program in Civil Engineering

Boğaziçi University

2023

ACKNOWLEDGEMENTS

Firstly, I would like to express my sincere gratitude to my thesis supervisor Assist. Prof. İrem Zeynep Yıldırım, for her guidance, dedication, and continuous support. Her expertise, mentorship and utmost attention to detail were instrumental in shaping the research direction and refining the quality of this work.

I would also like to thank Prof. Özer Çinicioğlu and Assist. Prof. Berrak Teymür for serving on my thesis committee and providing insightful feedback.

I would like to acknowledge my dearest friends Umut and Müge who have supported me throughout the course of my master's thesis. Completing this research would not have been possible without their invaluable companionship and encouragement. I am truly fortunate to have them as my friends.

Most of all, I am grateful to my family for their constant encouragement and belief in my abilities. Their presence and support have been an endless source of strength and motivation.

Finally, I would like to acknowledge the financial support provided by Boğaziçi University Scientific Research Projects (BAP Project Code: 16961) for this study.

ABSTRACT

THREE-DIMENSIONAL SHORT-TERM STABILITY ANALYSIS OF CLAYEY SLOPES STABILIZED WITH PILES

In this study, the short-term (undrained) behavior of pile-stabilized clayey slopes were investigated via three-dimensional (3D) finite element analysis. Deformations and stability conditions were investigated considering various soil strength parameters, slope geometries, pile material behavior, pile head conditions, and pile spacing-to-diameter ratios for slopes with and without surcharge loads. For the slopes without surcharge loads, the slopes were modeled as a representative slice model and the loaded slopes were modeled using the complete geometry of the problem to capture the 3D failure mechanism induced by the local surcharge loads. Initial case selection was performed using limit-equilibrium based slope stability analysis and based on the initial factor of safety values, slopes that were deemed feasible to be stabilized with piles were selected for the parametric study. Factor of safety values, internal pile forces, pile head displacements, and failure mechanisms were recorded and used to evaluate the performance of various pile-stabilized slope cases. The results indicate that using elasto-plastic pile models improves the accuracy of the analysis by better simulating pile behavior and coupled failure mechanisms, resulting in more reliable factor of safety values. The effectiveness of soil arching and pile stabilization decrease as the pile spacing-to-diameter ratios and slope heights increase. In cases of high and steep, natural slopes (slope height, $H \geq 25$m, slope angle, $\beta \geq 56.3°$), and high and gentle, loaded slopes (slope height, $H \geq 15$m, slope angle, $\beta \leq 33.7°$), marginal improvements were observed through stabilization by a single row of piles. For other slope geometries, pile stabilization performed reasonably well. When the factor of safety of a slope reduces below 1 due to surcharge loads, significant deformations occur, and stabilizing the slope with piles becomes an inefficient solution. In locally loaded slopes, central piles experience severe loading, leading to structural failure and subsequent slope failure. The employment of a pile cap to constrain pile head movements improves stability by ensuring an even load distribution among row of piles. The results highlighted the importance of 3D analysis when pile stabilized slopes are considered.

ÖZET

KAZIKLARLA STABİLİZE EDİLMİŞ KİLLİ ŞEVLERİN ÜÇ BOYUTLU KISA DÖNEM STABİLİTE ANALİZİ

Bu çalışmada kazıklarla stabilize edilmiş killi şevlerin kısa süreli (drenajsız) davranışı üç boyutlu (3D) sonlu elemanlar analizi ile incelenmiştir. Sürşarj yüklü ve yüksüz şevler için çeşitli zemin mukavemeti parametreleri, şev geometrileri, kazık malzemesi davranışları, kazık başı koşulları ve kazık aralığı-kazık çapı oranları dikkate alınarak, deformasyon ve stabilite koşulları incelenmiştir. Sürşarj yükü etkisi altında olmayan şevler için, şevler temsili bir dilim model olarak modellenmiştir. Bölgesel yüklü şevlerde ise, sürşarj yüklerinin neden olduğu 3D göçme mekanizmasını gözlemlemek için modellerde problemin bütün geometrisi kullanılmıştır. Parametrik çalışma için durum seçimi, limit-denge bazlı şev stabilite analizi kullanılarak yapılmıştır ve elde edilen güvenlik faktörlerine dayanarak, kazıklarla stabilize edilmesi uygun görülen şevler seçilmiştir. Güvenlik faktörü değerleri, kazık iç kuvvetleri, kazık başı deplasmanları ve göçme mekanizmaları, kazıklarla stabilize edilmiş şevlerin performansını değerlendirmek için kullanılmıştır. Sonuçlar, elasto-plastik kazık modellerinin kullanılmasının, kazık davranışını ve bütünleşik göçme mekanizmalarını daha iyi simüle ederek analizin doğruluğunu arttırdığını ve bunun sonucunda daha güvenilir güvenlik faktörü değerlerinin hesaplandığını göstermektedir. Kazık aralığı-kazı çapı oranları ve şev yükseklikleri arttıkça zemin kemerlenme ve kazık stabilizasyonu etkilerinin azaldığı görülmüştür. Yüksek ve dik doğal şev (şev yüksekliği, $H \geq 25m$, şev açısı, $\beta \geq 56,3°$) ve yüksek ve hafif eğimli yüklü şev (şev yüksekliği, $H \geq 15m$, şev açısı, $\beta \leq 33,7°$) durumlarında, tek sıra kazıklar ile stabilizasyon sonucu sınırlı iyileştirmeler gözlemlenmiştir. Diğer şev geometrileri için, kazıklarla stabilizasyonun iyi performans sergilediği görülmüştür. Sürşarj yükleri nedeniyle şevin güvenlik katsayısının 1'in altına düştüğü durumlarda ciddi deformasyonlar meydana gelmektedir ve şevin kazıklarla stabilizasyonu verimsiz bir çözüm haline gelmektedir. Bölgesel yüklü şevlerde, ortadaki kazıklar, ciddi yüklemeye maruz kalmakta ve bu durum yapısal göçmeye ve ardından şev göçmesine yol açmaktadır. Kazık başlarının hareketlerini kısıtlamak için başlık kirişi kullanılması, kazıklar arasında eşit yük dağılımı sağlayarak stabiliteyi arttırabilmektedir. Sonuçlar, kazıklarla stabilize edilen şevlerin analizinde 3D analizin önemini vurgulamıştır.

TABLE OF CONTENTS

ACKNOWLEDGEMENTS iii
ABSTRACT iv
ÖZET v
LIST OF FIGURES viii
LIST OF TABLES xiii
LIST OF SYMBOLS xv
LIST OF ACRONYMS / ABBREVIATONS xvii
1. INTRODUCTION 1
1.1. General 1
1.2. Objectives 1
1.3. Scope 2
2. LITERATURE REVIEW 3
2.1. Concept of Slope Stability and Landslides 3
2.2. Slope Stability Analysis 4
2.2.1. Limit Equilibrium Approaches 4
2.2.2. Finite Element and Finite Difference Approaches 6
2.3. Stability Analysis of Surcharge Loaded Slopes 8
2.4. Slope Stabilization Methods 10
2.5. Pile-stabilized Slopes 14
2.6. Stability Analysis of Pile-stabilized Slopes 18
2.6.1. Analytical Solutions 18
2.6.2. Numerical Solutions 23
2.6.3. Other Studies and Gaps in The Literature 30
3. METHODOLOGY 33
3.1. FEM Software and Units 33
3.2. Material Modeling 33
3.2.1. Modeling of Soils 33
3.2.2. Modeling of Piles 39
3.2.3. Modeling of Interfaces 40
3.3. Boundary Conditions 41

3.4. Model Dimensions and Extrusion Depth Sensitivity 41
3.5. Mesh Generation and Mesh Density Sensitivity 45
3.6. Initial Loading Conditions and Staged Construction Steps 49
3.7. Selection of Cases for Stabilization and Summary of Cases 50
4. RESULTS AND DISCUSSION 53
4.1. Effect of Pile Material Model on Coupled Failure Modes 53
4.2. Types of Failure Modes in Pile-stabilized Slope Cases 55
4.3. Types of Failure Modes in Pile-stabilized Loaded Slope Cases 57
4.4. Effect of Pile Stabilization on Slope Displacements in Loaded Cases 60
4.5. Effects of Slope Geometry on Normalized F_s of Pile-stabilized Slopes 62
4.6. Effect of Pile Spacing and Soil Arching on Results 67
4.7. Effect of Pile Cap Beam on Results 88
5. CONCLUSION AND RECOMMENDATIONS 92
REFERENCES 95

LIST OF FIGURES

Figure 2.1. Maximum displacements versus SRF from PLAXIS 3D. 7

Figure 2.2. A simple pile-stabilized slope model. 14

Figure 2.3. Summary of failure modes and bending moment diagrams for landslide-stabilizing rigid piles (modified after Viggiani, 1981)..... 18

Figure 2.4. State of plastic deformation around the piles (modified after Ito and Matsui, 1975). 19

Figure 2.5. Load transfer scheme (modified after Liang and Yamin, 2009). 26

Figure 3.1. Mohr-Coulomb failure envelope. 34

Figure 3.2. Determination of E_{50}^{ref} and E_{ur}^{ref} values from drained triaxial test results... 36

Figure 3.3. Determination of E_{oed}^{ref} value from oedometer test result. 36

Figure 3.4. 2D geometry of the analyzed pile-stabilized slopes. 42

Figure 3.5. 3D geometry of the analyzed pile-stabilized slopes. 42

Figure 3.6. 3D geometry of the analyzed pile-stabilized loaded slopes. 43

Figure 3.7. The effect of mesh density on the F_s of pile-stabilized slope cases: (a) smallest model, (b) largest model. 47

Figure 3.8. The effect of mesh density on the F_s of pile-stabilized loaded slope cases: (a) smallest model, (b) largest model. 48

Figure 3.9. Typical mesh distribution of piles and adjacent soil. 48

Figure 3.10. Typical mesh distribution of pile-stabilized slopes in slice model. 49

Figure 3.11. Typical mesh distribution of pile-stabilized loaded slopes in full model . 49

Figure 3.12. Staged construction steps for pile-stabilized loaded slope cases. 50

Figure 4.1. Exaggerated deformed mesh outputs (left) and incremental shear strain contours (right) of piles from safety analysis for the pile-stabilized slope case with β=45°, H=8 m, S_u=25 kPa, S/D=4: (a) LEP model, (b) EPP model.. 54

Figure 4.2. Deformed mesh outputs (cross section view) from safety analysis for the pile-stabilized slope case with β=26.6°, H=8 m, S_u=25 kPa: (a) S/D=2, (b) S/D=5..... 56

Figure 4.3. Exaggerated deformed mesh outputs (cross section view) from the deformation analysis at the loading phase for the pile-stabilized loaded slope cases: (a) β=26.6°, H=5 m, S_u=35 kPa, S/D=2, (b) β=45°, H=8 m, S_u=50 kPa, S/D=2. 58

Figure 4.4. Exaggerated deformed mesh outputs (cross section view) from the safety analysis for the pile-stabilized loaded slope cases: (a) β=26.6°, H=5 m, S_u=35 kPa, S/D=2, SPM, (b) β=45°, H=8 m, S_u=50 kPa, S/D=2, LPM..... 59

Figure 4.5. Total displacements of the unstabilized slope from deformation analysis at the loading phase for the case with β=45°, H=10 m, S_u=50 kPa (a) plan view, (b) cross-section view.. 61

Figure 4.6. Total displacements of the pile-stabilized slope from deformation analysis at the loading phase for the case with β=45°, H=10 m, S_u=50 kPa (a) plan view, (b) cross-section view. 61

Figure 4.7. Incremental displacements of the unstabilized slope from safety analysis for the case with β=45°, H=10 m, S_u=50 kPa: (a) plan view, (b) cross-section view.. 62

Figure 4.8. Incremental displacements of the pile-stabilized slope from safety analysis for the case with β=45°, H=10 m, S_u=50 kPa, S/D=2: (a) plan view, (b) cross-section view. 62

Figure 4.9. Normalized F_s (F_s x p / S_u) with respect to a range of H and β values for pile-stabilized slope cases: (a) S/D=2, (b) S/D=5. 64

Figure 4.10. Normalized F_s (F_s x p / S_u) with respect to a range of H and β values for pile-stabilized loaded slope cases: (a) S/D=2, (b) S/D=4. 65

Figure 4.11. Plan view of incremental displacements from safety analysis of pile-stabilized loaded slope cases with: (a) β=26.6°, H=5 m, S_u=35 kPa, S/D=3, (b) β=26.6°, H=15 m, S_u=50 kPa, S/D=3. 66

Figure 4.12. Normalized F_s (F_s x p / S_u) with respect to a range of H values and S/D ratios: (a) pile-stabilized slope cases with β=45°, (b) pile-stabilized loaded slope cases with β=26.6° and β=63.4°..... 68

Figure 4.13. S/D ratio versus ΔF_s for a range of for pile-stabilized slope geometries with: (a) H=8-20 m range, (b) H=25-30 m range..... 69

Figure 4.14. S/D ratio versus ΔF_s for pile-stabilized loaded slope cases with a range of β values: (a) H=5 m, (b) H=8 m. 71

Figure 4.15. S/D ratio versus ΔF_s for pile-stabilized loaded slope cases with a range of β values: (a) H=10 m, (b) H=15 m. 72

Figure 4.16. Incremental displacements (plan view) from safety analysis of pile-stabilized slope cases with β=33.7°, H=8 m, S_u=25 kPa: (a) S/D=2, (b) S/D=3, (c) S/D=4, (d) S/D=5. 74

Figure 4.17. Incremental displacements (plan view) from safety analysis of pile-stabilized slope cases with β=45°, H=8 m, S_u=25 kPa: (a) S/D=2, (b) S/D=3, (c) S/D=4, (d) S/D=5. 74

Figure 4.18. Incremental displacements (plan view) from safety analysis of pile-stabilized slope cases β=45°, H=15 m, S_u=50 kPa: (a) S/D=2, (b) S/D=3, (c) S/D=4, (d) S/D=5. 75

Figure 4.19. Incremental displacements (plan view) from safety analysis of pile-stabilized slope cases with β=45°, H=20 m, S_u=75 kPa: (a) S/D=2, (b) S/D=3, (c) S/D=4, (d) S/D=5. 75

Figure 4.20. Incremental displacements (plan view) from safety analysis of pile-stabilized slope cases with β=56.3°, H=20 m, S_u=75 kPa (a) S/D=2, (b) S/D=3, (c) S/D=4, (d) S/D=5. 76

Figure 4.21. Incremental displacements shown on plan and cross section views from the safety analysis for the pile-stabilized loaded slope cases with β=26.6°, H=5 m, S_u=35 kPa: (a) S/D=2, (b) S/D=3, (c) S/D=4. 78

Figure 4.22. Incremental displacements shown on plan and cross section views from the safety analysis for the pile-stabilized loaded slope cases with β=45°, H=10 m, S_u=50 kPa: (a) S/D=2, (b) S/D=3, (c) S/D=4. 79

Figure 4.23. Incremental displacements shown on plan and cross section views from the safety analysis for the pile-stabilized loaded slope cases with β=63.4°, H=15 m, S_u=75 kPa: (a) S/D=2, (b) S/D=3, (c) S/D=4. 80

Figure 4.24. Pile bending moments versus the depth for pile-stabilized loaded slope case with β=26.6°, H=5 m, S_u=35 kPa, S/D=2: (a) deformation analysis, (b) safety analysis. 81

Figure 4.25. Pile bending moments versus the depth for pile-stabilized loaded slope case with β=63.4°, H=15 m, S_u=75 kPa, S/D=2: (a) deformation analysis, (b) safety analysis. 81

Figure 4.26. Pile bending moments versus the depth for pile-stabilized loaded slope case with β=45°, H=8 m, S_u= 50 kPa S/D=2: (a) deformation analysis, (b) safety analysis. 83

Figure 4.27. Pile bending moments versus the depth for pile-stabilized loaded slope case with β=45°, H=8 m, S_u= 50 kPa S/D=4: (a) deformation analysis, (b) safety analysis. 83

Figure 4.28. S/D ratio versus M_{Max} / $M_{Max\text{-}S/D=2}$ for pile-stabilized loaded slope cases with a range of β values: (a) H=5 m, (b) H=8 m. 84

Figure 4.29. S/D ratio versus M_{Max} / $M_{Max\text{-}S/D=2}$ for pile-stabilized loaded slope cases with range of β values: (a) H=10 m, (b) H=15 m. 85

Figure 4.30. S/D ratio versus y_{Max} / $y_{Max\text{-}S/D=2}$ for pile-stabilized loaded slope cases with a range of β values: (a) H=5 m, (b) H=8 m. 86

Figure 4.31. S/D ratio versus y_{Max} / $y_{Max\text{-}S/D=2}$ for pile-stabilized loaded slope cases with a range of β values: (a) H=10 m, (b) H=15 m. 87

Figure 4.32. Pile bending moment along depth for pile-stabilized loaded slope case with β=56.3°, H=10 m, S_u=50 kPa, S/D=3 89

Figure 4.33. Incremental displacements from safety analysis for pile-stabilized loaded slope case with β=56.3°, H=10 m, S_u=50 kPa, S/D=4 with piles in: (a) free head condition, (b) constrained head condition. 90

Figure 4.34. Incremental displacements from safety analysis of pile-stabilized loaded slope cases with β=56.3°, H=10 m, S_u=50 kPa: (a) S/D=2 with free head condition, (b) S/D=2 with constrained head condition, (c) S/D=3 with free head condition, (d) S/D=3 with constrained head condition, (e) S/D=4 with free head condition, (f) S/D=4 with constrained head condition. 91

LIST OF TABLES

Table 2.1. Number of unknown parameters (Abramson *et al*., 1996)..... 5

Table 2.2. Number of known equations (Abramson *et al.*, 1996)..... 6

Table 2.3. Satisfied equilibrium conditions in various LE based approaches (Abramson *et al.*, 1996). 6

Table 2.4. Summary of slope stabilization methods (After Abramson *et al.*, 1996).. 11

Table 2.5. Pile-stabilized slope case studies reported in literature..... 15

Table 3.1. Units used in the PLAXIS 3D software. 33

Table 3.2. Parameters used in the HS and HSS models (Brinkgreve *et al*., 2021). ... 35

Table 3.3. Soil properties used in the parametric study. 38

Table 3.4. Pile material properties (adopted from Gerolymos *et al.,* 2014)..... 40

Table 3.5. The effect of extrusion depth on the deformation analysis results..... 44

Table 3.6. The effect of extrusion depth on the F_s. 44

Table 3.7. The effect of mesh density on the deformation analysis results. 46

Table 3.8. The parameter ranges used for the case selection of pile-stabilized slopes..... 51

Table 3.9. Selected cases for the parametric study. 52

Table 4.1. F_s of the cases analyzed with linear-elastic and elasto-plastic pile models. 55

Table 4.2. Results of deformation analysis at the loading phase and the F_s of the case with β=45°, H=10 m, S_u=50 kPa, S/D=2. 60

Table 4.3. Results of deformation analysis at the loading phase for various S/D ratios and pile head conditions. 88

Table 4.4. Results of safety analysis for different S/D ratios and pile head conditions… 89

LIST OF SYMBOLS

A_c	Area of the reinforced concrete section under compression
A_t	Area of the reinforced concrete section under tension
B	Surcharge load width
c	Cohesion intercept
d	Distance between loading and slope crest
D	Pile diameter
D_1	Center-to-center pile spacing in a row
D_2	Clear spacing between the piles
E	Young's modulus
E_{50}^{ref}	Secant stiffness in standard drained triaxial test
E_{oed}^{ref}	Tangent stiffness for primary oedometer loading
E_{ur}^{ref}	Unloading/ reloading stiffness
F_s	Factor of safety
F_{s0}	Factor of safety of the original slope prior to pile stabilization
F_{sl}	Factor of safety of the loaded slope prior to pile stabilization
G_0^{ref}	Reference shear modulus at very small strains
H	Slope height
L	Surcharge load length
L_d	Diagonal length
l_e	Target element size
L_p	Total pile length
L_s	Pile socket length
m	Power for stress-level dependency of stiffness
M	Bending moment
M_{max}	Maximum bending moment
N	Axial force
N_c	Undrained bearing capacity factor
p_a	Atmospheric pressure
p	Lateral force per unit length of the pile

p^{ref}	Reference stress for stiffnesses
q	Surcharge load magnitude
r_e	Relative element size factor
R_f	Failure ratio
R_{inter}	Interface strength reduction factor
R_{rf}	Reinforcement ratio
s	Spacing
S_u	Undrained shear strength
u_x	Displacement at the x direction
u_y	Displacement at the y direction
u_z	Displacement at the z direction
v	Poisson ratio
v_{ur}	Poisson's ratio for unloading - reloading
x_0	Abscissa of the neutral axis
β	Slope angle
δ	Allowable shaft deflection
η	Load transfer factor
σ_c	Compressive stress
σ_t	Tension cut-off stress
γ	Unit weight
$\gamma_{0.7}$	Threshold shear strain
ψ	Dilatancy angle
ϕ	Friction angle

LIST OF ACRONYMS / ABBREVIATONS

2D	Two-dimensional
3D	Three-dimensional
DSF	Deep-seated Failure
EPP	Elasto-plastic Pile
ERCAP	Earth Retaining Capacity of Piles
FD	Finite Difference
FDM	Finite Difference Method
FE	Finite Element
FEM	Finite Element Method
HS	Hardening Soil Model
HSS	Hardening Soil Model with Small Strain Stiffness
LE	Limit Equilibrium
LEM	Limit Equilibrium Method
LEP	Linear-elastic Pile
LPM	Long Pile Mode
MC	Mohr-Coulomb
M-c	Moment-curvature
MSE	Mechanically Stabilized Earth
RF	Resistance Force
S/D	Spacing to Diameter Ratio
SPM	Short Pile Mode
SRF	Strength Reduction Factor
SRM	Strength Reduction Method
USF	Upper Slope Failure
VP	Volume Pile

1. INTRODUCTION

1.1. General

One of the slope stabilization techniques is to install piles along a slope to increase the forces that resist movements. Since piles can be employed in a wide range of slope geometries, this approach offers greater practicality and versatility when compared to other slope stabilization measures. Utilizing piles for slope stabilization offers engineers a cost-effective and efficient solution to improve the stability of an existing slope. Despite its widespread use, a generalized design approach is not currently available for slopes stabilized with piles. Additionally, the behavior of pile-stabilized slopes, including the coupled-failure mechanisms are not completely understood or explained. The main challenge in this stability problem stems from the requirement of the simultaneous analysis of both the slope and the piles. Slope stabilizing piles experience lateral loads as a result of slope or landslide movements. The analytical solutions proposed for predicting the lateral loads exerted on piles have their limitations, primarily due to oversimplifications, and these solutions are applicable to a limited range of soil-pile interaction cases. Moreover, the shape of the failure mechanism is influenced by the location, spacing, and properties of the piles, highlighting the coupled nature of the problem that involves both the stability of the slope and the pile. Additionally, the introduction of surcharge loads and variations in drainage conditions adds further complexity to the analysis. Thus, a coupled analysis is necessary to accurately assess the safety of pile-stabilized slopes. This type of deformation and stability analysis, that account for the spacing between the piles and limited-size surcharge loads can be conducted using three-dimensional (3D) finite element (FE) methods. FE analysis facilitates the integration of slopes and piles within a unified continuum mechanics model, enabling the assessment of slope stability without the need for oversimplifications.

1.2. Objectives

The literature on slope stabilization using piles indicates that a clear understanding of the effect of each pile and slope related parameter on the factor of safety (F_s) of the slope have not been yet fully established. 3D analyses are still less commonly preferred, and 3D

effects on the results are unidentified. The results of the uncoupled analysis, in which piles and slope stability analysis are performed non-simultaneously, indicate the need for coupled analysis. 3D FE method can be utilized to understand soil-structure interaction, failure mechanisms, and to obtain F_s values, displacements, and internal pile forces in the pile-stabilized slope problem. A holistic approach, that allows the accurate definition of the surcharge load and the pile location, is required for the rigorous solution of this problem. This study aims to assess the behaviour of clayey slopes stabilized using piles socketed in sand. Due to loading, short-term stability conditions were employed using various soil properties, surcharge loading conditions, slope geometries, pile material behavior, pile head conditions and pile spacing-to-pile diameter (S/D) ratios.

For the selection of pile-stabilized slope cases, seven slope heights in the 5m to 30m range, five slope angles in the 26.6° to 63.4° range and six undrained shear strength (S_u) values in 25 kPa to 200 kPa range were analyzed with and without surcharge loads. For the initial case selection and calibration, cases were run in two-dimensional (2D) limit equilibrium (LE) software and their F_s values were recorded. Based on the recorded F_s values from these preliminary analyses, slopes that are deemed feasible for stabilization with piles were selected for the 3D FE parametric study. For the pile-stabilized slope cases, four S/D ratios (2 to 5), two pile head conditions (free and restrained) and two pile material models (linear-elastic and elasto-plastic) were considered in the 3D FE analysis. F_s values, internal pile forces, pile head displacements and failure mechanisms were then recorded and used to evaluate the performance of various pile-stabilized slope cases.

1.3. Scope

This thesis is structured into five primary chapters and is laid out in the following sequence. In Chapter 1, the thesis topic is briefly described, and the study's goals and scope are outlined. Chapter 2 introduces basic concepts and traditional methods for slope stability analysis, discusses stability analysis of slopes under surcharge loads, and provides a detailed examination of slope stabilization methods, with a focus on pile-based solutions. In chapter 3, methodology used in the study and details of the 3D FE software are explained. Chapter 4 contains the findings and discussions of the numerical analyses, while Chapter 5 provides a summary of the results.

2. LITERATURE REVIEW

Basic slope stability concepts and traditional slope stability analysis methods are introduced in this chapter. Stability analysis of slopes with and without surcharge loads and 3D effects in slope stability are discussed. Typical slope stabilization methods are introduced, with an emphasis on the use of piles. A detailed literature review of stability analysis of pile-stabilized slopes is presented.

2.1. Concept of Slope Stability and Landslides

Slope stability refers to the ability of a slope, embankment, or any sloping soil or rock surface to maintain its integrity and resist failure. Slope stability concerns are commonly encountered in construction projects such as highway cut slopes, levees, embankments, dams, and various excavation activities. The stability of a slope can be expressed by the factor of safety (F_s) that may be expressed in various ways. In simplest terms, it is the ratio of resisting forces to driving forces. In any case, when the driving forces exceeds the resisting forces, stability of the slope becomes compromised, and landslides may occur. Resisting forces in slope stability comes from the shear strength along the failure surface while the driving forces can be associated with the shear stresses.

According to Abramson *et al.* (1996), landslide can be triggered either when increases in shear stresses or reduction in shear strength occurs. Shear stresses can increase due to several factors, including removal of support, removal of underlying material, overloading, increase in lateral stresses and, seismic events. On the other hand, reduction in shear strength can occur as a result of the changes occurring in the nature and structure of the material such as weathering, physicochemical effects and increase in pore pressures. The combination of such geotechnical factors can result in very complex slope failures. According to Abramson *et al.* (1996), failures observed in clay slopes can be in the form of rotational, compound, translational and flow type failures, which shows that slope failure shapes and mechanisms are a complex phenomenon influenced by many factors. These factors cover a wide range of parameters, including slope material properties, slope geometry, the thickness of the unstable soil layer, geological conditions, and other environmental factors. For these reasons, slope

stability analysis and methods to stabilize slopes have been the focus of extensive research by civil engineers and various approaches to assess the stability of the slopes have been developed.

2.2. Slope Stability Analysis

Slope stability analysis is generally performed either using Limit Equilibrium (LE) or methods that employ continuum mechanics such as Finite Element (FE) and Finite Difference (FD) both of which are widely accepted and used by researchers and practicing engineers. LE methods rely on the force and/or moment equilibrium to determine the stability of slopes. On the other hand, FE and FD methods, utilize strength reduction technique to assess the safety of the slope analysed. Both LE and FE/FD methods are widely used to determine F_s of slopes and their outcomes are generally expected to be comparable to each other (Duncan, 1996; Griffiths and Lane, 1999; Lechman and Griffiths, 2000; Dawson *et al.*, 2000; Cheng *et al.*, 2007; Sloan, 2013). Slope stability design charts were also developed based on the aforementioned methods (Michałowski, 2002; Baker, 2003; Gao *et al*., 2013; Lim *et al*., 2016). At the preliminary design stages, these simplified charts can provide a preliminary estimate of the F_s of slopes.

2.2.1. Limit Equilibrium Approaches

LE methods consider the force and/or moment equilibrium to assess the stability of slopes. The F_s in LE analysis can be defined as the ratio of shear strength to mobilized shear forces, as the ratio of resisting moments to the driving moments or simply as the ratio of resisting forces to the driving forces. Typically, F_s values greater than 1 indicates stability, while a F_s value less than 1 suggests the presence of out of balance forces and instability. Infinite slope analysis, planar surface analysis, block analysis, and the Swedish circle method are straightforward limit equilibrium-based approaches used to determine the F_s. In the infinite slope analysis, it is assumed that the sliding portion of the slope extends along a long surface, and the sliding surface is parallel to the slope surface. Thus, small portion of a relatively long slope is analyzed and equilibrium of forces acting on the small failure plane is used to assess the F_s. This method is particularly useful for analyzing shallow slip surfaces. In the planar surface analysis, single planar sliding surface is selected, and F_s is calculated

as the ratio of resisting and driving forces along that surface. In block analysis, sliding slope section is divided into moving blocks and equilibrium of each block is used to determine the overall stability of the slope. Lastly, the Swedish circle method employs a geometric approach to assess the short-term stability of a slope by adjusting the position of the center of a circular failure surface to achieve moment-based equilibrium. More rigorous LE based methods involve dividing the slope into slices. These LE methods that use slices rather than a single-body diagram are known as the method of slices. In these methods (*e.g.,* Bishop's simplified, Janbu's simplified, Spencer *etc.*) sliding portion of the slope is divided into slices and equilibrium condition of each slice is analyzed separately based on the resisting forces (*i.e.,* shear strength) and driving forces (*i.e.,* weight of slice and external loads) (Abramson *et al.* (1996).

Considering n number of slices in a sliding slope section, number of unknown parameters and number of known equations used for the calculation of F_s are given in Table 2.1 and 2.2, respectively. As seen from the tables, the number of equations and unknowns are not equal, which makes the system statically indeterminate. To address this issue, the problem is generally simplified, and various assumptions are employed to determine which equations are satisfied.

Table 2.1. Number of unknown parameters (Abramson *et al*., 1996).

Variables	**Number of unknowns**
Factor of safety	1
Normal force at the base of the slice	n
Location of the normal force	n
Shear force at the base of the slice	n
Interslice force	n-1
Angle of interslice force	n-1
Location of the interslice force	n-1
Total	6n-2

Table 2.2. Number of known equations (Abramson *et al.*, 1996).

Conditions	Number of known equations
Moment equilibrium	n
Force equilibrium in X direction	n
Force equilibrium in Y direction	n
Mohr-Coulomb shear strength relationship	n
Total	4n

Satisfied equilibrium conditions for various LE based slope stability methods are summarized in Table 2.3. These methods involve numerical analysis using computer software to improve the accuracy and efficiency of the assessment of the F_s. The results obtained from the LE based approaches can be sensitive to the selection of failure surface and the satisfied equilibrium conditions.

Table 2.3. Satisfied equilibrium conditions in various LE based approaches (Abramson *et al.*, 1996).

Method	Force Equilibrium		Moment Equilibrium
	X Axis	Y Axis	
Ordinary method of slices	-	-	✓
Bishop's simplified	✓	-	✓
Janbu's simplified	✓	✓	-
Lowe and Karafiath's	✓	✓	-
Corps of Engineers	✓	✓	-
Spencer 's	✓	✓	✓
Janbu's generalized	✓	✓	-
Sarma's	✓	✓	✓
Morgenstern-Price	✓	✓	✓

2.2.2. Finite Element and Finite Difference Approaches

Finite element method (FEM) and Finite Difference Methods (FDM) are a numerical modelling approaches used to describe physical model in a continuum. In these methods, the geometry of the problem is divided into finite number of domains that are interconnected with respective boundary conditions. Each domain has an area and a set of nodes which

constructs a mesh. The mesh is then used to calculate displacements based on the defined stress-strain relationship and differential equations. The accuracy of the analysis is dependent on the quality of the mesh and rigor of the selected constitutive model (Obrzud and Truty, 2018). With the advanced computational power of today's computers, FEM and FDM have become useful and reliable tools for modelling failure mechanisms of various soil mechanics problems. For the slope stability problems analysed with FEM and FDM tools, failure conditions are simulated via strength reduction method (SRM). This is defined as a safety phase at the end of plastic analysis phases. SRM is an iterative process where shear strength related parameters, tangent of effective friction angle (φ') and effective cohesion intercept (c') or S_u values are equally reduced until failure occurs. Failure condition is obtained when a small increase in strength reduction factor (SRF) yields relatively high displacements which compromises the stability of the model (Griffiths and Lane, 1999; Brinkgreve *et al.*, 2021). Figure 2.1 shows an example plot obtained at the end of safety phase of a 3D slope stability analysis which demonstrates the convergence of F_s at failure condition.

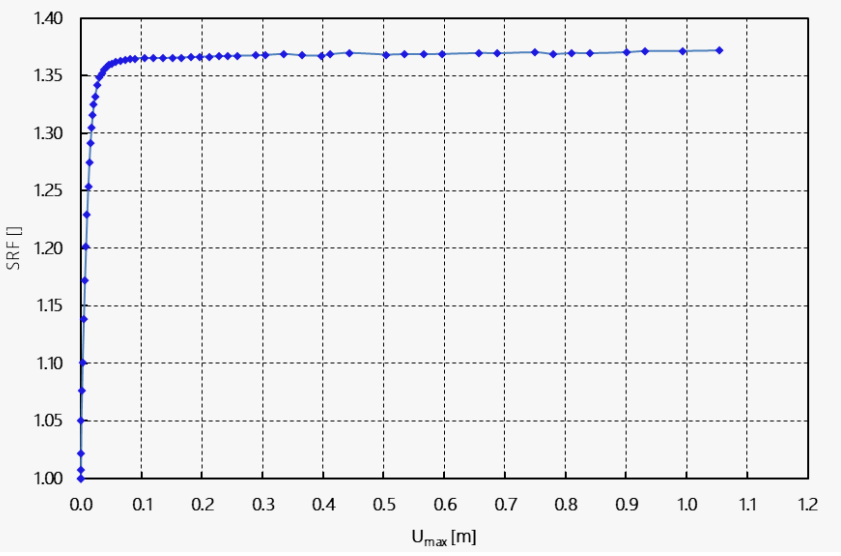


Figure 2.1. Maximum displacements versus SRF from PLAXIS 3D.

Cheng *et al.* (2007) summarized the main advantages of the SRM. Firstly, the critical failure surface is automatically defined by analysing shear strains without assuming its location or shape. Moreover, it does not rely on any assumptions of interslice shear forces unlike the case of LE approaches.

For the calculation of SRF in the FE analysis of slopes, typically four main phases/stages are introduced in calculations. First one is the initial phase where stress field and pore pressures are calculated. After the first phase, calculated displacements are reset to zero. The second phase is the plastic nil phase, which is run without any changes in the model and only used to stabilize any out-of-balance conditions that may be present from the initial phase. The third phase allows the user to introduce excavations, surcharge loadings, interfaces, supports, etc. Displacements calculated during this phase are retained, and the newly generated field conditions are used in the last phase, which is the safety analysis. Finally, during the safety analysis SRF value is obtained. SRF value is then accepted as F_s of the slope.

2.3. Stability Analysis of Surcharge Loaded Slopes

Surcharge refers to any additional load imposed on ground surface or on a slope. Surcharge loads can impact the stability of slopes by increasing the driving forces acting along a potential failure surface and reduce the F_s of slopes. Stability analysis of a surcharge load positioned at the top of a slope should be analyzed carefully, as it can also lead to a bearing capacity type failure. Both bearing capacity and slope stability analysis may be used to analyze these problems. While bearing capacity analysis offers a F_s value regarding the applied load, conventional slope stability analysis provides a F_s concerning forces along a potential failure surface, and these two approaches can yield significantly different results (Pantelidis and Griffiths, 2015). The failure surface of a surcharge loaded slope is dependent on factors such as geometry of the slope, strength parameters of soil, geometry of the loaded area, location of the loading and magnitude of the loading. To examine the effects of some of these parameters, Pantelidis and Griffiths (2015) conducted a parametric study on a 10 m high homogeneous slope. Their study involved the investigation of various foundation widths, loading distances with respect to the slope crest, and surcharge load magnitudes. In their study, short term stability condition was investigated, and undrained shear strength values were used. Various design approaches from Eurocode 7 were utilized, and the results were compared with the results of slope stability analysis obtained from 2D FE analysis to distinguish between slope stability dominant and bearing capacity dominant failures. Typical failure surfaces and F_s values obtained for various methods were presented by Pantelidis and Griffiths (2015). Three distinct failure surfaces were observed in a surcharge loaded slope:

deep-seated failure, toe failure and bearing capacity failure. Based on their results, it was concluded that the failure mechanism is mostly dependent on the surcharge load magnitude and with increasing magnitude, the failure mechanism changes from deep-seated to toe failure and then from toe failure to bearing capacity failure. Their findings indicated that surcharge load magnitudes of approximately 170 kPa or higher may be required to for bearing capacity failure to appear in a typical 10 m high slope in undrained conditions, and slope stability analysis could be more critical in cases below those magnitudes.

Georgiadis (2010) conducted a series of 2D FE analyses to investigate the parameters affecting undrained bearing capacity of strip footings placed near slope crests. His study included various foundation widths, loading distances with respect to the slope crest, and slope heights. The findings from the FE analyses were then compared with established bearing capacity equations such as Meyerhof, Hansen, Vesic, Bowles etc., which rely on limit equilibrium or upper bound plasticity methods. In his results, some of these bearing capacity equations yielded satisfactory comparisons to the results of FE analysis under specific combinations of geometric factors and soil characteristics, but they were generally non-conservative, in-essence FE analysis provided lower F_s values compared to that produced by the conventional bearing capacity equations. Additionally, Georgiadis (2010) proposed design charts, equations, and a design procedure to obtain the undrained bearing capacity factor (N_c) to be used for slopes under surcharge loads based on the results of FE analysis.

Shiau *et al.* (2011) studied the short-term bearing capacity of strip foundations placed near clayey slope crests. Loaded slope models were analyzed using 2D FE analyses based on the lower and upper bound methods for a wide range of input parameters. Their research demonstrated the existence of a critical strength ratio that can be used to separate two failure modes, namely, bearing capacity failure and slope failure. Proposed strength ratio is calculated through the expression $S_u/\gamma B$, by using S_u, unit weight of the soil (γ) and foundation width (B). If the $S_u/\gamma B$ ratio is greater than its critical value, $(S_u/\gamma B)_{critical,}$ bearing capacity failure is expected, otherwise, slope failure is expected. A design procedure for determining the bearing capacity of strip foundations placed on slopes was proposed based on their findings.

Wei *et al.* (2009) carried out 3D slope stability analysis using both the LE method and FD method coupled with SRM considering various cases, including vertical cut stability analysis, vertical cut stability analysis with the inclusion of a weak layer, locally loaded slope stability analysis, and failure modes resulting from the self-weight of infinite slopes. The results of this study showed that, convergence criteria, model boundary conditions, and mesh optimization significantly affect the performance of 3D SRM analysis. The Authors pointed out that the dimensionality (*i.e.,* whether it is 2D or 3D) of the critical failure surface for a slope with local loading is mainly determined by the magnitude of the applied load.

Zhang *et al.* (2011) used both 2D and 3D FD method coupled with SRM to analyze parameters that influence the slope failure mechanisms. Effects of boundary conditions, shear strength parameters and surcharge loads were investigated. The Authors emphasized that the failure mode of a 3D slope model is significantly influenced by the boundary conditions. The failure mode can be regarded as near plane strain conditions when the ratio of the failure shape length to slope height is greater than or equal to ten (10). It was concluded that a 3D failure can be obtained when a load is applied near the crest of a slope. This 3D failure occurs when the ratio of loading length to slope height is smaller than six (6). In other conditions, the failure shape is considered to be associated with state of plane strain conditions.

2.4. Slope Stabilization Methods

Slope stabilization techniques are commonly employed to mitigate the risk of slope failure by reducing the driving forces and/or increasing the resisting forces within slopes. In cases where limitations exist with respect to changing the geometry of the slope, increasing the resisting forces becomes a more viable option. According to Abramson *et al.* (1996), it is possible to increase resisting forces by: (*i*) improving drainage conditions to increase the shear strength of soil, (*ii*) removing weak layers or areas susceptible to failure, (*iii*) constructing retaining structures or additional supports, (*iv*) implementing in situ ground reinforcement, and (*v*) employing chemical treatments to increase the shear strength of soil (Abramson *et al.*, 1996). Table 2.4 provides a summary of commonly employed slope stabilization methods along with their general uses and descriptions.

Table 2.4. Summary of slope stabilization methods (After Abramson *et al.*, 1996).

Treatment	**Stabilization method**	**Description and general use of the method**
Unloading	Excavation	Weight of the upper portion of the slopes can be reduced, benching can be applied at the slope surface or the slope can be flattened to decrease the slope angle to decrease driving forces. Excavation methods provide low-cost solutions when they are applicable.
	Lightweight fill	Lightweight materials can be preferred for constructing embankments or as a replacement material for the upper portion of slopes.
Buttressing	Soil and rock fill	Soil and rock fills can be placed near toe of the slopes to counterbalance driving forces. Dead-weight fill solutions are easy and cost-effective when suitable materials are available and accessible.
	Counterberms	Counterberms decrease resisting forces when placed near the toe of the slopes. They are especially useful when positioned between embankments and hills to prevent bulging near the toe of the slopes.
Drainage	Surface drainage	Drainage systems help mitigate seepage forces, prevent piping, and reduce erosion. Surface drainage methods, such as using sandbags to divert water, sealing cracks, and employing surface covers, can be employed as temporary solutions in landslide areas.
	Subsurface drainage	Stability of failure surfaces below water table can be significantly improved by subsurface drainage. Subsurface drainage can be facilitated through the construction of drain blankets, trenches, cut-off drains, horizontal drains, relief drains, and drainage tunnels.
Surface protection	Shotcrete	The goal of most surface slope protection measures such as shotcrete covering, is to reduce or prevent rainwater infiltration to ensure that the slope remains either dry or mostly dry. Shotcrete covers can be reinforced with steel mesh or other fiber reinforcements when needed.
	Rip-rap	The gradual erosion of the slope's toes by flowing water in rivers, streams, and oceans can also result in instability. To prevent this erosion, layers of dumped or hand-placed rip-rap (medium and large sized rocks) can be placed along the toe of the slopes.

Table 2.4. Summary of slope stabilization methods (After Abramson et al., 1996). (Cont.)

Treatment	Stabilization method	Description and general use of the method
Reinforcement	Soil nails	Soil nailing involves reinforcing the slopes by introducing passive elements that mobilizes when there is movement in slopes. In soil nail applications, the reinforcement typically comprises metal rods, steel bars, or metal tubes designed to withstand tensile stresses, shear stresses, and bending moments caused by slope movements. Soil nailing offers numerous advantages, including its flexibility, which enables it to adapt to significant total and differential settlements. In the event that a single nail fails for any reason, it will not compromise the integrity of the entire wall system. Instead, it redistributes any excess stress to surrounding nails, thus ensuring the overall stability of slope.
	Stone columns	The construction of stone columns enhances the average shear strength (resisting forces) on a potential sliding surface by substituting the existing soil with compacted stone columns. Stone columns can also serve as drains to increase the stability of clayey slopes.
	Reticulated micropiles	Reticulated micropiles are similar to soil nails. The main difference between them is that the geometric configuration of micropiles has an important impact on their performance.
Retaining walls	Gravity and cantilever walls	Earth retaining structures such as traditional gravity and cantilever retaining walls can be used to stabilize unstable slopes.
	Tieback walls	Tieback wall designs utilize a concept in which the lateral earth pressures are stabilized through a tie system that transfers the exerted forces to zone behind the potential failure plane. Tieback walls provide an alternative to conventional walls in cases where excavation limitations exist.
	Mechanically stabilized earth (MSE) walls	MSE walls are constructed using a combination of backfill soil and thin metallic strips, mesh, or geosynthetic reinforcement to create a hybrid structure that can withstand significant loads. The typical practice involves confining backfill material with facings such as, metal, concrete, shotcrete, or geosynthetic wrapping. MSE walls, due to their versatility, can be employed in various applications, including bridge abutments, highway systems, levees, etc.
	Tire soil walls	Similar to MSE walls, tire soil walls are constructed with scrap tires as reinforcement in earth walls. This practice provides a low-cost solution and promotes recycling.

Table 2.4. Summary of slope stabilization methods (After Abramson et al., 1996). (Cont.)

Treatment	Stabilization method	Description and general use of the method
Deep foundations	Drilled shafts	When slope flattening or counterweight fills are not viable option to increase slope stability, drilled shafts can be used as an alternative solution. The drilled shafts should be inserted to adequate depths within stable layers below the anticipated depth of failure surface to provide the necessary stabilization against lateral forces generated by slope movements or landslides.
	Driven piles	Similar to drilled shafts, driven piles are also effective slope stabilization measures, particularly for shallow slides where the soil does not flow between the piles. In cases of deep-seated failures, driven piles may be unable to withstand the substantial lateral loads imposed by the deep failure surface. Additionally, driveability of piles could be an issue in certain geologies.
Vegetation	Erosion control mats	Utilizing vegetation is an effective method for protecting slopes against erosion. Erosion control mats and blankets made out of synthetic material can be used to protect seeds during the growth process.
	Biotechnical stabilization	Biotechnical stabilization is the use plant of stems and vegetation as reinforcement, drainage and surface protection to prevent erosion and surficial movements. Use of this method is mostly limited to earth fill slopes and embankments.
Soil hardening	Compacted soil-cement fill	Improving the stability of slopes through drainage might not be possible in cohesive soils with low permeability. Mixing cement with cohesive soil material increases the shear strength and reduces the permeability of the soil. Thus, soil-cement fills can be used for the restoration of a failed slopes and construction of embankments made out of cohesive soils.
	Electro-osmosis	Clay particles within silty soil can harden when moisture is removed from the soil. Drainage in silty slopes can be conducted through an electric field.
	Grouting	Grouting is a commonly applied to stabilize shallow landslides in stiff clays and shales. Grouting is accomplished by pushing water out of the cracks or openings in the ground by filling them with cement to create a stable soil mass.
	Lime injection	Injection of lime columns can be used in clayey and silty slopes to enhance the strength of soils.

2.5. Pile-stabilized Slopes

One of the main techniques used to stabilize slopes is to construct deep foundations (either drilled shafts or driven piles) along the slope to increase the resisting forces. A simple pile-stabilized slope model is illustrated in Figure 2.2. Deep foundations are commonly used to stabilize large landslides in challenging environments. The case studies of pile stabilized slopes/landslides in literature are summarized in Table 2.5. As seen in Table 2.5, both drilled shafts and driven piles are extensively used in various slope geometries, soil profiles and pile configurations. In the majority of the cases, piles are socketed into stable layers to effectively transfer loads to these stable layers. Reported cases cover a wide range of scenarios related to landslide prevention and slope stability. They involve various efforts aimed at preventing landslides, as well as improving the stability of highway cut slopes and railway embankments. In addition, these cases address challenges caused by sudden river drawdowns, slow-moving creep-type mass sliding failures, and active mudslides. They also involve implementation of preventive measures near excavation sites. These examples demonstrate the application versatility of using piles as a method for stabilizing slopes. Even though piles are commonly employed to stabilize slopes, generally accepted design method has yet to be established. The current literature is far from providing useful design insights to the practicing engineer and 3D effects are generally not recognized. The following section discusses the proposed methods for assessing the stability of pile-stabilized slopes.

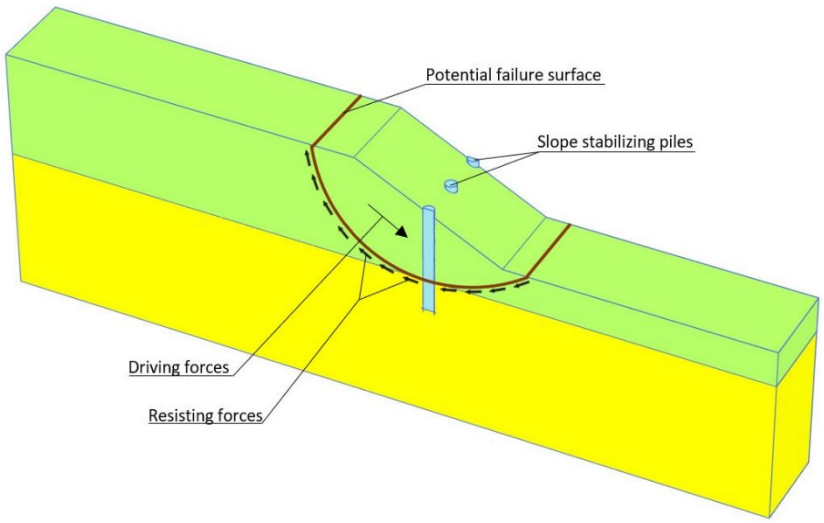


Figure 2.2. A simple pile-stabilized slope model.

Table 2.5. Pile-stabilized slope case studies reported in literature.

No	Reference	Soil Profile	Reason for Stabilization	Stabilization Method	Pile Location	Pile Diameter (m)	S/D Ratio	Socket Length / Total Pile Length Ratio
1	Ito and Matsui (1975)	Clay layers mixed with mudstone pieces over mudstone and shale	To prevent landslide	2 rows of hollow reinforced concrete piles or steel pipe piles placed in staggered configuration	-	0.3-0.318	6.67	35%-50%
2	Poulos (1995)	High plasticity clay over claystone and siltstone	To increase the stability of highway cut slopes	Reinforced concrete drilled shafts	Near mid slope	1.2	2.5 to 5	50%
3	Smethurst and Powrie (2007)	Weald clay fill and weathered weald clay over intact weald clay	To increase the stability of a railway embankment	Reinforced concrete drilled shafts	Near mid slope	0.6	4	55%
4	Liang *et al.* (2009)	Silty clay fill and sometimes mixed with gravel and cobbles over weathered mudstone bedrock	To remediate substantial settlement due to the sliding of the embankment slope in a roadway	Reinforced concrete drilled shafts	Near mid slope	1.05	2	44%
5	Bodour and Liang (2010)	Cohesive and granular fill materials over colluvium / alluvium layers above bedrock	To remediate the failure due to sudden drawdown of a river	Concrete drilled shafts reinforced with H profile beams	Near mid slope	0.83	2.75	30%
6	Gregory (2011)	Very soft bentonite seam over shale	To prevent the slow moving creep type mass sliding failure	Reinforced concrete drilled shafts	Near mid slope	0.9	2	46%
7	Lirer (2012)	Soft clayey mudslide body over varicolored clay	To stabilize an active mudslide	Steel pipe pile	Near mid slope	0.4	2.25	50%

Table 2.5. Pile-stabilized slope case studies reported in literature. (cont.)

No	Reference	Soil Profile	Reason for Stabilization	Stabilization Method	Pile Location	Pile Diameter (m)	S/D Ratio	Socket Length / Total Pile Length Ratio
8	Ashour and Ardalan (2012)	Sand over bedrock	To prevent the periodic slope movement	Augured holes filled with grout and 10 x 42 H piles	Between crest and mid slope	0.457	2.67	14%
9	Yamasaki *et al.* (2013)	Mudstone over sandstone	To prevent landslide	Reinforced concrete drilled shafts	Near toe	0.9	3	50%
10	Sengor *et al.* (2013)	Colluvium underlain by gravelly sandy silty clay layers with limestone blocks, weathered tuff and unweathered tuff	To remediate the instability due to excavation works near the toe of the slope	2 rows of reinforced concrete drilled shafts	Between mid-slope and toe	1.2	1-2	60%
11	Zhou *et al.* (2014)	Gravel, silty clay, clay soils over mudstone and sandstone	To stabilize a reactivated landslide after the construction of a dam and the rise of the lake level	2.5m x 3m rectangular reinforced concrete drilled shafts	Between mid-slope and toe	-	3	39%
12	Kahyaoğlu (2017)	Brown, gray–yellow and gray–white clayey and silty sand over sandstone	To prevent landslide	Double row of reinforced concrete drilled shafts connected with a rigid pile cap	Near toe	1.2	2	60% to 100%
13	Xue *et al.* (2018)	Exposed weak layers within highly weathered basalt	To increase the stability of a highway cut slope	3 rows of 2m x 3m rectangular reinforced concrete drilled shafts	-	-	3	-

Table 2.5. Pile-stabilized slope case studies reported in literature. (cont.)

No	Reference	Soil Profile	Reason for Stabilization	Stabilization Method	Pile Location	Pile Diameter (m)	S/D Ratio	Socket Length / Total Pile Length Ratio
14	Zhao and Deng (2018)	Gravelly soil with soft plastic clay weak layer over sandstone	To improve the stability of a landslide considering the future deterioration that may be caused by tunnel construction	2.4m x 3.6m rectangular reinforced concrete drilled shafts	Near mid slope	-	2.5	55%
15	Yildirim (2019)	High plasticity clays with swelling and collapsing potential and occasionally fine sand / silt layers sandwiched between clay layers	To avoid failure due to compulsory loading of a levee	Steel pipe pile	Near mid slope	0.605	2	-
16	Ersoy *et al.* (2020)	High plasticity clay over andesitic bedrock	To stabilize a landslide triggered by uncontrolled slope excavation	Double row reinforced concrete drilled shafts supported with grouted tiebacks	Near toe	1	1	27%
17	Li and Du (2021	Loess over sandstone	To increase the stability of a highway slope	2m x 3m rectangular reinforced concrete drilled shafts	Near toe	-	3	38%
18	Khan *et al.* (2022)	Fully softened weathered high plasticity Yazoo clay over unweathered Yazoo clay	To prevent the extreme shrink–swell movement of highly plastic clay due seasonal moisture variations	14 x 73 H-piles and two layers of uniaxial geogrid	Near mid slope	-	2.5	83%

2.6. Stability Analysis of Pile-stabilized Slopes

Stability analysis of pile-stabilized slopes can be performed using both analytical solutions, such as LE methods, pressure-based methods, and displacement-based methods, as well as numerical solutions based on continuum mechanics approaches such as FE and FD analysis. A literature review of analytical and numerical solutions is presented in the following sections.

2.6.1. Analytical Solutions

Analytical methods used for the stability analysis for pile-stabilized slopes are LE methods, pressure-based methods, and displacement-based methods. Analytical methods generally consider uncoupled analyses, as pile and slope stability are evaluated separately. Initially, Broms (1964) used the coefficient of subgrade reaction method to study the ultimate lateral resistance of piles in cohesive soils. Based on his work, Viggiani (1981) defined failure modes for landslide-stabilizing piles and developed LE based analytical formulations to calculate the ultimate lateral loads on landslide stabilizing piles. Only rigid piles in cohesive soils were considered in his study. Summary of failure modes and bending moment diagrams proposed by Viggiani (1981) are shown in Figure 2.3.

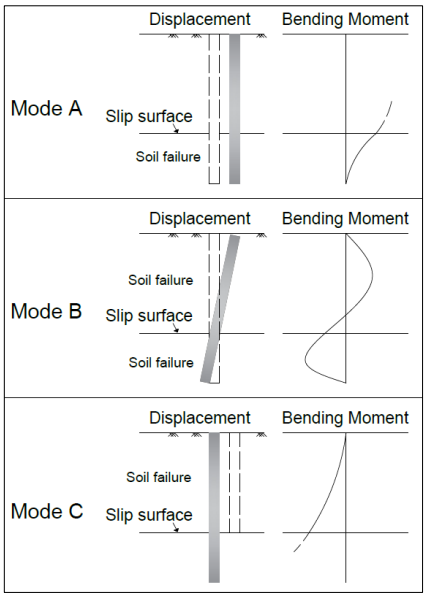


Figure 2.3. Summary of failure modes and bending moment diagrams for landslide-stabilizing rigid piles (modified after Viggiani, 1981).

As seen in Figure 2.3, in mode A, the pile and the unstable soil layer moves together displacing horizontally; by ripping through the stable soil layer below. In mode B, both stable and unstable soil layers fail, resulting in a rigid body rotation of the pile. In mode C, the pile is firmly socketed in the stable layer and the unstable soil layer flows around the pile. This study showed that all of these failure modes are possible and the development of one of these specific failure modes is influenced by the pile length, pile diameter, ultimate bending moment capacity of the pile cross section, thickness of the unstable soil layer, and undrained shear strength of both stable and unstable soil layers.

Ito and Matsui (1975) carried out one of the most significant analytical research studies on pile-stabilized slopes considering rigid piles with restrained pile heads. The researchers described how lateral load develops in a slope stabilizing pile by pointing out two soil states between the piles: (*1)* plastic deformation and *(2)* plastic flow. State of plastic deformation around the piles considered in their theory is shown in Figure 2.4.

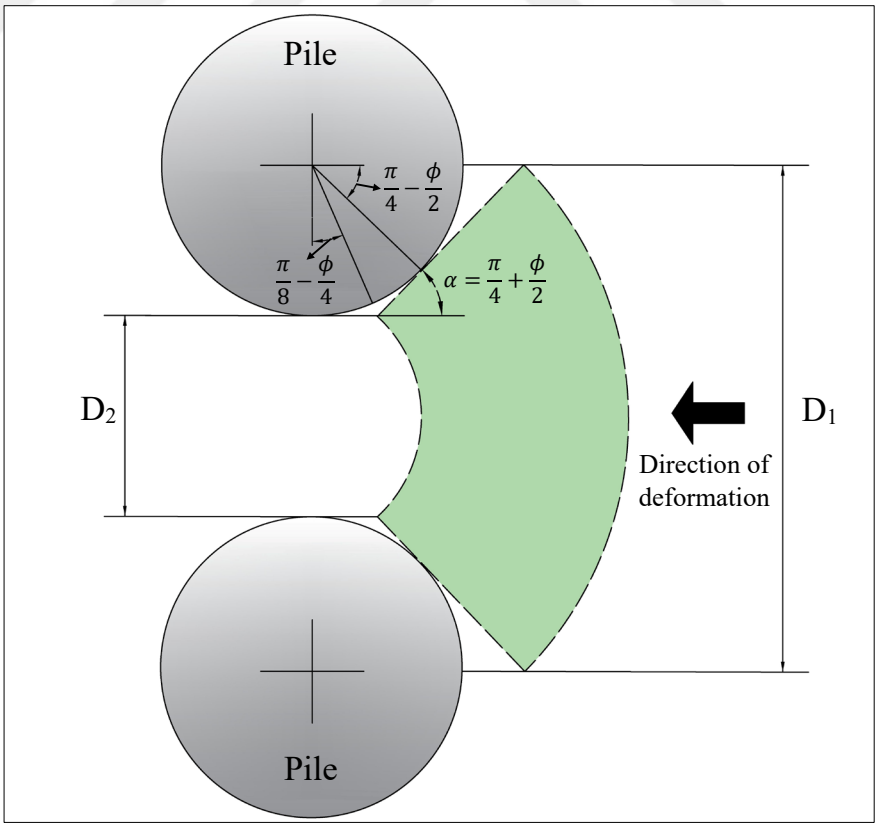


Figure 2.4. State of plastic deformation around the piles (modified after Ito and Matsui, 1975).

Based on the plastic deformation theory, Ito and Matsui (1975) introduced a formulation for calculating the lateral force acting on stabilizing piles. In their formulation lateral force per unit length of the pile (p) was defined as,

$$p = cD_1\left(\frac{D_1}{D_2}\right)^{\left(N_\phi^{1/2}\tan\phi+N_\phi-1\right)}\left[\frac{1}{N_\phi\tan\phi}\left\{exp\left(\frac{D_1-D_2}{D_2}N_\phi\tan\phi\ x\tan\left(\frac{\pi}{8}+\frac{\phi}{4}\right)\right)-2N_\phi^{1/2}\tan\phi-1\right\}+\frac{2\tan\phi+2N_\phi^{1/2}+N_\phi^{-1/2}}{N_\phi^{1/2}\tan\phi+N_\phi-1}\right]-c\left\{D_1\frac{2\tan\phi+2N_\phi^{\frac{1}{2}}+N_\phi^{-\frac{1}{2}}}{N_\phi^{\frac{1}{2}}\tan\phi+N_\phi-1}-2D_2N_\phi^{-\frac{1}{2}}\right\}+\frac{\gamma}{N_\phi}\left\{D_1\left(\frac{D_1}{D_2}\right)^{\left(N_\phi^{1/2}\tan\phi+N_\phi-1\right)}x\ exp\left(\frac{D_1-D_2}{D_2}N_\phi\tan\phi\ x\tan\left(\frac{\pi}{8}+\frac{\phi}{4}\right)\right)-D_2\right\} \quad (2.1)$$

where γ is the unit weight of the soil, c is the cohesion intercept of soil, ϕ is the friction angle of soil, D_1 is the center-to-center pile spacing in a row, D_2 is clear spacing between the piles and N_ϕ is $\tan^2(45+\phi/2)$.

Ito *et al.* (1981, 1982) carried out parametric studies considering one and two rows of piles based on the analytical framework introduced by Ito and Matsui (1975). In their research, they proposed a revised formulation to determine the F_s of the pile-stabilized slope, considering the lateral load capacity of the piles. In their formulation F_s was defined as,

$$F_S = \frac{F_{rs}+F_{rp}}{F_d} \quad (2.2)$$

where F_{rs} is the resisting forces supplied by the slip surface, F_{rp} is the resisting forces supplied by the piles and, F_d is the driving forces. While F_{rs} and F_d can be determined using limit equilibrium approaches, such as the method of slices, F_{rp} can be obtained through Equation 2.1 or considered as the ultimate shear force capacity of piles in the event of pile failure.

Using the plastic deformation theory developed by Ito and Matsui (1975), Hassiotis *et al.* (1997) presented a thorough and meticulous design procedure to analyze the slopes stabilized with single row of piles. In their approach, reaction force mobilized due to the lateral loads exerted onto the piles was calculated. The calculated lateral loads were integrated into LE based friction-circle method to determine the F_s that accounts for the contribution of the piles. Pile displacements and internal forces were also calculated. For the pile section above the slip surface, the lateral resistances were calculated using the Ito and

Matsui (1975) formulation, whereas for the pile section below the slip surface, Winkler foundation model was adopted using FD analysis. The suggested design procedure was demonstrated on an example slope, investigating the effects of pile diameter, pile spacing and pile location on F_s. The Authors recommended to position the piles between the crest and the mid-height of the slope, and to restrain the pile head movement to reduce the bending moments and shear forces acting on the pile.

Poulos (1995) presented a new design procedure for pile-stabilized slopes using traditional LE methods coupled with simplified boundary element analysis to include lateral response of piles. ERCAP (Earth Retaining Capacity of Piles) software was used to implement his analytical method. Pile behavior under lateral soil movements can be analyzed by this software, based on factors such as the thickness of sliding layer, pile diameter and pile flexibility. Based on the results of the ERCAP analyses performed to investigate pile behavior, four pile failure modes were defined: *(1)* flow mode, *(2)* short-pile mode, *(3)* intermediate mode and, *(4)* long-pile mode. The first three failure modes are associated with soil failure, whereas the final mode of failure considers the failure of the pile element itself. In the flow mode, the relatively shallow unstable soil layer flows between the piles. In the short pile mode, the unstable soil layer is comparatively deeper while the portion of the pile socketed in the stable soil is relatively shorter. In this mode, the sliding layer pushes the pile through the stable soil layer, leading to the complete utilization of the strength of the stable layer. In the intermediate mode, complete utilization of the strength occurs in both unstable and the stable layers. In the long-pile failure mode, the pile element fails as it reaches the ultimate bending moment capacity of the pile cross section.

Lee *et al.* (1995) introduced a simple uncoupled method for the analysis of pile-stabilized slopes by considering the response of piles and stability of the slope independently. A modified boundary element method that can model non-linear pile soil interaction was utilized to analyze the response of stabilizing piles under lateral loads. The Bishop slip circle method, which defines the F_s based on resisting and overturning moments, was modified by including the supplementary resisting moments resulting from pile stabilization to evaluate the F_s of the pile-stabilized slope. Based on this uncoupled approach, the Authors emphasized that optimal location of the piles may be either at the crest or at the toe of a homogeneous soil slope. Additionally, the performance of piles is influenced by the

pile diameter, the pile spacing, and the maximum pressure allowed at the interface between the pile and the soil in a layered profile. The performance of piles is maximized when they are embedded through soft soils and socketed into stable layers.

Ausilio *et al.* (2001) used the kinematic approach of limit analysis to study pile-stabilized slopes. Initially, the Authors focused on slopes without piles and proposed a method for computing the F_s. The calculated F_s values were compared/verified with the traditional LE and upper and lower bound limit analysis results. Then, they expanded their method to include the contribution of piles and proposed analytical expressions that can be used for designing pile-stabilized slopes. In their study, a single row of piles was deemed to be a practical solution to improve the stability of a slope, particularly when the slip surface is shallow. Furthermore, based on their analytical expressions, the most advantageous placement of piles was recommended as near the toe of the slope.

Ashour and Ardalan (2012) presented an iterative approach to study pile behavior and F_s of pile-stabilized slopes using strain-wedge method coupled with LE analysis. Their approach considers the interaction between the piles and the adjacent soil, with the assumption that the soil's displacements would surpass the deflection of the piles. The Authors emphasized that the proposed model was verified via multiple full-scale load tests obtained from reported case studies in the literature. Their findings suggested that the ultimate force a pile can transmit to the stable soil is influenced by various factors, including the pile's location within the slope, the depth of the failure surface at the pile location, the type of soil, the diameter of the pile, and the spacing between piles.

He *et al.* (2015) investigated the effect of slope angle on the distribution of the soil-pile pressure acting on stabilizing piles considering infinite sandy slopes and proposed a LE based new method to calculate lateral forces acting on the piles. The proposed method was verified via 3D FD analysis.

Zuo *et al.* (2023) presented a kinematic approach to evaluate the stability of pile-stabilized slopes. Kinematic expressions were developed based on failure mechanisms involving rotational slip surfaces to calculate resisting forces and F_s values of the slopes. Proposed mathematical expressions were then used to produce stability charts for

preliminary design of pile-stabilized slopes. Their results showed that if piles are closely spaced and have adequate length, a shallow slip surface is expected instead of a deep seated failure surface that passes beneath the piles. Generally, the highest value of F_s is obtained when piles are positioned in the upper-middle section of the slope.

2.6.2. Numerical Solutions

Numerical methods used for the stability analysis for pile-stabilized slopes include the continuum mechanics based approaches such as FE and FD analysis. Numerical methods enable the execution of coupled analyses, where pile and slope stability are evaluated simultaneously. With the advances in computer technology and 3D software, recent research work started to reveal more about the behavior of slope stabilizing piles.

Chow (1996) proposed a numerical method to analyze pile-stabilized slopes where piles were modeled using finite beam elements and the soil was characterized using the subgrade reaction modulus. The interaction between the piles and the soil was considered in accordance with the principles of elasticity theory. Based on the proposed method, the evaluation of pile performance in slope stabilization was conducted by analyzing two case studies, one focusing on a single pile and the other on a group of piles. The results indicated that the proposed method has the ability to estimate the pile behavior and the performance of pile groups was notably affected by the interaction between the piles and the surrounding soil.

Cai and Ugai (2000) investigated the influence of spacing between piles, the pile head conditions, the elastic modulus of piles, and the placement of the piles on F_s of pile-stabilized slopes using 3D FE analysis coupled with SRM. Numerical results were subsequently compared to the F_s values obtained by a modified version of the Bishop's simplified method, where the contribution of pile resistance is incorporated through the Ito and Matsui (1975) formulation. Their results highlighted that the pile head condition and the elastic modulus of piles can influence F_s significantly and this influence cannot be accurately determined using LE methods. The Authors also emphasized that the free pile head conditions yield considerably lower F_s values compared to those obtained with the restrained pile head

condition. They recommended that the pile row should be positioned at the middle of the slope height to achieve the maximum improvement in F_s.

Chen and Martin (2002) studied and quantified the effect of soil arching in passive piles by conducting a series of 2D FD analysis. Undrained behavior for fine grained soils and drained behavior for coarse grained soils were considered in their numerical study. Effects of dilatancy angle, pile-soil interface roughness, and pile group effects were investigated. The presence of an arching zone was identified by examining the patterns of displacement in the direction of soil movement and the rotation of principal stress directions between the piles. The Authors highlighted that ultimate state conditions, with sufficient soil displacement to induce plastic deformation in the soil may be required for the formation of an arching zone. Their findings indicate that the development of the soil arch between piles depend on factors such as pile configuration, pile displacement, pile shape, pile-soil interface roughness, and the dilatancy angle.

Liang and Zeng (2002) studied the impact of soil arching phenomenon on the load transfer mechanism of slopes stabilized with drilled shafts. They utilized 2D FE analysis to investigate the effects of pile spacing, pile diameter, pile shape (square, and circular) and soil strength considering both cohesive and cohesionless soils. Based on their results, practical design tables that include S/D ratio, pile diameter and soil strength were proposed. The Authors demonstrated that the loads transferred to the piles increase rapidly with larger soil movements, due to the stress transfer facilitated by soil arching. Additionally, after reaching a threshold value of maximum load experienced by the piles, soil movement continues without further loading of the piles. Single pile behavior was observed for S/D ratios larger than eight (8). This study also emphasized that the S/D ratio is the most influential parameter, and the pile diameter has a minor effect for a constant S/D ratio. The Authors concluded that smaller S/D ratios and higher friction angles increases the loads transferred to piles and cohesive soils are more likely to develop full arching. The Authors also highlighted that the outcomes of their parametric analysis were in good agreement with the experimental findings.

Jeong *et al.* (2003) investigated the impact of a single row piles on the stability of weathered slopes through analytical and numerical methods. 3D FE analysis was conducted

to obtain pile response based on various S/D ratios and pile head conditions. Based on the limited results of 3D FE analysis, the Authors proposed a simplified uncoupled method to analyze pile-stabilized slopes. In their analytical study, the Authors first obtained ultimate soil resistance values from single pile p-y curves. Subsequently, they quantified load transfer curves through 3D FE analysis. Then, these two findings were integrated into the Bishop simplified method to calculate the F_s of pile-stabilized slope. Their results showed that F_s of the uncoupled analysis is significantly more conservative than the F_s of the 3D FE analysis but rate of change in F_s with respect to S/D ratio was similar in both approaches. Moreover, use of restrained pile heads (either hinged or fixed) was recommended to attain higher F_s values.

Wei and Cheng (2009) analyzed the failure surfaces of pile-stabilized slopes for various pile spacing and pile locations. Slope geometry used by Cai and Ugai (2000) was utilized in their parametric study. Failure surfaces were determined by the maximum shear strain approach. Their results showed that the point at which the maximum shear force is concentrated within a pile may not necessarily correspond to the depth of the critical failure surface of a pile-stabilized slope. Additionally, it was shown that the optimal pile placement is generally close to the midpoint of the slope for sandy soils, but for clayey soils, it tends to shift slightly toward the crest.

Liang and Yamin (2009) studied the soil arching phenomenon and the load transfer mechanisms in slopes stabilized with one row of rock-socketed drilled shafts using 3D FE simulations. An extensive parametric study was performed considering large range of pile, soil, and rock properties. The Mohr–Coulomb constitutive model was employed to describe the behavior of the soils, while both the drilled shaft and rock were represented as linear-elastic materials. Load transfer factor (η) and allowable shaft deflection (δ) values were introduced to quantify the effect of various parameters considered in the study. η was defined as the ratio of the forces exerted on the drilled shafts from the upslope section divided by the forces transferred to the downslope section of the slope. Load transfer scheme used to calculate the η values is shown in Figure 2.5. As a result of the analyses, preliminary design charts were proposed based on the statistical analysis obtained from the numerical η - δ data. It was concluded that, substantial enhancements in F_s can be obtained by using a single row

of drilled shafts that are adequately embedded in a stable layer and have a S/D ratio in the 2-4 range.

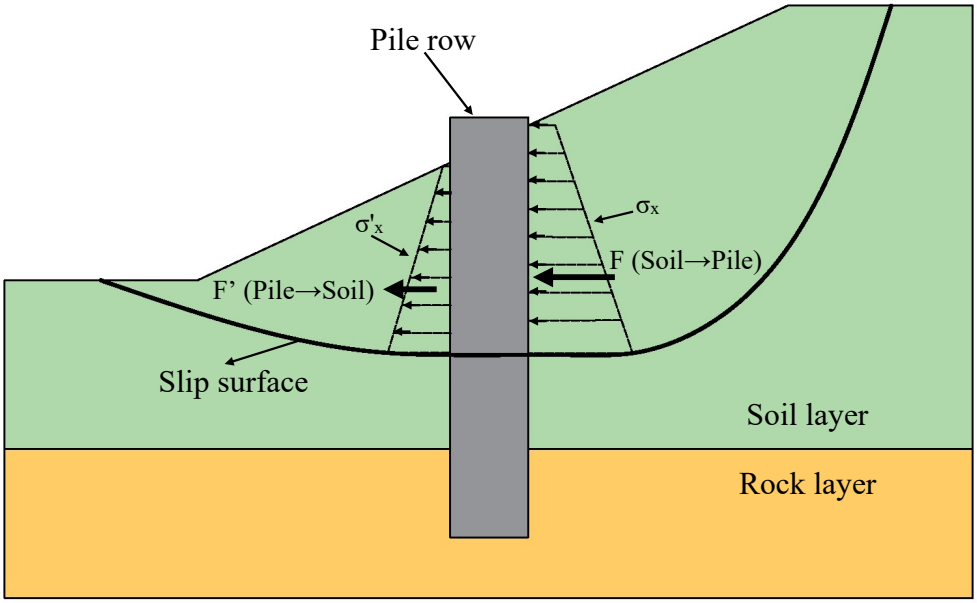


Figure 2.5. Load transfer scheme (modified after Liang and Yamin, 2009).

Ellis *et al.* (2010) studied impact of pile location, pile diameter and pile spacing on a generic pile-stabilized clayey slope that had F_s value of 1 prior to any stabilization measure, using 2D-3D FD tools and SRM. In their research, flexural failure of the piles was not considered, and the piles were modeled as linear-elastic material. A simple analytical model was proposed to calculate the force needed to achieve a desired improvement in F_s for preliminary design purposes. The results obtained from the proposed model were in good agreement with the results of the numerical analyses.

Kanagasabai *et al.* (2011) conducted 3D FD analysis to investigate stabilizing pile behavior in soil masses experiencing lateral displacements. The pile failure modes proposed by Viggiani (1981) were utilized to assess the performance of the piles placed in various slope inclinations and various interface strength values (between the sliding and stable soil layers). Three slope inclinations: 0°, 14°, and 22° were considered in their analysis. The findings of their study highlighted the significance of soil layering and soil strength in the failure mode of the piles. Additionally, the Authors emphasized that the effect of slope inclination on pile behavior becomes notably pronounced beyond a specific angle, while

below this specific angle, the pile's behavior closely resembles that observed in the case of a flat ground surface (0° slope.)

Yang *et al.* (2011) examined the influence of pile length in pile-stabilized slope stability analysis using 3D FE analysis coupled with SRM. Additionally, impacts of pile spacing, the conditions at the pile head, the stiffness of the pile, and the properties of the surrounding soil on both the length and behavior of the pile were analyzed in their study. The results of this study showed that the F_s value increase as the pile length increases until it stabilizes as the pile length surpasses a critical length. The critical pile length is shorter for slopes with clayey soil compared to slopes with sandy soil when free (*i.e.,* unrestrained) pile heads are considered. On the other hand, critical pile length is longer when piles heads are restrained in clayey soils. Even though, the Authors recommended the use of restrained pile head conditions, this study noted that achieving a restrained head condition with a single row of piles can be challenging unless the pile heads are securely anchored in practice.

Kourkoulis *et al.* (2011, 2012) introduced a two-step hybrid method for the analysis of pile-stabilized slopes to reduce the computation time by decoupling the slope geometry and the calculation of pile lateral capacity. Proposed method consists of two main steps: *(1)* performing conventional LE analysis using the whole slope model to obtain the lateral resistance force (RF) needed to increase the F_s to a pre-determined target F_s, and *(2)* conducting 3D FE analysis for a selected pile arrangement capable of supplying the RF determined in the first step considering an allowable deformation threshold. A parametric study was presented based on the proposed approach. The effects of pile spacing, pile diameter, pile socket length, pile group configurations, unstable soil layer thickness and soil strength considering both cohesive and non-cohesive soils were investigated in their parametric study. Kourkoulis *et al.* (2011, 2012) concluded that in case of relatively small pile embedment, the short pile failure mode is dominant, and the pile's full structural capacity cannot be utilized, resulting in an uneconomical design. In order to establish effective soil arching between the piles, it is crucial to maintain a S/D ratio of 4 or below. When the S/D ratio exceeds 5, the piles function as single piles, and the soil flow in between the piles may be initiated. Additionally, the required socket length for achieving fixed conditions at the pile base ranges from 0.7 to 1.5 times the thickness of the unstable layer, depending on the strength of the stable layer.

Liang *et al.* (2014) proposed a LE based design procedure for the design of slopes stabilized with one row of drilled shafts. Semiempirical load transfer factors representing soil arching effects was formulated and integrated into a 2D LE slope stability software via regression analysis considering various slope geometries, soil profiles, and groundwater table conditions. The results of the 2D LE analysis, including F_s and the net force applied to the piles, were compared, and validated using a 3D FE tool. The Authors emphasized that there is no unified general rule of thumb that can be applied for determining optimum location, spacing, or size of drilled shafts and these parameters should be investigated case by case.

Keleşoğlu (2015) utilized FDM coupled with SRM to study the effects of the slope curvature, local surcharge loading and pile-stabilization on the F_s and failure mechanism of gentle slopes. His results showed that when the local surcharge loading is near the crest of the slope, 3D failure is expected. Otherwise, slope's own weight is more influential on the shape of the failure surface, leading to 2D failure. Moreover, the results of this study indicated that the optimal pile row placement is closer to the slope crest to ensure local and global stability of the slope, especially when surcharge loads are present.

Pirone and Urciuoli (2018) used 2D and 3D FE method to analyze infinite slopes stabilized with continuous and discontinuous pile rows. The study examined how slope inclination, residual friction values on the slip surface, and the distance between piles influenced the ultimate soil strength at the interface between the piles and the soil. SRM was adopted in FE analysis to study pile-stabilized slopes at the ultimate limit state (*i.e.,* slope failure). In the analysis, linear-elastic perfectly plastic soil constitutive model with the Mohr-Coulomb failure criterion was used for the frictional soil layers and the piles were modeled as elastic materials. Failure of piles were not considered in the analysis since shallow landslides are mainly observed in purely frictional slopes and in such cases failure mode is governed by soil failure. Ultimate lateral loads exerted on piles were obtained by 2D and 3D analyses and then compared with the analytical rigid-plastic solutions by extending the existing solutions in the literature. Failure modes proposed by Viggiani (1981) shown in Figure 2.3 were used in calculations. Simple design charts for landslide mitigation are proposed based on the results of their parametric study considering ultimate limit state

conditions. Their results highlighted that soil arching was effective up to S/D ratio 3 and 6 for failure modes B and C (*see* Figure 2.3), respectively.

González *et al.* (2020) studied pile reinforced slope stability problem to assess the impact of pile location, spacing, embedment depth, and pile diameter on the F_s using 2D-3D LE and FE methods. The study utilized mathematical and statistical methods to quantify the sensitivity of various inputs on the F_s of pile-stabilized slopes. The results showed that pile location, embedment depth, and spacing significantly influenced the F_s. Moreover, it was concluded that the optimum location of piles can change with respect to the strength parameters of soils and the slope geometry. For c - ϕ soils, optimal pile location varies between middle of the slope and the slope crest depending on the location of middle point of the critical failure surface. In cohesive soils, the best pile location is near the slope's toe and the location shifts upwards as cohesion increases. However, this change in pile location only has a marginal impact on the F_s. For purely frictional soils, highest F_s values were observed in the middle to three-quarter point of the slope, but again improvement in F_s due to pile location was minor.

Li and Du (2021) conducted a field study to monitor the movements of large-scale reinforced concrete piles used to stabilize an excavated loess slope that had a pre-existing slip surface. Field measurements were compared with numerical results obtained from 3D FE analysis. Then, a parametric study was executed via 3D FE using the same slope geometry to examine how variations in pile length, embedment ratio, spacing, and cross-section impact the stress and deformation properties of the piles. The Authors emphasized that extending the pile and increasing the embedment ratio can decrease the displacements at the pile head. When the embedment ratio exceeds 0.68, the probability of having shallow critical surface that yields a lower F_s value increase. Increasing the spacing between the piles leads to a decrease in the F_s, while also causing a gradual increase in the displacement and bending moment of the pile. Based on the results of their analysis, a pile spacing to pile diameter ratio of 4 was identified as the most cost-effective spacing option.

Fantera *et al.* (2022) used 2D and 3D FD methods to study the effects of pile spacing, pile embedded length, soil properties, and slope inclination on the efficiency of pile-stabilized fine-grained slopes considering fixed and unconstrained movement of the

complete pile shaft. Simple preliminary design charts were proposed for the calculation of ultimate resisting forces provided by piles, which are based on analytical relationships obtained for two layered infinite slopes with gentle ground inclinations, ranging from 0° to 12°. It was concluded that the 2D analyses significantly overestimate soil arching and this overprediction decreases as pile spacing increases. In cases where S/D>7, soil arching significantly reduces and piles behave as isolated piles. The result of the 3D analyses indicated that assuming fixed piles can lead to an overestimation of pile efficiency in reducing slope movements. Thus, it was recommended to model piles as unconstrained where piles are free to move for a more accurate assessment. Moreover, it was concluded that the effectiveness of piles in stabilizing slopes is also significantly affected by the magnitude of slope movements in addition to the spacing between the piles.

Wang *et al.* (2023) introduced a probabilistic approach for assessing the stability of pile-stabilized slopes using a weighted uniform simulation method integrated into 3D FE software via Python code. Using the proposed method, the Authors investigated the influence of different pile design parameters such as pile length, pile diameter, pile spacing and pile location using the pile-stabilized slope example presented by Wei and Cheng (2009). Based on obtained reliability indices and most probable failure points, optimum pile designs were discussed.

2.6.3. Other Studies and Gaps in The Literature

The piles have been modeled as linear-elastic materials in most of the slope stability analysis studies that utilize numerical methods to date (Wei and Cheng 2009; Ellis *et al.* 2010; Kanagasabai *et al.* 2011; Liang *et al.* 2014; Fantera *et al.* 2022). However, in the short-term stability analysis of clayey slopes, deep-seated failure surfaces are often observed, and it is important to model the piles as elasto-plastic elements since the structural capacity of the slender pile is likely to govern the failure mode. To investigate the effect of pile structural capacity, Pradel *et al.* (2010) carried out 2D FD analysis coupled with strength reduction method to determine the F_s of a pile-stabilized slope, using the pile-stabilized slope model presented by Hassiotis *et al.* (1997). In their study, concrete piles were modeled assuming they are materials with *(1)* linear-elastic (*i.e.,* unlimited bending moment capacity) properties and *(2)* limited strength (*i.e.,* maximum bending moment capacity). The piles modeled with

maximum bending moment capacity accurately estimated the critical failure mode and the F_s of pile-stabilized slopes subjected to plastic bending moments.

Jiang *et al.* (2022) investigated the impact of pile location and reinforcement ratio on internal pile forces, displacements, and the F_s of pile-stabilized slopes via 3D FD analysis. In their research, the piles were modeled using both linear-elastic constitutive model and a damage constitutive model. The damage constitutive model is a novel modeling approach that is capable of representing the plastic deformations, fracturing, and crushing of piles when subjected to lateral loads which was implemented in 3D FE using the FISH programming language. Based on their findings, the Authors emphasized that the elastic constitutive model tends to overestimate the contribution of piles in terms of stabilization. As a result, adopting the damage constitutive model can yield more critical F_s values and internal pile forces.

Kourkoulis *et al.* (2011) investigated pile structural non-linearity in their two-step hybrid method. Structural non-linearity aspect of the reinforced concrete piles was modeled based on moment-curvature (M-c) relationships of the selected pile cross sections. It was observed that in shallow slides, pile non-linearity has minor influence on the results. However, in deep slides, significant soil movement apply substantial thrust on the piles, nearing their structural capacity. Their findings highlight the importance of incorporating pile failure into the analysis of pile-stabilized slopes, especially in cases where deep-seated failures are expected.

Lirer (2012) reported substantial volume of experimental data, including recordings such as groundwater levels, rainfall measurements, slide movements, pile displacements, and pile strains obtained from a row of instrumented steel piles constructed in an active mudslide. The extensive dataset was analyzed to investigate the impact of the pile row on the stability of the mudslide. It was found that the single row of steel piles could not prevent the mudslide entirely, but it does influence surrounding displacement field. The Authors noted that the piles behaved elastically until a plastic hinge gradually formed just beneath the sliding surface. Furthermore, 3D FD analysis was performed to estimate lateral loads exerted on the piles. It was concluded that, the lateral forces exerted on the piles estimated

via numerical analysis were in compliance with the field data highlighting the potential of 3D numerical analysis as a valuable research tool.

The results of the uncoupled analysis, in which piles and slope stability analysis are performed non-simultaneously, indicate the requirement for coupled analysis that can be performed using rigorous FE analysis. The literature on the numerical analysis of pile-stabilized slopes indicates a range of results, however, a clear understanding of the effect of pile and slope related parameters on the F_s of the slope, and the effect of 3D analysis have not been yet fully established. Especially, the effects of surcharge loads on the 3D failure shapes of pile-stabilized slopes are not identified. Additionally, the studies that account for the critical-failure surfaces generating from the structural-failure of the piles are scarce.

3. METHODOLOGY

Pile-stabilized slope cases considered in this study were analyzed via 3D FEM. The definition of the investigated problem, details of the used 3D FE software, analysis steps and case selection approach used in this study are presented in this chapter.

3.1. FEM Software and Units

Pile-stabilized slope models were simulated in the three-dimensional finite element software PLAXIS 3D that is widely used in geotechnical practice (Brinkgreve *et al*., 2021). The units used in the PLAXIS 3D software are presented in Table 3.1.

Table 3.1. Units used in the PLAXIS 3D software.

Basic Units			**Geometry**		**Forces and Stresses**	
Length	Force	Time	Coordinates	Displacements	Distributed Loads	Stresses
m	N	day	m	m	kN/m^2	kN/m^2

3.2. Material Modeling

3.2.1. Modeling of Soils

FEM is a numerical modelling approach used to describe a physical model in a continuum. In this method, displacements are calculated based on the defined stress-strain relationship and differential equations. Accuracy of the analysis is dependent on the capabilities of the selected constitutive model (Obrzud and Truty, 2018). Thus, selection of the material model is an important step in the FEM analyses. PLAXIS 3D offers a variety of well-known constitutive models that are commonly used in geotechnical analysis, including simple linear-elastic, Mohr-Coulomb (MC), hardening soil (HS), hardening soil with small strain stiffness (HSS), modified cam-clay, NGI-ADP, Hoek-Brown, and jointed rock models. For more advanced analysis, soft soil, soft soil creep, UDCAM-S, UBC3D-PLM and concrete models are also available in PLAXIS 3D. Additionally, users can also define their own constitutive model and use it in their analysis if needed (Brinkgreve *et al*., 2021).

The simplest constitutive model commonly used to represent stiff structures in soil is the linear-elastic model. This model is based on Hooke's law of linear elasticity, and the stress-strain relationship is defined by Young's modulus (E) and Poisson's ratio (ν). The Mohr-Coulomb model is the second most commonly used model. In this model, the stress-strain relationship is defined as an elastic perfectly-plastic model with Mohr-Coulomb failure criterion as shown in Figure 3.1. A constant average elasticity modulus is assumed to model deformations and for this reason, this model is considered to be a crude approximation of soil behavior and its application is more suitable for analyzing failure conditions (Obrzud and Truty, 2018). So, the MC model is not the ideal choice for analyzing the deformation of soft or clayey soils, and more advanced models are recommended for such analyses. However, in Plaxis 3D, the parameters commonly employed in these advanced models are automatically simplified to fit the MC model for factor of safety analyses by excluding stress-dependent stiffness behavior and hardening effects to apply strength reduction method and obtain a F_s value (Brinkgreve *et al*., 2021).

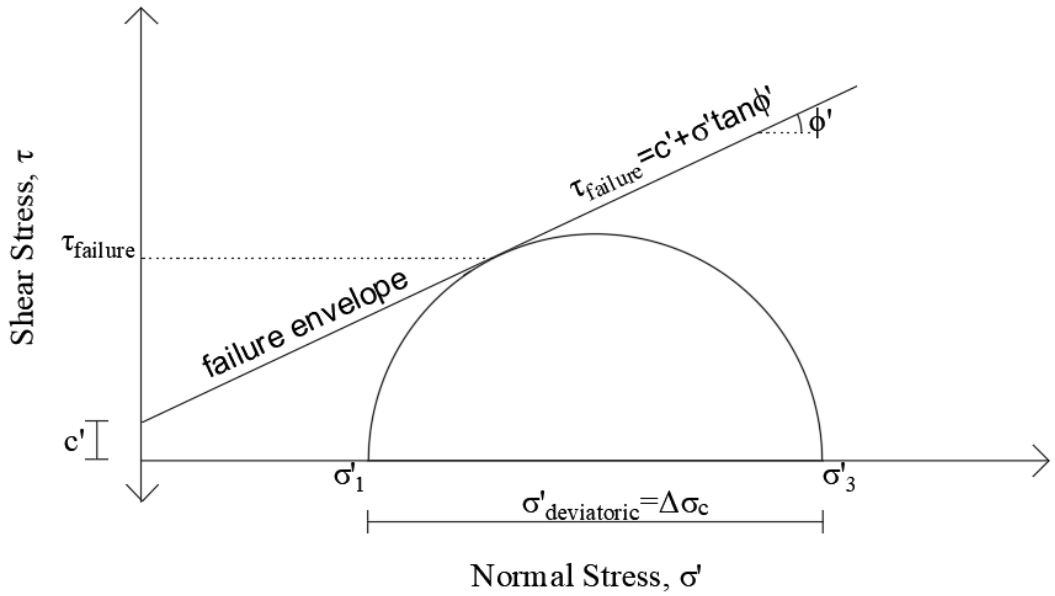


Figure 3.1. Mohr-Coulomb failure envelope.

HS and HSS models are rigorous constitutive soil models defined using the principles of hardening plasticity. Compared to the elastic perfectly-plastic MC model, the HS and HSS models are better suited for soft or clayey soils because they allow the yield surface to expand

when plastic strains occur (Brinkgreve *et al*., 2021). Summary of parameters used to simulate soil behavior in the hardening soil models are provided in Table 3.2.

Table 3.2. Parameters used in the HS and HSS models (Brinkgreve *et al*., 2021).

Parameter	**Symbol**	**Unit**
Parameters for the HS Model		
Effective cohesion intercept	c'	kPa
Effective friction angle	ϕ'	Degree
Dilatancy angle	ψ	Degree
Tension cut-off	σ_t	kPa
Secant stiffness in standard drained triaxial test	E_{50}^{ref}	kPa
Tangent stiffness for primary oedometer loading	E_{oed}^{ref}	kPa
Unloading / reloading stiffness	E_{ur}^{ref}	kPa
Power for stress-level dependency of stiffness	m	-
Poisson ratio for unloading-reloading	ν_{ur}	-
Reference stress for stiffnesses	p^{ref}	kPa
Failure ratio	R_f	-
Additional Parameters for the HSS Model		
Reference shear modulus at very small strains	G_0^{ref}	kPa
Threshold shear strain	$\gamma_{0.7}$	-

The main distinction between the MC and hardening soil models is the modeling of stiffness. In the hardening soil models, three different stiffness parameters are introduced to better simulate the stress-dependent stiffness characteristics of soils which are tangent stiffness for primary oedometer loading (E_{oed}^{ref}), secant stiffness in standard drained triaxial test (E_{50}^{ref}), and unloading / reloading stiffness (E_{ur}^{ref}). E_{50}^{ref} value is defined by secant stiffness at 50% of the maximum deviatoric stress, at the reference stress level. The reference stress value for stiffness parameters is taken as 100 kPa by default in PLAXIS 3D. It is suggested and commonly employed to set E_{oed}^{ref} equal to E_{50}^{ref} and E_{ur}^{ref} equal to $3E_{50}^{ref}$ in most geotechnical engineering applications. The determination of E_{50}^{ref} and E_{ur}^{ref} values from drained triaxial test results is illustrated in Figure 3.2 and the determination of E_{oed}^{ref} value from oedometer test result is demonstrated in Figure 3.3.

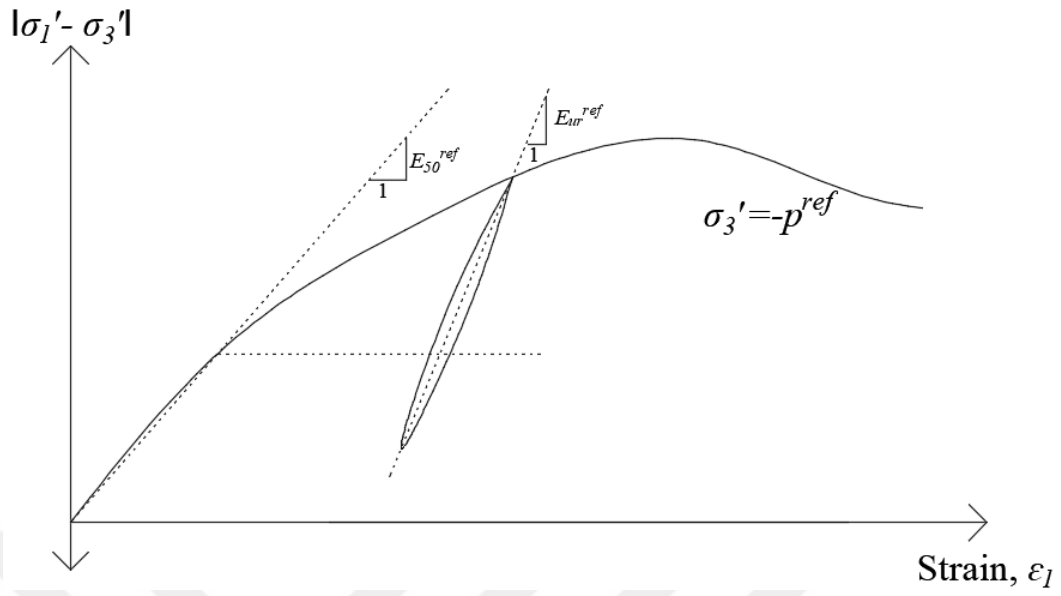


Figure 3.2. Determination of E_{50}^{ref} and E_{ur}^{ref} values from drained triaxial test results.

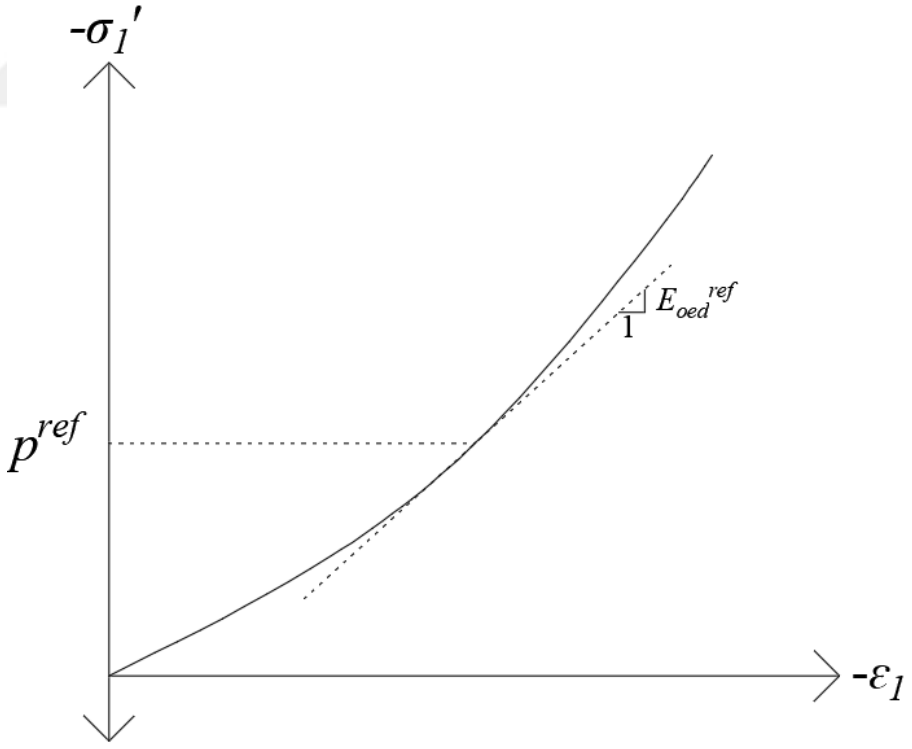


Figure 3.3. Determination of E_{oed}^{ref} value from oedometer test result.

In the HS and HSS models, stress dependency of soil stiffness for oedometer conditions is expressed as,

$$E_{eod} = E_{eod}^{ref} \left(\frac{\sigma}{p^{ref}}\right)^{m}. \quad (3.1)$$

As seen in the expression, stress-dependent stiffness characteristics of the soil is controlled by the power m. This m value is typically considered to be around 1 for clays and varies between 0.5 and 1 for silts and sands (Brinkgreve *et al*., 2021). Another parameter used to simulate plastic yielding of soils is the Failure ratio (R_f) which is the ratio of the ultimate deviatoric stress (q_f), and the asymptotic value of the shear strength (q_a) defined with respect to MC failure criterion. The R_f value is used to limit the deviatoric stress at the threshold where the MC failure criteria is activated. R_f value of 0.9 is set as default in PLAXIS 3D (Brinkgreve *et al*., 2021).

The HS model operates under the assumption that the material behaves elastically when soil experiences unloading and reloading. However, the soil's capacity to experience elastic deformation and fully recover from the applied strain is limited to a very small range (Brinkgreve *et al*., 2021). The HSS model is an adaptation of the HS model, that considers the increased stiffness of soils when subjected to small strains. At low strain levels, the soils generally tend to demonstrate greater rigidity compared to when subjected to engineering strain levels. As shown in Table 3.2, the HS and HSS models are very similar with respect to their constitutive model parameters. In the HSS model two new parameters are introduced, that are the initial small-strain shear modulus (G_0^{ref}) and the shear strain level ($\gamma_{0.7}$) at which the secant shear modulus G_s is reduced to about 70% of G_0^{ref}. These parameters are can be correlated with respect to soils in-situ stress state and void ratio (Brinkgreve *et al*., 2021). G_0^{ref} value can also be calculated as,

$$G_0^{ref} = \frac{E}{2(1+\nu_{ur})} \quad (3.2)$$

by using to small strain Young's modulus (E) and Poisson ratio for unloading-reloading (ν_{ur}) which is suggested as 0.2 by default in PLAXIS 3D. The Second parameter, $\gamma_{0.7}$ value can be expressed as,

$$\gamma_{0.7} = \frac{1}{9\,G_0}[2c'(1+\cos(2\phi')) - \sigma_1'(1+K_0)\sin(2\phi')] \quad (3.3)$$

by using Hardin-Drnevich relationship and the MC failure criterion (Brinkgreve *et al*., 2021).

In the PLAXIS 3D manuals, the HSS model is suggested as one of the best standard constitutive models for modeling over-consolidated clays and sands. HSS model is known to provide reasonable results when it is used to model normally-consolidated clays and undrained loading conditions. Moreover, for slope stability analyses, the HSS model is again recommended as one of the best standard models to be used in determining deformations (Brinkgreve *et al.* 2021). For these reasons, HSS model was selected for clayey and sandy materials used in the models created in this study. This study investigated the short-term stability analysis of clayey slopes that are stabilized with piles. Additionally, in the models, surcharge loads were also introduced. Accordingly, undrained conditions were considered for clays that have low permeability. Undrained conditions can be simulated with two different drainage options in PLAXIS 3D when HSS model is employed. The first option involves using effective stress parameters for stiffness and strength, which is denoted as 'Undrained A'. In this option, undrained shear strength (S_u) is an output calculated by the software with respect to the generated pore pressures and this option is typically recommended for consolidation analyses. The second option requires effective stress parameters for stiffness and undrained strength parameters, which is denoted as 'Undrained B'. In this option, the S_u value is an input parameter, making it more suitable for analyses in cases where effective strength parameters are not available (Brinkgreve *et al*., 2021). In this study, the 'Undrained B' drainage option was employed for clay layers, while the 'Drained' drainage option was utilized for sand layers. The unit weights of the soils were considered as 16 kN/m^3 and 18 kN/m^3 for clay and sand layers, respectively. A summary of the material properties used in this study is provided in Table 3.3.

Table 3.3. Soil properties used in the parametric study.

Soil	S_u **(kPa)**	c' **(kPa)**	ϕ' **(Degree)**	E_{50}^{ref} **(kN/m^2)**	E_{oed}^{ref} **(kN/m^2)**	E_{ur}^{ref} **(kN/m^2)**	ψ **(Degree)**
Clays	25 - 200	-	-	6000-48000	6000-48000	18000-144000	0
Dense Sand	-	1	42	70000	70000	210000	12

3.2.2. Modeling of Piles

PLAXIS 3D offers various options for modeling piles. The suitability of these options depends on the nature of the problem and volume pile (VP) option is considered to be the best choice for the simulation row of piles under lateral soil movement condition (Brinkgreve *et al.* 2021). For this reason, volume piles with interface elements were used to model the slope stabilizing piles in this study. Additionally, the structural capacity of the of the reinforced concrete piles were evaluated in the parametric study by comparing linear-elastic pile (LEP) and elasto-plastic pile (EPP) material modeling approaches. In the LEP approach, the Elastic Modulus (E) of the pile was assumed as 30 GPa. In the EPP approach, Mohr-Coulomb (MC) constitutive model parameters were assigned for reinforced concrete elements. In the EPP model, a macroscopic reinforced concrete material approach proposed by Gerolymos *et al.* (2014) was adopted for the piles. This approach was called macroscopic because reinforcement details and concrete volumes are considered as one uniform element. In this approach, a MC-based uniaxial stress-strain constitutive model was employed to simulate the response of circular reinforced concrete elements under the influence of both bending moments (M) and axial forces (N). The model considered two equilibrium equations. The first equation considers force equilibrium in the axial direction with respect to the axial load and the pile cross-sectional area, this equation is expressed as,

$$\left(\sigma_c - \frac{4\,N}{\pi\,D^2}\right) A_c = \left(\sigma_t - \frac{4\,N}{\pi\,D^2}\right) A_t. \tag{3.4}$$

In this expression, the area of the reinforced concrete section under compressive stresses (A_c) and tensile stresses (A_t) formulated with respect abscissa of the neutral axis (x_0) are computed as,

$$A_c = \int_0^{x_0} 2\sqrt{x\,(D-x)}dx, \text{ and} \tag{3.5}$$

$$A_t = \int_{x_0}^{D} 2\sqrt{x\,(D-x)}dx. \tag{3.6}$$

The second equation represents the moment limit equilibrium at the center of the pile section, that can be written as,

$$M = \sigma_c \int_0^{x_0} 2\sqrt{x(D-x)}\,(x_0 - x)dx + \sigma_t \int_{x_0}^{D} 2\sqrt{x(D-x)}\,(x_0 - x)dx + \left(\frac{D}{2} - x_0\right) N. \tag{3.7}$$

These equations were utilized to derive the MC parameters based on the conditions of structural failure under bending moments and axial forces. M-N failure envelopes, friction angle (ϕ), cohesion intercept (c), pile diameter (D), pile reinforcement ratio (R_{rf}), and abscissa of the neutral axis (x_0) are unknown parameters that should satisfy the two equilibrium equations. For a given pile diameter and reinforcement ratio, Gerolymos *et al.* (2014) obtained M-N failure envelopes using a fiber analysis tool, and the next step of their study was to find the best fit of parameters for a predefined M-N failure envelope by minimizing the relative root mean squared error of the bending moment at the point of failure. Equations were solved by Gerolymos *et al.* (2014), by employing a genetic algorithm-driven optimization approach implemented in MATLAB and ϕ, c, and x_0 parameters were obtained for various pile diameters and reinforcement ratios. Then the model was adjusted to Tresca criterion by setting the compressive strength in the force equilibrium to $\sigma_c = 2c$ and equating the tensile strength to the tension cut-off.

The main advantages of this approach are its simplicity and direct applicability to bending moment-based failure in the context of the studied pile-slope problem. Moreover, the accuracy of the model can be manually verified by monitoring whether the increase in F_s approaches zero as the maximum bending moment in the piles approaches the ultimate bending moment capacity of the selected pile section. A summary of the material properties, corresponding to C30 concrete, used in each pile modeling approach is presented in Table 3.4.

Table 3.4. Pile material properties (adopted from Gerolymos *et al.,* 2014).

Pile model	**E (gPa)**	**v**	**c (kPa)**	**ϕ (Degree)**	**σ_t (kPa)**
Linear- elastic pile	30	0.2	-	-	-
Elasto-plastic pile	30	0.2	15262	0	7534

3.2.3. Modeling of Interfaces

Interfaces are surface elements that are composed of 12-nodes. Each face of the interface surface can be connected to the 6-noded triangular soil elements. Thus, interface elements enable the simulation of complex soil-structure interactions between volume elements or other structural elements in PLAXIS 3D. Interfaces are also used to control the

amount of stresses transferred between soil and structural elements by introducing an interface strength reduction factor (R_{inter}). While a R_{inter} value of one (1) corresponds complete contact and stress transfer (*i.e.,* rigid contact) between soil and structural elements, a low R_{inter} value (*i.e.,* 0.01) corresponds to almost no friction between the same elements.

Piles in this study were modeled using volume elements with interfaces. Interface elements were placed around the pile and at its base to allow the formation of gaps between the volume piles and the surrounding soil. Skin friction coefficients between soils and construction materials proposed by Potyondy (1961) were used to determine R_{inter} values. For the interaction between the soil and concrete surfaces, R_{inter} value was chosen as 0.6 for clay layers and 0.9 for the dense sand layers.

3.3. Boundary Conditions

Boundary conditions that are preset in PLAXIS 3D were utilized. Vertical model boundaries parallel to the yz plane were fixed in x direction (*i.e.,* $u_x = 0$) and free in y and z direction. Vertical model boundaries parallel to the xz plane were fixed in y direction (*i.e.,* $u_y = 0$) and free in x and z directions. Boundary at the bottom of the model was fixed in all directions (*i.e.,* $u_x = u_y = u_z = 0$) and the top surface is free in all directions ($u_x = u_y = u_z = 0$). (Brinkgreve *et al.*, 2021).

3.4. Model Dimensions and Extrusion Depth Sensitivity

In this study, undrained clay over dense sand soil profile was considered. Geometry of the analyzed slope is shown in Figure 3.4. As it can be seen from the figure, slope height and slope angle parameters were selected to be variables in the 2D cross section. The distance between the surcharge load and the slope model boundary at the left side, was selected as three (3) times of the surcharge width (B) to eliminate the boundary effects on F_s (Keleşoğlu, 2015). The same approach was used to determine the length between the toe of the slope and the model boundary at the right side. Pile socket length is selected to be in the 27- 32% range of the total pile length to ensure that the pile is socketed in the stable dense sand layer. The thickness of the dense sand layer was selected within the range of 4 to 6 times the pile socket length to prevent potential boundary effects.

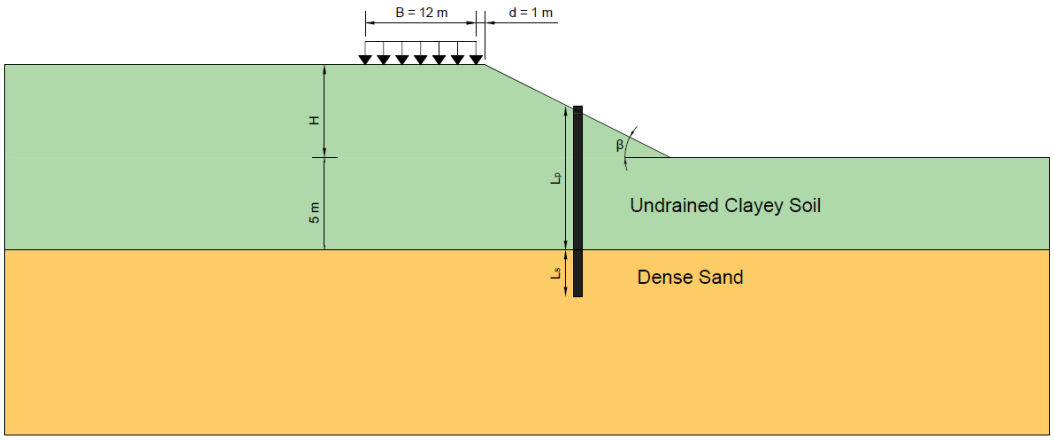


Figure 3.4. 2D geometry of the analyzed pile-stabilized slopes.

For the pile-stabilized slope problem without surcharge loading, the slope was modeled as representative slice model with three (3) equally-spaced piles as demonstrated in Figure 3.5. Preliminary studies demonstrated that the simple slice model was effective in capturing the soil arching behavior for unloaded slope cases. Additionally, the results showed that the depth of extrusion did not influence the deformation and stability analysis results as the conditions are similar to plane-strain deformations. So, the extrusion depth of these cases was selected based on the respective pile spacing of the studied case.

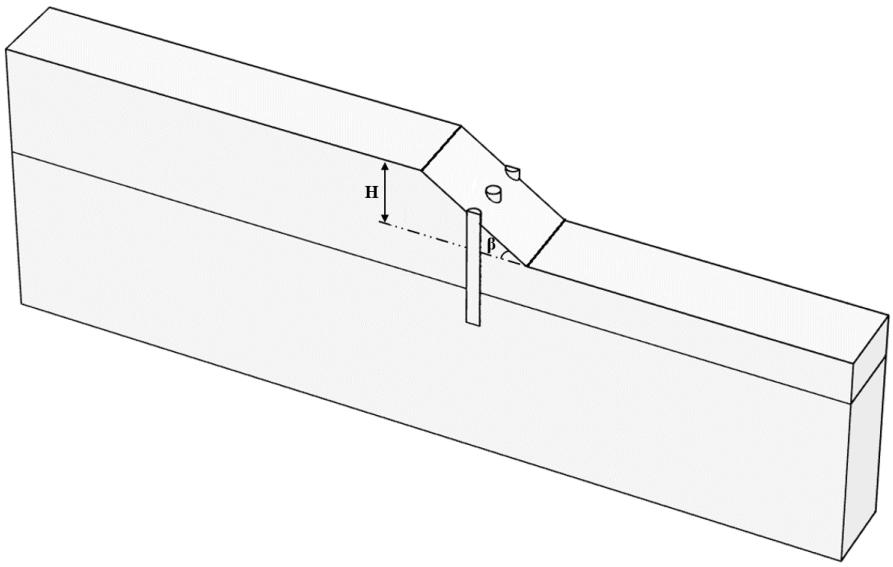


Figure 3.5. 3D geometry of the analyzed pile-stabilized slopes.

In order to capture the 3D failure mechanism induced by the surcharge loads, pile-stabilized loaded slope was modeled using the complete geometry of the problem. Surcharge magnitude was selected as 100 kPa and a 12 m by 24 m rectangular surcharge load was placed 1 m away from the slope crest. 3D geometry of the analyzed pile-stabilized loaded slopes is shown in Figure 3.6.

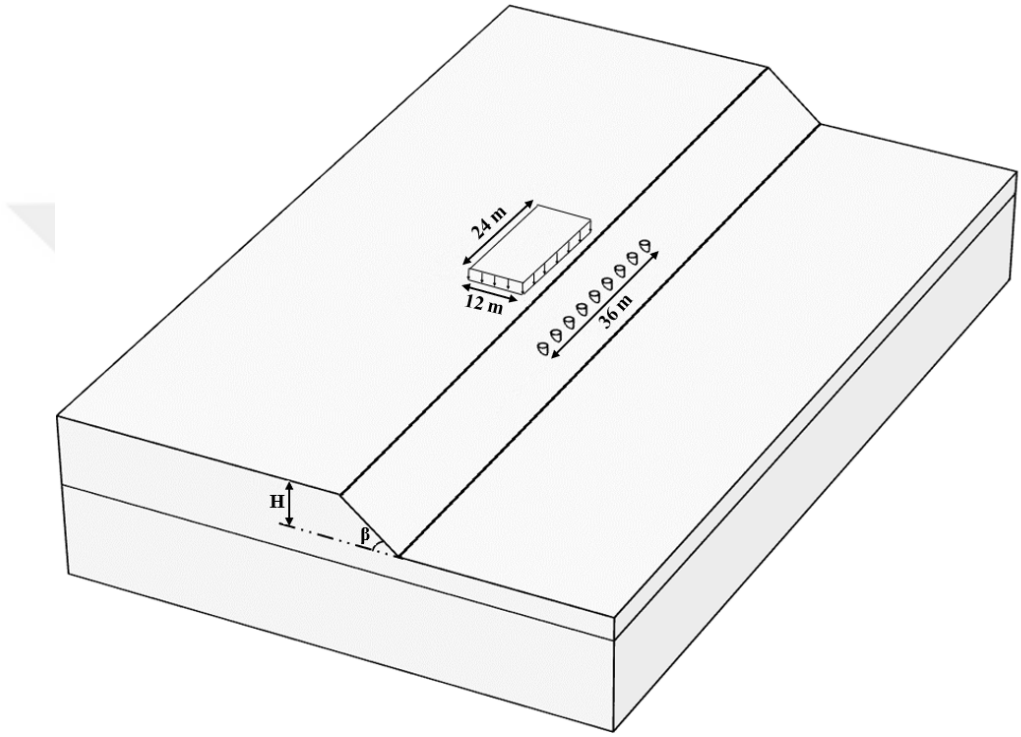


Figure 3.6. 3D geometry of the analyzed pile-stabilized loaded slopes.

A sensitivity analysis was conducted to determine the extrusion depth of the full model. Four extreme model geometries were used in this analysis: *(1)* shortest slope with lowest slope angle, *(2)* highest slope with lowest slope angle, *(3)* shortest slope with highest slope angle, and *(4)* highest slope with highest slope angle. In the analysis, the pile material was selected as elasto-plastic pile and the S/D ratio was selected as four (4). In all of the cases, pile diameter of 1.5 m was used, and the piles were placed on the middle of the slope. Three extrusion depths, 60 m, 150 m and 250 m were considered in the analysis. F_s of the slope, pile head displacement, applied maximum pile shear stress and applied maximum pile bending moment outputs are used to determine the effect of different extrusion depths on various slope models. Deformation and stability analysis results are presented in Table 3.5

and Table 3.6, respectively. Based on Table 3.5, no significant difference was observed in pile internal forces and head displacements between cases with 150 m and 250 m extrusion depths. Similar results were observed in F_s values presented in Table 3.6. Based on the sensitivity analysis results, the extrusion depth of 150 m was deemed sufficient to eliminate boundary effects.

Table 3.5. The effect of extrusion depth on the deformation analysis results.

Extrusion Depth (m)	**Center Pile Head Displacement U_x (cm)**	**Center Pile Max Shear Force (kN)**	**Center Pile Max Bending Moment (kNm)**
β=26.6°, H=5 m, S_u=35 kPa, S/D=4			
60	5.7	669	2045
150	5.7	673	2026
250	5.6	662	2005
β=26.6°, H=15 m, S_u=50 kPa, S/D=4			
60	5.3	939	2662
150	4.6	819	2371
250	4.6	827	2364
β=63.4°, H=5 m, S_u=50 kPa, S/D=4			
60	5.3	621	2048
150	5.2	602	1981
250	5.2	606	1992
β=63.4°, H=15 m, S_u=75 kPa, S/D=4			
60	6.8	822	3614
150	6.7	805	3536
250	6.7	800	3541

Table 3.6. The effect of extrusion depth on the F_s.

Case	**Extrusion Depth (m)**		
	60	**150**	**250**
β=26.6°, H=5 m, S_u=35 kPa, S/D=4	1.381	1.380	1.380
β=26.6°, H=15 m, S_u=50 kPa, S/D=4	1.317	1.337	1.345
β=63.4°, H=5 m, S_u=50 kPa, S/D=4	1.533	1.531	1.532
β=63.4°, H=15 m, S_u=75 kPa, S/D=4	1.333	1.347	1.347

3.5. Mesh Generation and Mesh Density Sensitivity

The distribution and density of the mesh elements have a significant effect on the outputs of the FE analysis (Tschuchnigg *et al.*, 2015). In the process of generating a mesh in PLAXIS 3D, the initial step involves the computation of the model's diagonal length (L_d) with respect to its dimensions across the X, Y, and Z directions. Then, the user selects a unitless relative element size factor (r_e) for the entire model based on the refinement requirements of the analysis. To illustrate, r_e value of two (2) corresponds to a very coarse mesh, r_e value of 1.5 corresponds to a coarse mesh, r_e value of one (1) corresponds to a medium mesh, r_e value of 0.7 corresponds to a fine mesh and, r_e value of 0.5 corresponds to a very fine mesh in PLAXIS 3D (Brinkgreve *et al.*, 2021). Typically, medium or fine mesh options are used in these types of analyses. Then, the target element size (l_e) of the model is calculated using the expression, $l_e = r_e \times 0.05 \times L_d$ (Brinkgreve *et al.*, 2021).

The calculated l_e is unique to each model's geometry. Then the element size of each element is calculated by multiplying the l_e with assigned coarseness factors of each element. The coarseness factors are selected based on the need for additional mesh refinement. For example, additional mesh refinement is required around structural elements, loads, and other areas that experience relatively higher displacements. The element size values determine the mesh density of each element in the model.

A sensitivity analysis was conducted to determine the impact of mesh density on both pile-stabilized slope (*i.e.,* slice model) and pile-stabilized loaded slope (*i.e.,* full model) cases. In both models, the cases with the highest and the lowest diagonal lengths were selected from the parametric study to investigate the effect of mesh density in cases with the highest and the lowest target element sizes. In the analysis, the pile material was selected as elasto-plastic pile, the pile diameter of 1.5 m was used, and the piles were placed on the middle of the slope. The models were divided into multiple regions and the mesh was refined in the regions close to the loading area, the piles, and the potential failure plane. Very small coarseness factors were assigned to the pile and soil volumes that experienced relatively higher displacements. The aim of the mesh optimization was to avoid convergence problems and to reduce the computation time. Five relative element size factors (r_e) corresponding to very coarse, coarse, medium, fine, very fine mesh distributions were considered in the

sensitivity analysis. For the pile-stabilized slope cases, piles are only loaded/activated at safety analysis via SRM. Thus, only the F_s values were used for comparison in these cases. For the pile-stabilized loaded slope cases, the surcharge loads at the crest are activated in the loading (deformation phase) and the loads induced by the surcharge are laterally transferred to the pile. Then the safety analysis is conducted using SRM. Accordingly, results from both deformation analysis at the loading phase and safety analysis are presented for these cases. For the pile-stabilized loaded slope cases, maximum pile head displacement and internal pile forces are presented in Table 3.7. In both of the pile-stabilized loaded slope cases, Table 3.7 shows similar pile head displacements for all mesh densities and a gradual increase in internal pile forces with increasing mesh densities. However, the difference between fine and very fine mesh distributions is observed to be relatively small.

Table 3.7. The effect of mesh density on the deformation analysis results.

Mesh Density	**Very Coarse Mesh**	**Coarse Mesh**	**Medium Mesh**	**Fine Mesh**	**Very Fine Mesh**
Smallest Model - β=63.4°, H=5 m, S_u=50 kPa, S/D=4					
# of Elements	29488	40578	72671	145694	335307
Center Pile Head Displacement, U_x (cm)	5.3	5.3	5.2	5.2	5.1
Center Pile Max Shear Force (kN)	475	524	575	602	625
Center Pile Max Bending Moment (kNm)	1462	1658	1852	1981	2093
Largest Model - β=26.6°, H=15 m, S_u=50 kPa, S/D=4					
# of Elements	49120	65122	131742	290468	703666
Center Pile Head Displacement, U_x (cm)	4.4	4.5	4.6	4.6	4.6
Center Pile Max Shear Force (kN)	589	676	760	819	857
Center Pile Max Bending Moment (kNm)	1689	1977	2201	2371	2508

The effect of mesh density on F_s values obtained from safety analysis for pile-stabilized slope and pile-stabilized loaded slope cases, are presented in Figure 3.7 and Figure 3.8, respectively. According to the results, both the smallest and largest models in both cases show a gradual convergence in the F_s value obtained with a very fine mesh distribution.

Given the considerable amount of computational time required for very fine mesh distributions, the differences observed in both deformation and factor of safety analyses between fine and very fine mesh distributions were relatively minor. Therefore, opting for a fine mesh distribution could be a suitable choice for achieving sufficient accuracy. Thus, the fine mesh distribution was deemed sufficient and utilized in parametric study. Typical mesh distribution of the piles and adjacent soil used in the analysis is shown in Figure 3.9. Selected typical mesh distributions for slice and full model are also demonstrated in Figure 3.10 and 3.11, respectively.

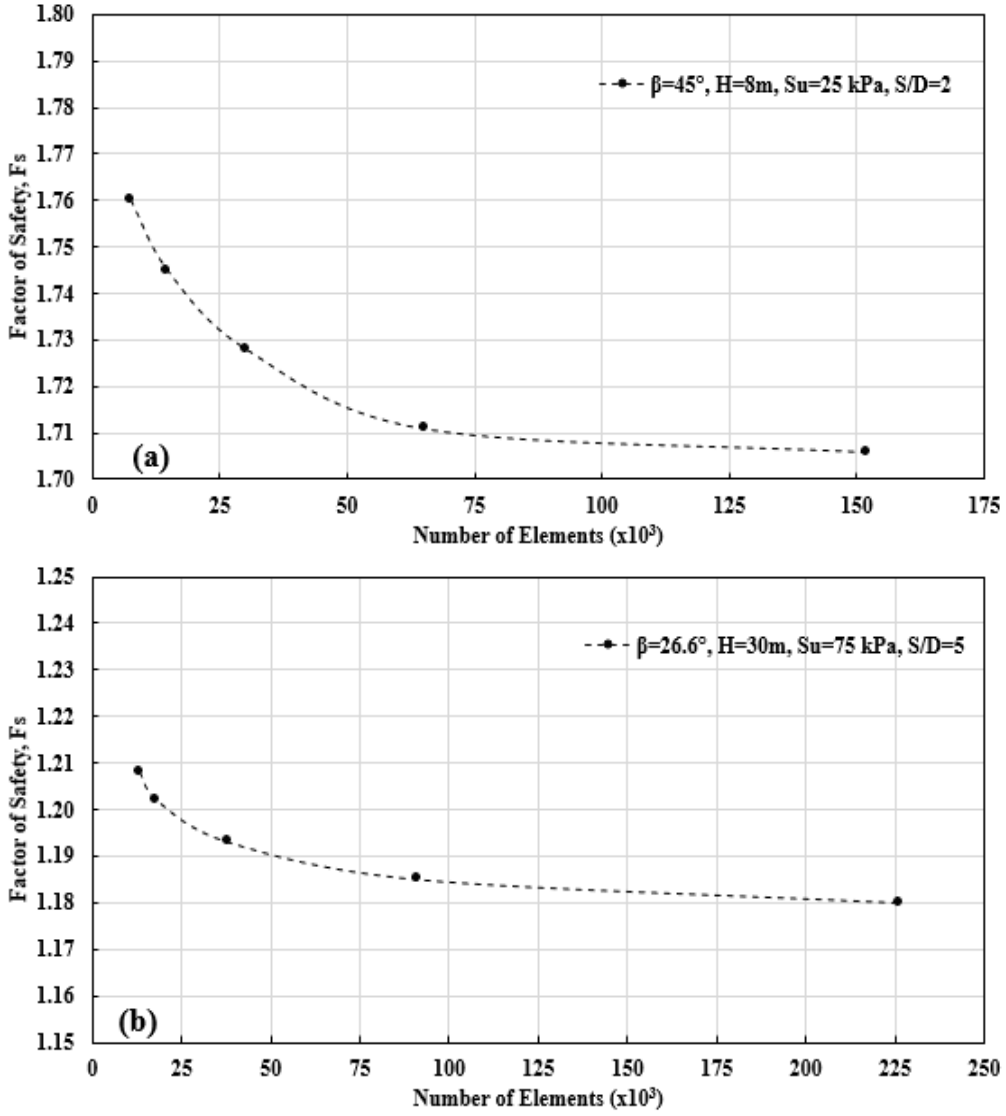


Figure 3.7. The effect of mesh density on the F_s of pile-stabilized slope cases: (a) smallest model, (b) largest model.

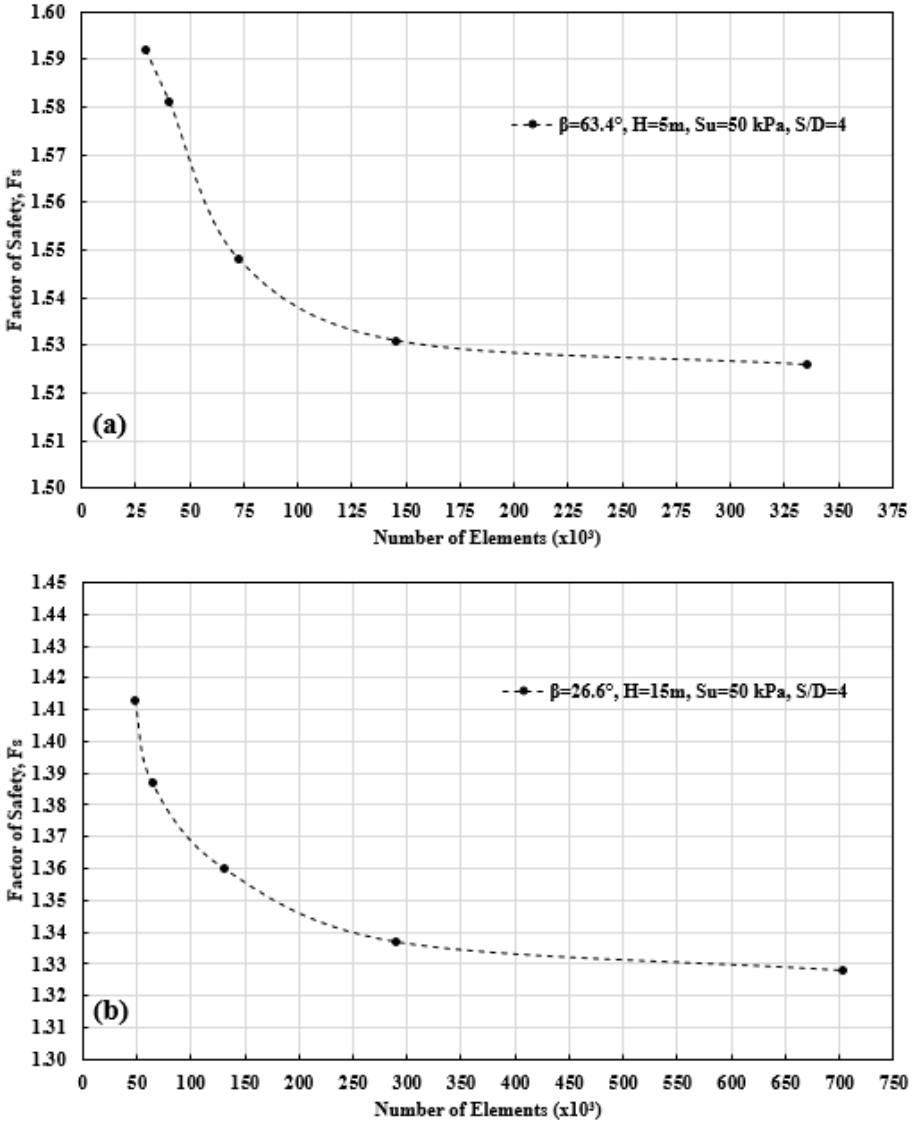


Figure 3.8. The effect of mesh density on the F_s of pile-stabilized loaded slope cases: (a) smallest model, (b) largest model.

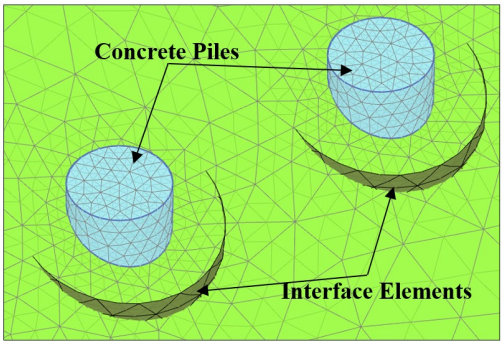


Figure 3.9. Typical mesh distribution of piles and adjacent soil.

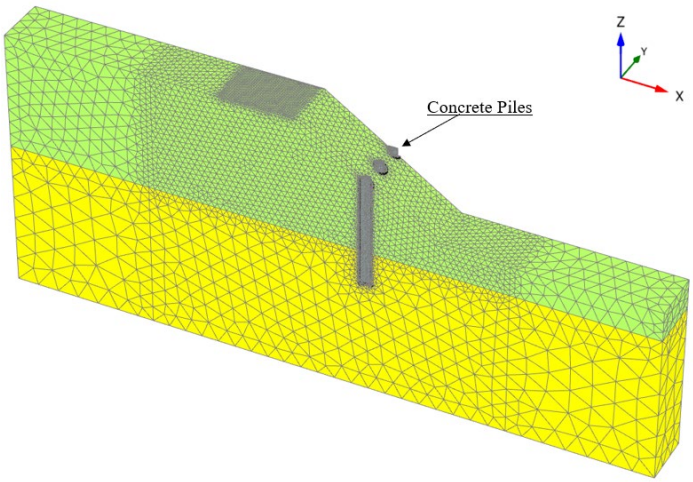


Figure 3.10. Typical mesh distribution of pile-stabilized slopes in slice model.

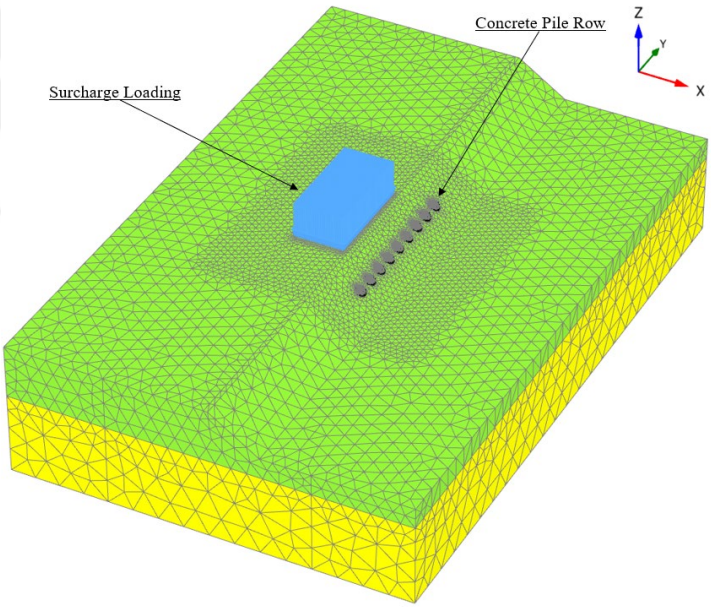


Figure 3.11. Typical mesh distribution of pile-stabilized loaded slopes in full model.

3.6. Initial Loading Conditions and Staged Construction Steps

Slope stability analysis in PLAXIS 3D consists of multiple construction steps that are simulated as plastic deformation phases, followed by a final safety phase where the overall F_s of the slope is determined via the SRM. Time effects are not taken into consideration in deformation or safety phases. First deformation phase is the initial phase where stress field

and pore pressures are calculated. To calculate the initial stress field in nonlevel ground (*i.e.,* slope) conditions, gravity loading option is utilized to calculate equilibrium of forces using the weight of the modeled geometry (Duncan, 1996). After the first phase, calculated displacements are reset to zero. The second phase is the plastic nil phase, which is run without any changes in the model and only used to stabilize any out-of-balance forces that may be present from the initial phase. In the third phase, volume piles and interface elements are activated in the model. Since the effects of pile installation cannot be effectively simulated in 3D FEM at the time of this study, volume piles are assumed to be constructed as 'wished-in place piles'. Displacements calculated during this phase are retained, and the newly generated field conditions are used in the next phase. For the pile-stabilized loaded slope cases an additional deformation step where the surcharge load is activated is also added before the safety phase. For the pile-stabilized slope cases, the final phase is the safety phase. In the safety phase, tan (φ') and c' or S_u values are equally reduced until failure and F_s value is obtained. Staged construction steps for pile-stabilized loaded slope cases are shown in Figure 3.12.

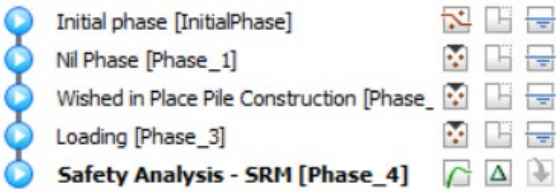


Figure 3.12. Staged construction steps for pile-stabilized loaded slope cases.

3.7. Selection of Cases for Stabilization and Summary of Cases

Parameter ranges used in the analysis for the pile stabilized slopes cases with and without surcharge loads are presented in the Table 3.8 below. Initial case selection was performed using an LE based slope stability analysis software Slide 2D (Rocscience Inc., 2023). A total of 210 slopes were analyzed, considering without and with surcharge load cases and the corresponding F_s values were recorded. Based on the recorded F_s values, slopes that were deemed feasible to be stabilized with piles (*i.e.,* $F_{s\text{-}3D\ FEM} \approx 1$ to 1.3) were selected for parametric study. This preliminary analysis was performed to decrease the number of 3D FE cases and to mainly focus on critical slopes that actually require stabilization. F_s of natural slopes was assumed to be greater than 1 (*i.e.,* stable) when no loading is present. When the

F_s of a slope reduces to a value below 1 due to surcharge loads, significant displacements occur. In such cases, our preliminary analysis results indicated that that stabilizing the slope with piles is not an efficient solution. Therefore, slope cases with initial F_s values in the 1 to 1.3 range were selected for stabilization using piles in 3D FE analysis of both unloaded (natural) and loaded slope cases.

Table 3.8. The parameter ranges used for the case selection of pile-stabilized slopes.

Slope Angle (Degree)	**Slope Height (m)**	**S_u (kPa)**	**Surcharge Magnitude (kPa)**
26.6 to 63.4	5 to 30	25 to 200	0 and 100

Before starting the parametric study, a comparative analysis was performed on two unloaded (natural) slope cases to investigate the effect of pile material selection, either linear-elastic pile (LEP) or elastoplastic pile (EPP) on the results. Based on the results of these cases, EPP model was utilized in the rest of the parametric study.

A total of 18 unloaded (natural) slope cases were selected for pile stabilization and a slice model of each case was prepared in 3D FE software. A total of 16 cases of loaded slopes were selected for pile stabilization and a full model of each case was prepared in 3D FE software. For the pile-stabilized slope cases, S/D ratio was selected in the 2-5 range. For the pile-stabilized loaded slope cases, S/D ratio was selected as 2, 3 and 4 for all cases. Pile head condition was free in the parametric study. In all of the cases, a pile diameter of 1.5 m was utilized to account for the high bending moment values that may occur due to deep-seated failures and the piles were positioned at the midpoint of the slope.

Additionally, one slope case was analyzed at the end of the parametric study to investigate the effect of constrained pile head movement on the results. A volume element as a cap beam with 1.7 m x 1.7 m dimensions was included to achieve the constrained pile head condition. The beam connected all pile heads to each other and allowed only a limited movement in comparison to piles with free head.

The cases analyzed considering a row of piles placed in the middle of the slope height are summarized in Table 3.9. Models were prepared and analyses were carried out using the parameters provided in Table 3.9. A total of 80 slopes cases were analyzed using the slice

model and 51 cases were analyzed using the full model in PLAXIS 3D. Internal pile forces and pile head displacements were then recorded from the deformation analysis step. F_s values and observed failure mechanisms were recorded from safety phase for each case for comparison purposes.

Table 3.9. Selected cases for the parametric study.

Case No	H (m)	β (Degree)	S_u (kPa)	F_s (3D FEM)	S/D Ratio	Pile Model	Pile Head Condition
Pile-stabilized slope cases							
A-1	8	26.6	25	1.18	2, 3, 4 and 5	EPP	Free
A-2	8	33.7	25	1.11	2, 3, 4 and 5	EPP	Free
A-3	8	45	25	1.04	2, 3, 4 and 5	LEP and EPP	Free
A-4	15	26.6	45	1.20	2, 3, 4 and 5	EPP	Free
A-5	15	33.7	50	1.22	2, 3, 4 and 5	EPP	Free
A-6	15	45	50	1.12	2, 3, 4 and 5	LEP and EPP	Free
A-7	20	45	75	1.27	2, 3, 4 and 5	EPP	Free
A-8	20	56.3	75	1.15	2, 3, 4 and 5	EPP	Free
A-9	20	63.4	75	1.05	2, 3, 4 and 5	EPP	Free
A-10	25	26.6	75	1.26	2, 3, 4 and 5	EPP	Free
A-11	25	33.7	75	1.14	2, 3, 4 and 5	EPP	Free
A-12	25	45	75	1.02	2, 3, 4 and 5	EPP	Free
A-13	25	56.3	100	1.22	2, 3, 4 and 5	EPP	Free
A-14	25	63.4	100	1.13	2, 3, 4 and 5	EPP	Free
A-15	30	26.6	75	1.08	2, 3, 4 and 5	EPP	Free
A-16	30	33.7	100	1.27	2, 3, 4 and 5	EPP	Free
A-17	30	45	100	1.14	2, 3, 4 and 5	EPP	Free
A-18	30	56.3	100	1.01	2, 3, 4 and 5	EPP	Free
Pile-stabilized loaded slope cases							
B-1	5	26.6	35	1.22	2, 3 and 4	EPP	Free
B-2	5	33.7	35	1.14	2, 3 and 4	EPP	Free
B-3	5	45	35	1.04	2, 3 and 4	EPP	Free
B-4	5	56.3	35	1.00	2, 3 and 4	EPP	Free
B-5	5	63.4	50	1.24	2, 3 and 4	EPP	Free
B-6	8	26.6	35	1.11	2, 3 and 4	EPP	Free
B-7	8	33.7	35	1.02	2, 3 and 4	EPP	Free
B-8	8	45	50	1.26	2, 3 and 4	EPP	Free
B-9	8	56.3	50	1.14	2, 3 and 4	EPP	Free
B-10	8	63.4	50	1.07	2, 3 and 4	EPP	Free
B-11	10	26.6	35	1.05	2, 3 and 4	EPP	Free
B-12	10	45	50	1.18	2, 3 and 4	EPP	Free
B-13	10	56.3	50	1.06	2, 3 and 4	EPP	Free and constrained
B-14	10	63.4	50	1.01	2, 3 and 4	EPP	Free
B-15	15	26.6	50	1.28	2, 3 and 4	EPP	Free
B-16	15	63.4	75	1.23	2, 3 and 4	EPP	Free

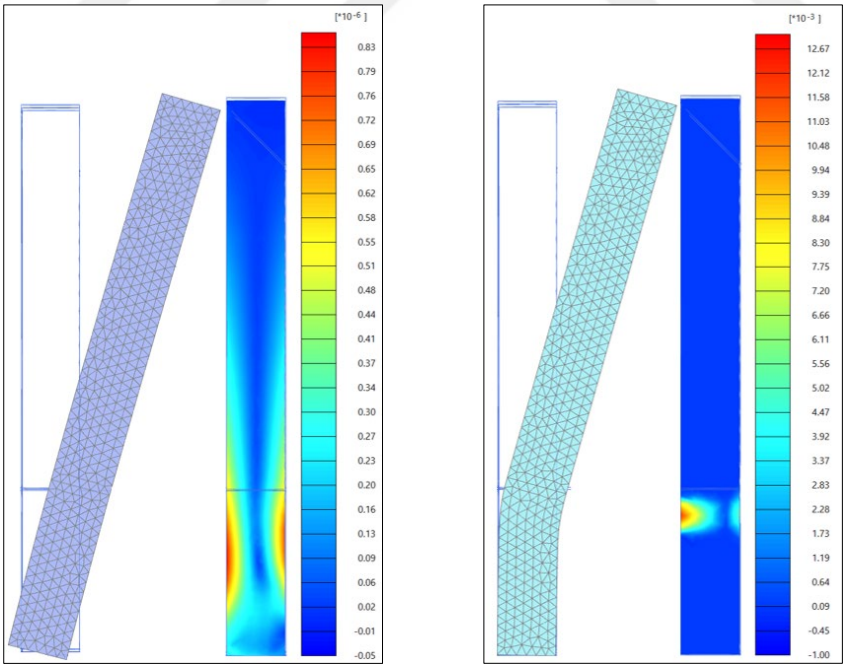
4. RESULTS AND DISCUSSION

In this chapter, typical failure modes of the pile-slope systems are presented, and the effects of slope geometry, pile spacing, soil arching and pile cap beam on the results are discussed. In all the loaded slope cases presented in this chapter, a 12 m by 24 m rectangular surcharge load with a magnitude of 100 kPa was placed 1 m away from the slope crest.

4.1. Effect of Pile Material Model on Coupled Failure Modes

Exaggerated deformed mesh outputs and incremental shear strain contours of β=45°, H=8 m, S_u=25 kPa, S/D=4 case considering LEP and EPP pile models are given in Figures 4.1a and 4.1b, respectively. As it can be seen in Figure 4.1a, the LEP approach showed no shear strain concentration along the piles to indicate structural failure at the end of the safety analysis. In this approach the piles never reached structural failure, and consequently short pile mode (SPM), defined by Poulos (1995), was observed. However, a deeper failure mechanism developing along the length of the piles is likely for a failure mode that allows the failure of the pile. Accordingly, the shear strain and deformation behavior observed in Figure 4.1a, that corresponds to an unlimited bending capacity, is rather unlikely. As shown with the shear strain concentration zones in Figure 4.1b, a single plastic hinge developed in the EPP model at the interface between clay and dense sand layer, and accordingly long pile mode (LPM), defined by Poulos (1995), was observed. EPP approach was capable of capturing the critical slope stability failure mode that resulted from the failure of the pile. Additionally, the accuracy of the EPP model in terms of structural capacity was verified by monitoring the increases in the F_s values and the maximum bending moments in the piles. The ultimate bending moment capacity of the reinforced concrete pile section with a diameter of 1.5 m was approximately estimated as 7250 kNm based on M-N failure envelopes presented by Gerolymos *et al.* (2014). In the EPP models, the increase in F_s approached to zero when the maximum bending moment in piles approached the ultimate bending moment capacity of the selected pile section. For two (2) slope conditions with four (4) different S/D ratios, F_s values obtained from the analysis performed with EPP models were compared with those ran with LEP models in Table 4.1. Factor of safety of the original slope prior to stabilization (F_{s0}) values are also provided in Table 4.1. In the β=45°, H=8 m,

S/D=2 case, the loads transferred onto the piles were below the structural capacity of the pile. As it can be seen in Table 4.1, both pile models for this case yielded similar F_s values. For other S/D ratios for the same case, pile structural capacity was exceeded in the safety analysis and the F_s values gradually decreased with the increase in S/D ratio. In these cases, when the structural capacity of the pile was exceeded, significant differences were observed in F_s values of the cases employing the LEP model and those employing the EPP model. For the slope case with β=45° and H=15 m, F_s values were observed to be quite different from each other for various S/D ratios. The analysis results indicated much lower F_s values for the cases of EPP model compared to those utilized the LEP model. The effect of pile model on F_s was observed to be more pronounced in cases with a high overestimation ratio ($M_{Max-LEP}$ / $M_{Max-EPP}$) of maximum pile bending moments from the safety analysis. These results suggest that use of elasto-plastic piles in coupled safety analysis of pile-stabilized slopes is required to model soil-structure interaction correctly and to eliminate the over estimation of the F_s values. Thus, EPP model was utilized in the rest of the parametric study performed in this study.



(a) (b)

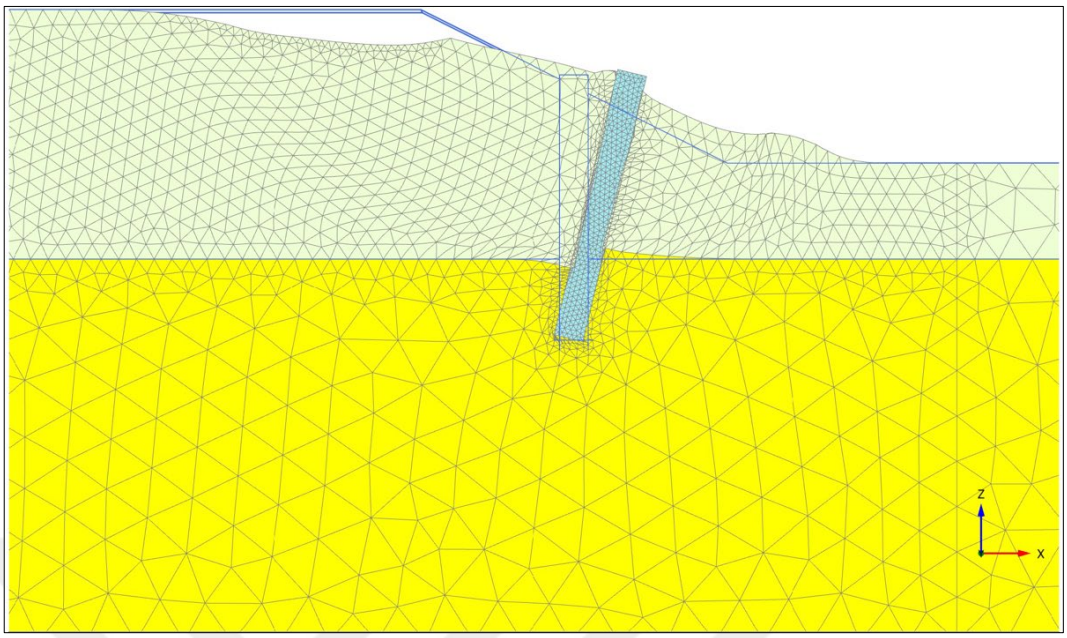
Figure 4.1. Exaggerated deformed mesh outputs (left) and incremental shear strain contours (right) of piles from safety analysis for the pile-stabilized slope case with β=45°, H=8 m, S_u=25 kPa, S/D=4: (a) LEP model, (b) EPP model.

Table 4.1. F_s of the cases analyzed with linear-elastic and elasto-plastic pile models.

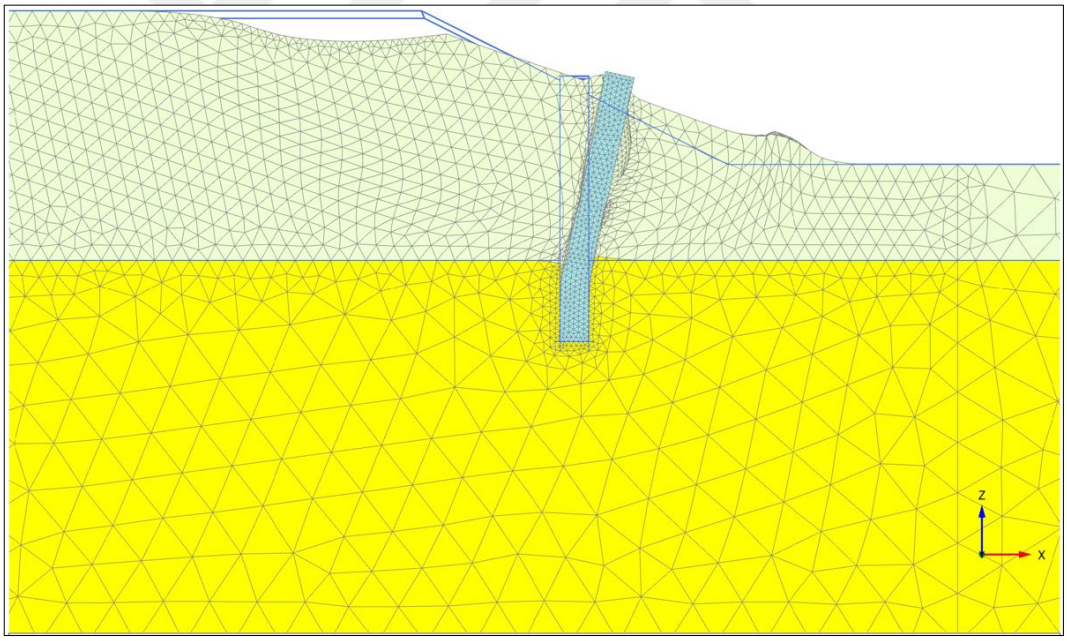
Case	S/D Ratio	Pile Failure Mode	F_s		$M_{Max\text{-}LE}$ / $M_{Max\text{-}EP}$
			LEP	EPP	
β=45°, H=8 m, S_u=25 kPa, F_{so}=1.04	2	SPM	1.71	1.71	1.0
	3	LPM	1.59	1.54	1.1
	4	LPM	1.46	1.39	1.3
	5	LPM	1.37	1.31	1.4
β=45°, H=15 m, S_u=50 kPa, F_{so}=1.12	2	LPM	1.61	1.43	1.7
	3	LPM	1.55	1.34	2.4
	4	LPM	1.48	1.29	3.0
	5	LPM	1.45	1.26	3.8

4.2. Types of Failure Modes in Pile-stabilized Slope Cases

For the pile-stabilized slope cases, piles were only loaded/activated at the safety phase via SRM. Thus, only the results from the safety analysis are presented for these cases. Figure 4.2 demonstrates the two typical failure modes obtained from the pile-stabilized slope cases where no surcharge load is present. Figure 4.2a shows the case with S/D=2 pile configuration. In this case the structural capacity of the pile was not reached, and a rotational movement was observed along the piles. Figure 4.2b shows the case with S/D=5 pile configuration. For this case of rather spaced, unfavorable pile spacing, the structural capacity of the pile was reached. The development of a plastic hinge was observed at the clay-sand interface, at the socket depth. These two main types of pile failure modes and deep-seated slope failures were observed in all of the pile-stabilized unloaded (natural) slope cases studied in this parametric study.



(a)

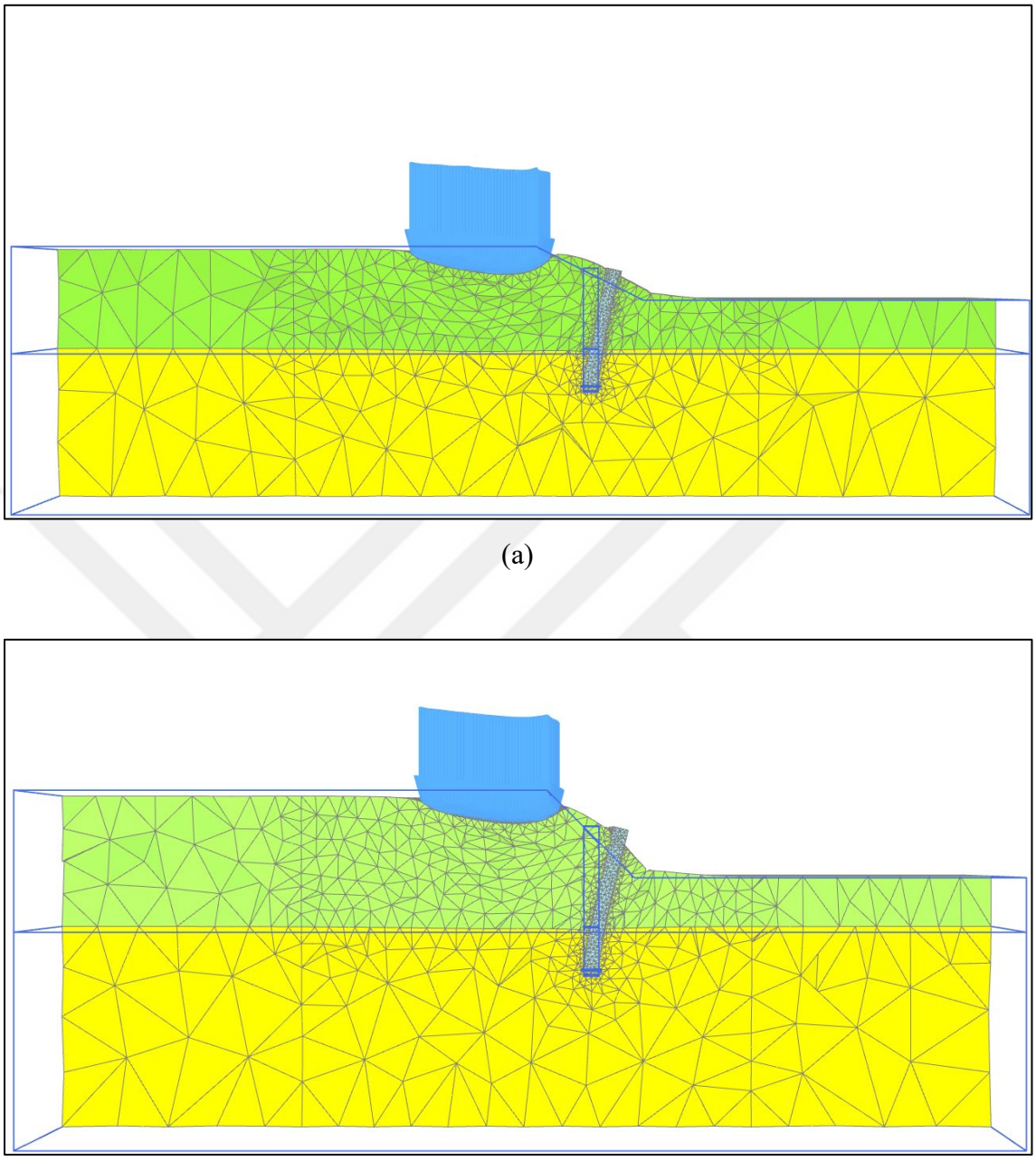


(b)

Figure 4.2. Deformed mesh outputs (cross section view) from safety analysis for the pile-stabilized slope case with β=26.6°, H=8 m, S_u=25 kPa: (a) S/D=2, (b) S/D=5.

4.3. Types of Failure Modes in Pile-stabilized Loaded Slope Cases

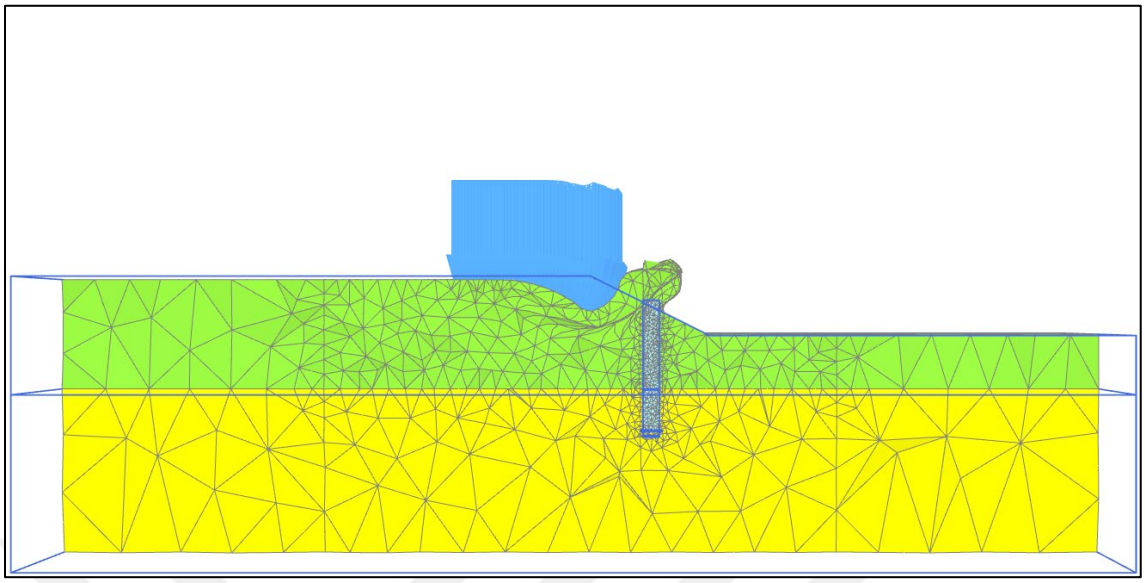
For the pile-stabilized loaded slope cases, the surcharge loads at the crest were activated in the loading (*i.e.,* deformation phase) and then the loads were laterally transferred onto the piles. Then, the safety analysis was conducted via SRM. Accordingly, results from both the deformation analysis at the loading phase and the safety analysis are presented for these cases. Figure 4.3a and Figure 4.3b show the deformations induced by surcharge loads for two different slope conditions with different pile failure modes at the safety phase. As it can be seen from the figures, coupled deformation mechanism of the surcharge loaded pile-slope system was similar in both of these cases. The structural capacity of the piles was not reached, and a rotational movement was observed along the piles. Deep seated soil movement was observed in both cases. Figure 4.4a and Figure 4.4b show the two different typical failure modes obtained from the pile-stabilized loaded slope cases. In Figure 4.4a, the structural capacity of the piles was not reached, and failure mechanism was limited to the upper section of the slope between the loading and the piles, this failure mode was defined as an upper slope failure (USF) in the context of this study. In Figure 4.4b, the structural capacity of the piles was reached, and a deep-seated failure mechanism (DSF) was observed. Definitions of these typical failure mechanisms as USF and DSF were found useful for interpreting the results obtained for various slope geometries and pile spacing values.



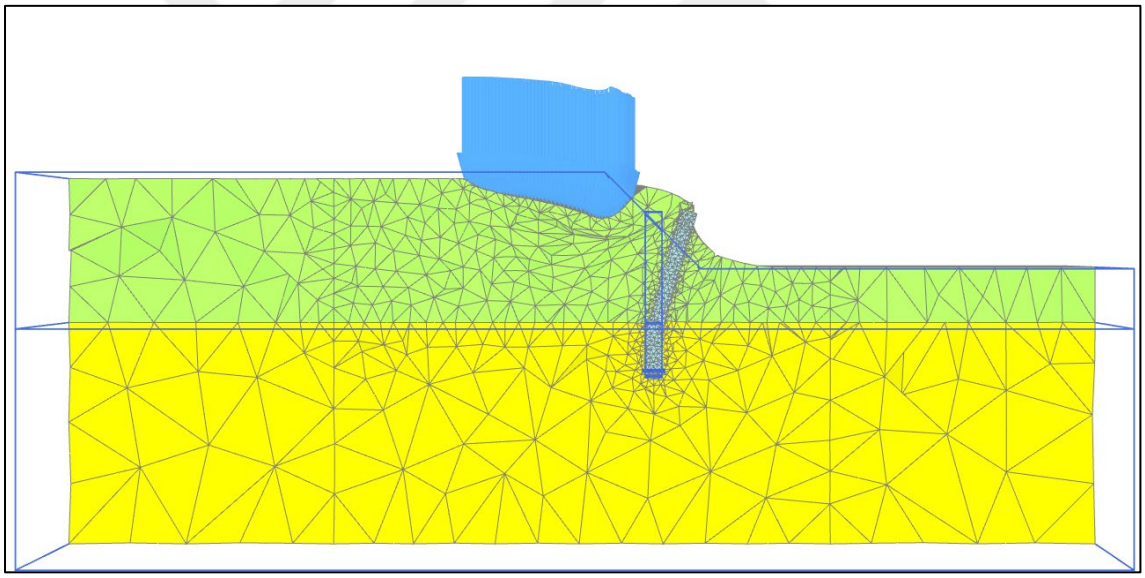
(a)

(b)

Figure 4.3. Exaggerated deformed mesh outputs (cross section view) from the deformation analysis at the loading phase for the pile-stabilized loaded slope cases: (a) β=26.6°, H=5 m, S_u=35 kPa, S/D=2, (b) β=45°, H=8 m, S_u=50 kPa, S/D=2.



(a)



(b)

Figure 4.4. Exaggerated deformed mesh outputs (cross section view) from the safety analysis for the pile-stabilized loaded slope cases: (a) β=26.6°, H=5 m, S_u=35 kPa, S/D=2, SPM, (b) β=45°, H=8 m, S_u=50 kPa, S/D=2, LPM.

4.4. Effect of Pile Stabilization on Slope Displacements in Loaded Cases

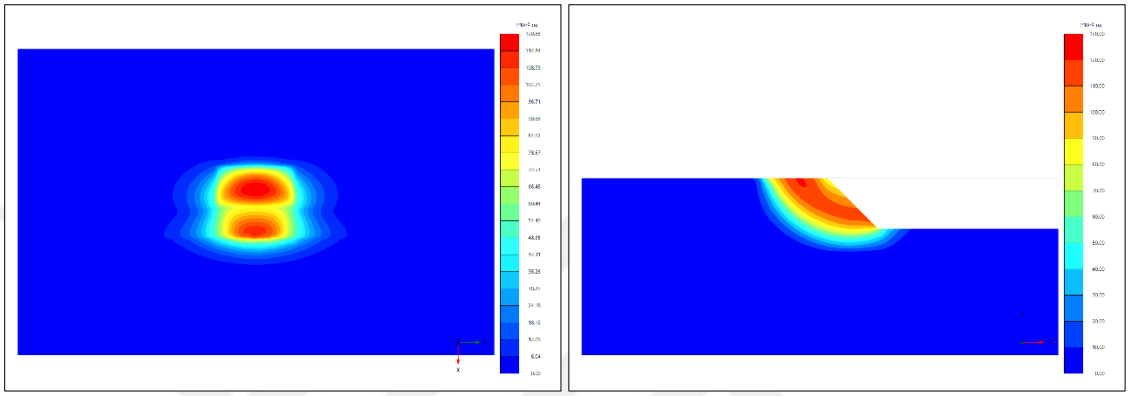
To observe the effect of pile stabilization on F_s and failure surfaces, β=45°, H=10m, S_u=50 kPa, S/D=2 case was examined to compare unstabilized loaded slopes and pile-stabilized loaded slopes. The results of the deformation analysis at the loading phase and safety analysis pertaining to this selected case are summarized in Table 4.2. Lateral displacements at the crest and toe of the slope and the vertical displacements caused by the surcharge loading were used to compare the unstabilized and pile-stabilized cases. As it can be seen from the table, the lateral and vertical displacements caused by the surcharge loading decreased significantly when the slope was stabilized with piles before the application of the surcharge load. This clearly shows the positive effect of stabilization. In the safety analysis, the surcharge load reduced the F_s of the natural slope by 0.5 (*i.e.*, ΔF_s =0.5), and the stabilization with piles could only restore 0.25 (*i.e.*, ΔF_s =0.25). However, the final F_s of the pile-stabilized slope was over 1.3, so the stabilization using the piles in this case can be considered sufficient.

Table 4.2. Results of deformation analysis at the loading phase and the F_s of the case with β=45°, H=10 m, S_u=50 kPa, S/D=2.

β=45°, H=10 m, S_u=50 kPa, S/D=2 Case	**Deformation Analysis at The Loading Phase**			**Safety Analysis**
	Vertical displacement at the center of the loading U_z (cm)	Slope crest lateral displacement at the center of the loading U_x (cm)	Slope toe lateral displacement at the center of the loading U_x (cm)	F_s
Before stabilization and loading	-	-	-	1.68
After loading without stabilization	10.7	6.0	6.7	1.18
After loading with stabilization	7.6	4.4	3.9	1.43

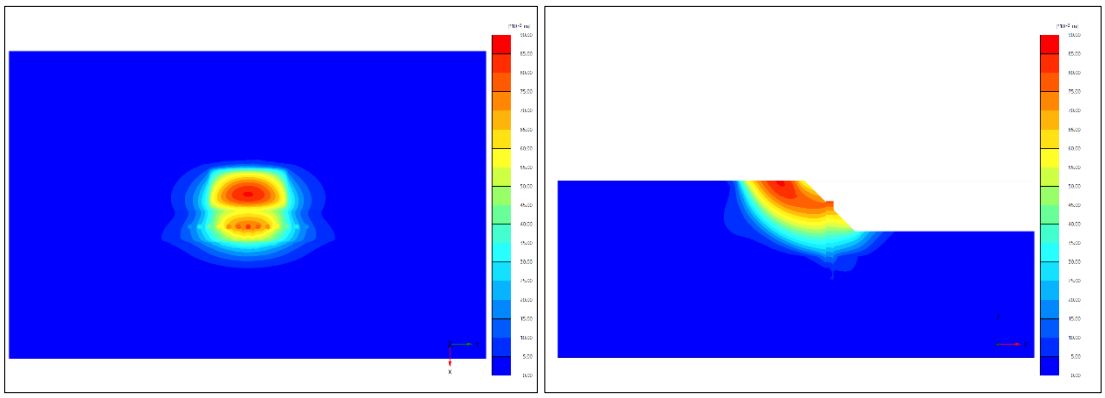
Total displacements obtained from the deformation analysis are shown in Figures 4.5 and 4.6. As it can be seen from the top and cross section views of the unstabilized and pile-stabilized slopes, piles caused a significant reduction in the magnitude of displacements. Significant displacements were confined in the upper section of the slope between the

loading and the piles. This effectively prevented the advancement of the displacements that could potentially lead to the development of a deep-seated failure surface. A similar behavior was observed in the results of the safety analysis shown in Figures 4.7 to 4.8. Similar improvements through pile stabilization were also observed in other studied cases, as discussed here.



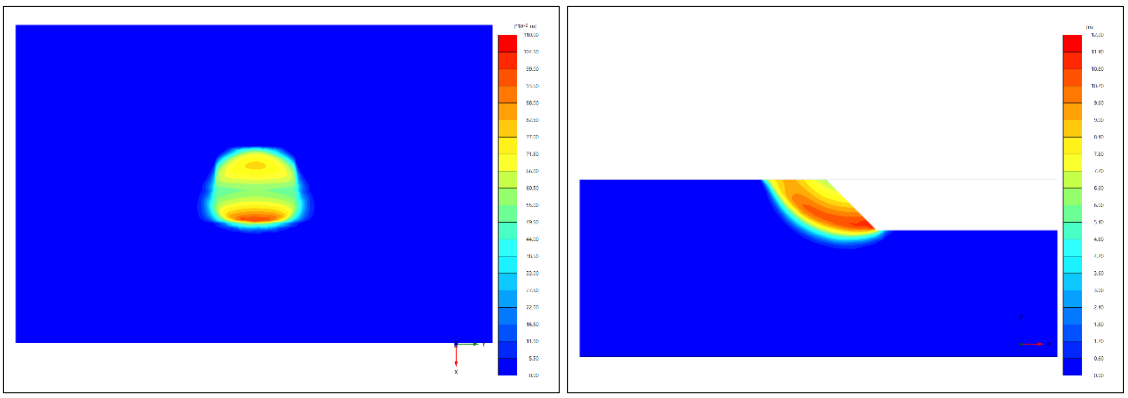
(a) (b)

Figure 4.5. Total displacements of the unstabilized slope from deformation analysis at the loading phase for the case with β=45°, H=10 m, S_u=50 kPa (a) plan view, (b) cross-section view.



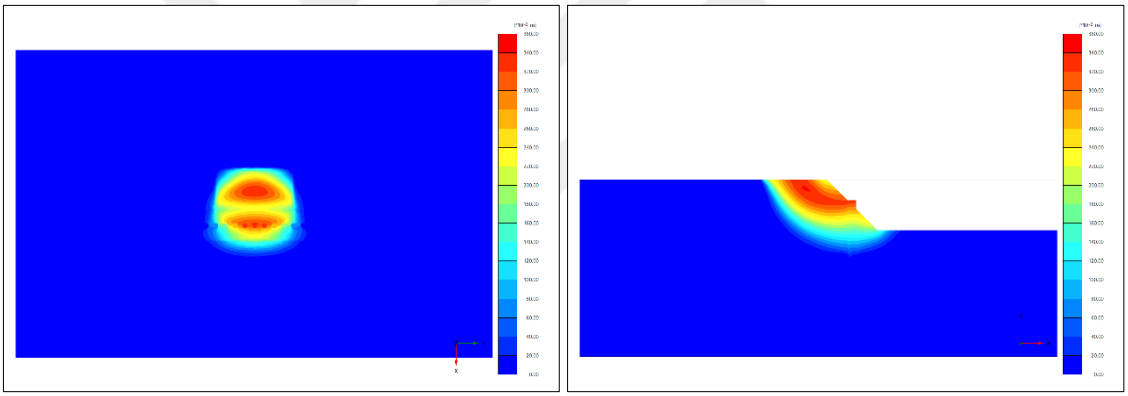
(a) (b)

Figure 4.6. Total displacements of the pile-stabilized slope from deformation analysis at the loading phase for the case with β=45°, H=10 m, S_u=50 kPa (a) plan view, (b) cross-section view.



(a) (b)

Figure 4.7. Incremental displacements of the unstabilized slope from safety analysis for the case with β=45°, H=10 m, S_u=50 kPa: (a) plan view, (b) cross-section view.



(a) (b)

Figure 4.8. Incremental displacements of the pile-stabilized slope from safety analysis for the case with β=45°, H=10 m, S_u=50 kPa, S/D=2: (a) plan view, (b) cross-section view.

4.5. Effects of Slope Geometry on Normalized F_s of Pile-stabilized Slopes

Figure 4.9a and 4.9b show the plot of normalized F_s values with respect to a range of H and β values for pile-stabilized slope cases with S/D=2 and S/D=5 pile configurations, respectively. F_s values were normalized by multiplying them with atmospheric pressure (*i.e.*, p_a=100 kPa) and then dividing them by their respective S_u values to obtain a unitless F_s value to compare various cases. This approach was applicable due to the linear correlation observed between S_u and F_s in pile-stabilized slope and pile-stabilized loaded slope cases.

As seen in Figure 4.9a, highest normalized F_s values were observed in H=8 m cases. SPM was the prevalent pile behavior for H=8 m, S/D=2 cases due to the close pile spacing and gentle H. This also resulted in relatively higher F_s values compared to the cases with higher slopes. As expected, normalized F_s values gradually reduces with the increase in H and β in all cases. Additionally, increase in H was found to be more influential on normalized F_s values than the increase in β. Except for the cases with H=8 m (as noted in Figure 4.9a as SPM), LPM was the dominant pile behavior, highlighting the importance of using EPP models in the coupled analysis of pile-stabilized slopes. Similar results were obtained for the cases with S/D=5 pile configuration, as shown in Figure 4.9b.

Figure 4.10a and 4.10b show the variation of normalized F_s with respect to a range of H and β values for pile-stabilized loaded slope cases considering S/D=2 and S/D=4 pile configurations, respectively. As it can be seen in Figure 4.10a, similar to the unloaded slopes (*i.e.,* slopes without surcharge loads), highest normalized F_s values were observed in cases with lower H values. SPM was observed in all H=5 m cases and since the piles did not reach their structural capacity, most critical failure surfaces were contained within the upper slope section between the loading and the piles, as previously defined as USF in Section 4.3. USF was not observed in cases with H values greater than 8 m or in some cases with relatively larger S/D ratios (*see* Figure 4.10b). This is because of the fact that piles go through structural failure in these cases due to relatively unfavorable loading conditions. Similarly, a gradual decrease was observed in normalized F_s values with the increase in H and β in loaded cases. The effect of the increase in H on the normalized F_s was more prominent than the effect of the increase in β. Additionally, wider, and deeper failure shapes were observed for high slopes and effect of surcharge on F_s was significantly lower in these cases compared to that of lower H values. It is important to note that, in the cases of higher slopes, the effect of the self-weight of the slope material was more significant in determining the failure shape than the effect surcharge. To illustrate this, Figure 4.11a depicts the local failure shape observed in the slope case with β=26.6° and H=5 m. On the other hand, in Figure 4.11b, depicts a failure shape that is similar to the plane strain conditions in the slope case with β=26.6° and H=15 m. Consequently, for the H=15 m case, the improvement in F_s due to local pile stabilization is mostly capped by the natural F_s of the slope prior to any loading or stabilization using piles.

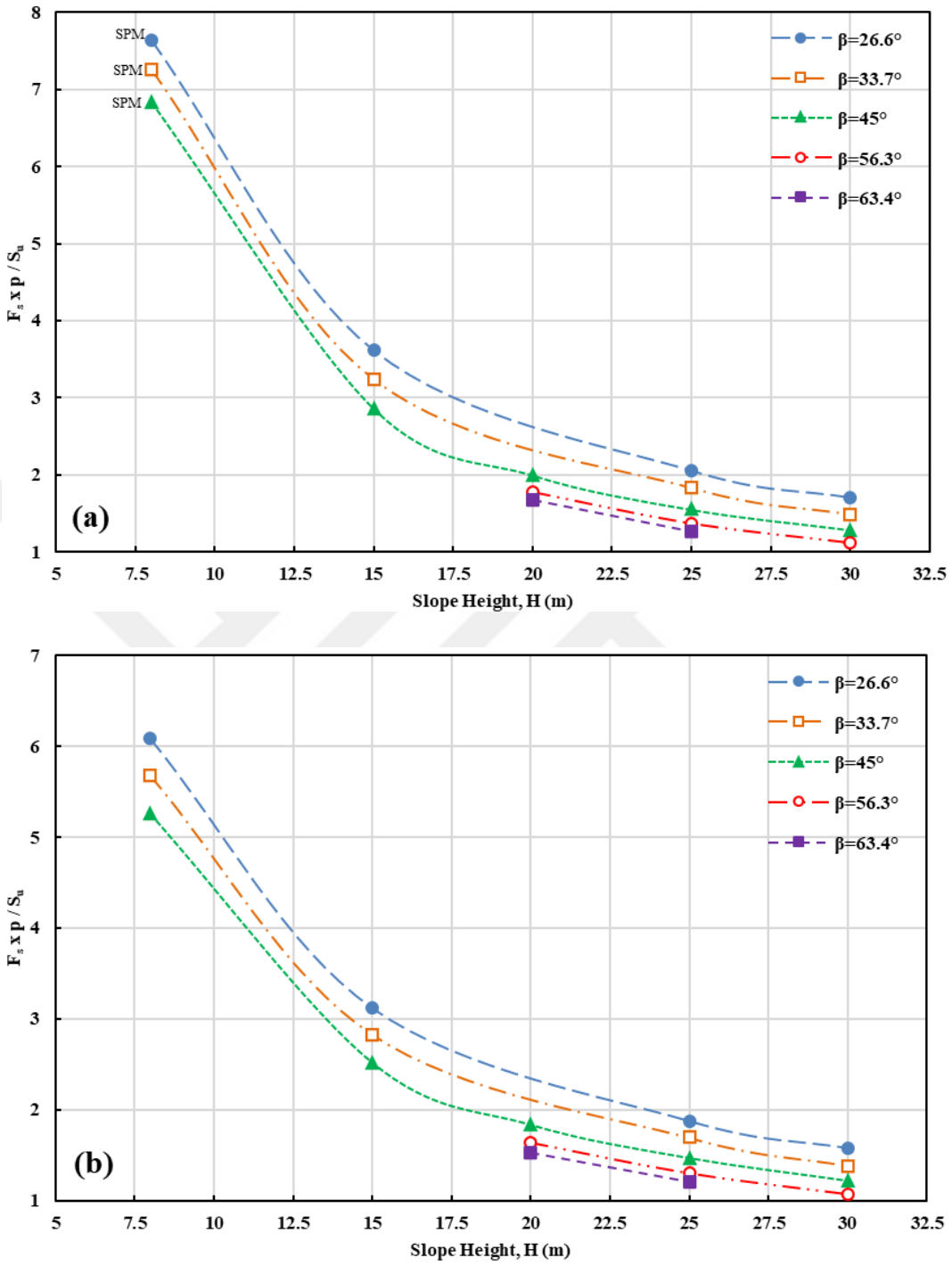


Figure 4.9. Normalized F_s (F_s x p / S_u) with respect to a range of H and β values for pile-stabilized slope cases: (a) S/D=2, (b) S/D=5.

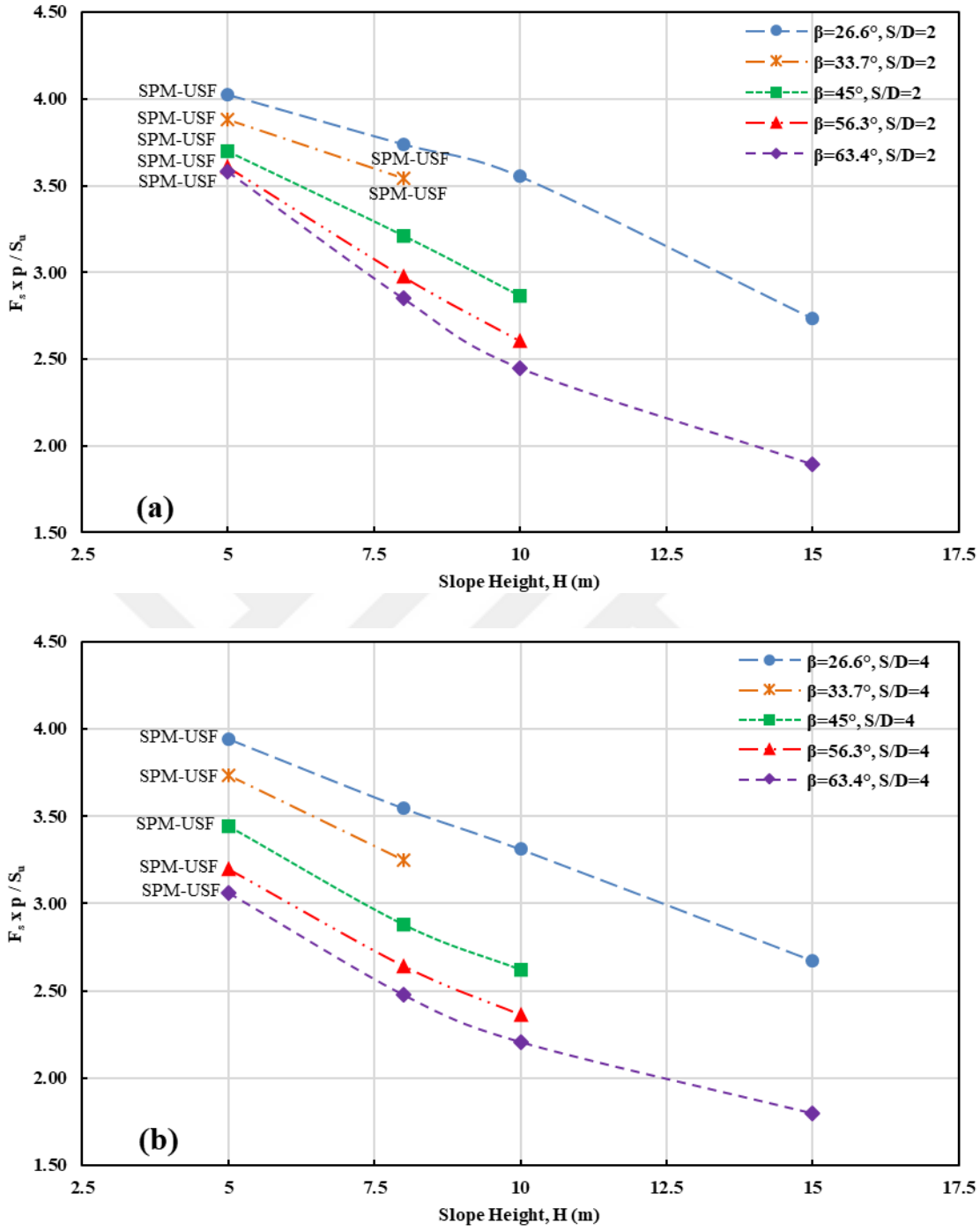
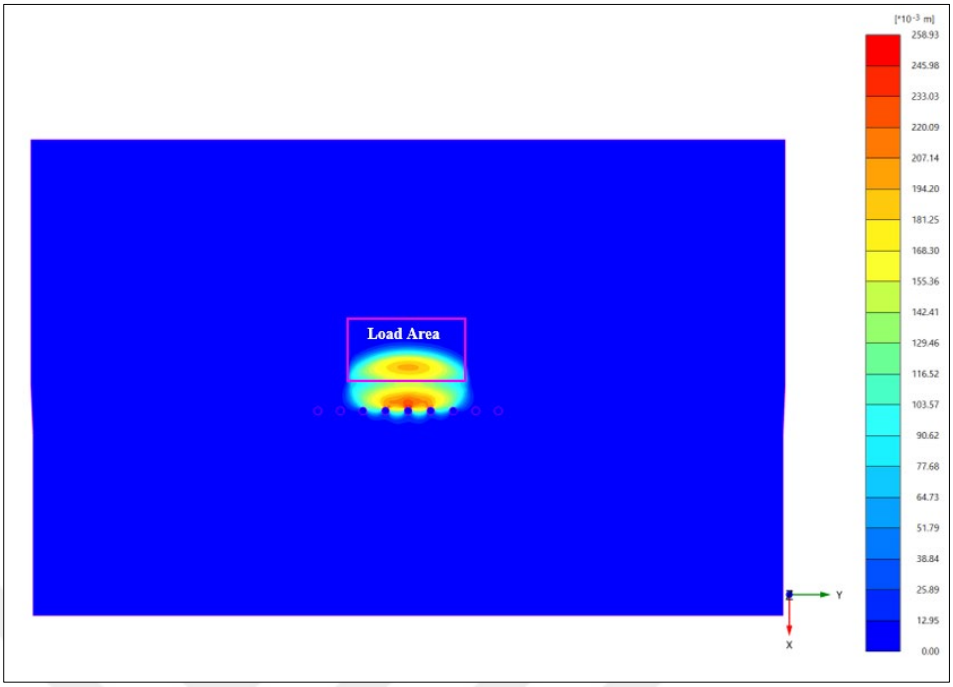
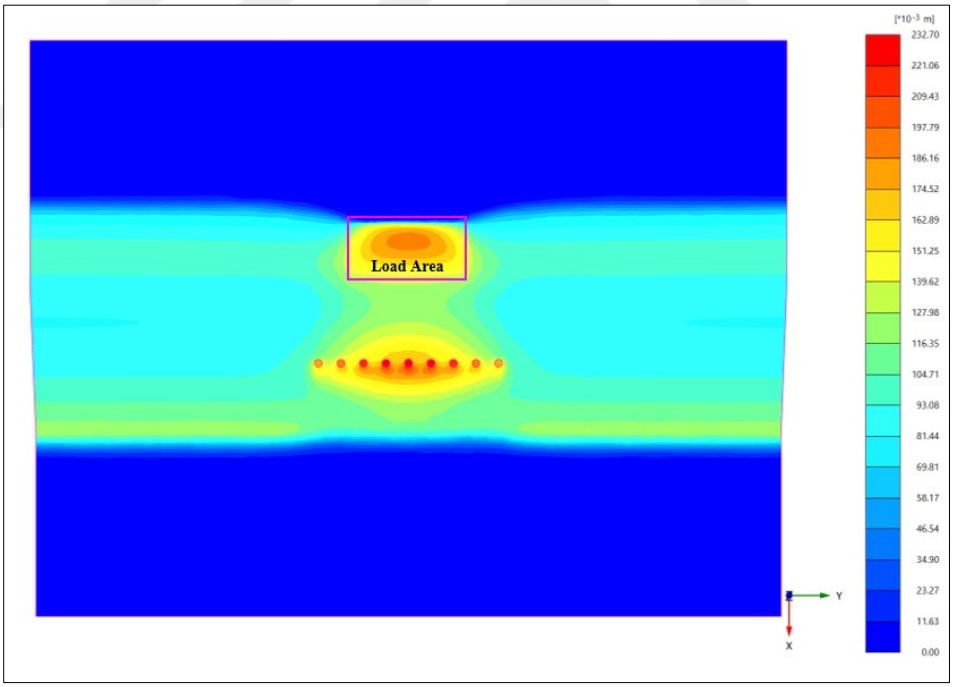


Figure 4.10. Normalized F_s (F_s x p / S_u) with respect to a range of H and β values for pile-stabilized loaded slope cases: (a) S/D=2, (b) S/D=4.



(a)



(b)

Figure 4.11. Plan view of incremental displacements from safety analysis of pile-stabilized loaded slope cases with: (a) β=26.6°, H=5 m, S_u=35 kPa, S/D=3, (b) β=26.6°, H=15 m, S_u=50 kPa, S/D=3.

4.6. Effect of Pile Spacing and Soil Arching on Results

Effect of pile spacing on F_s and internal pile forces are presented in this section along with observed failure mechanisms for various slope geometries. In Figure 4.12a, plot of normalized F_s values for pile-stabilized slope cases with β=45° is shown. The normalized F_s values decrease with the increase in spacing and the effect of S/D ratio is the most prominent in the case with the lowest H. The effect of pile spacing then significantly reduces with the increase in H and this behavior was similar for other β values investigated. In Figure 4.12b, plot of normalized F_s values for pile-stabilized loaded slope cases with lowest (β=26.6°) and highest (β=63.4°) slope angles are presented. LPM-DSF pile-slope failure mode was dominant in most of the cases with exceptions noted in the figures as SPM-USF. Figure 4.12b shows that for slopes with H=5 m, effect of spacing was most pronounced in the steepest slope case of β=63.4°. This can be mainly attributed to the narrow width of this slope (2.5 m from crest to toe) when the β is 63.4°. Considering that the selected pile diameter is 1.5 m and the width is 2.5 m, slope cases with H=5 m and β=63.4°, were significantly over-stabilized compared to the slope cases with same height and gentler slope angles. Additionally, for the loaded cases, while the effect of pile spacing was more distinct in H values of 5 m, 8 m and 10 m, this effect noticeably reduces in cases with H=15 m. This was due to the fact that the effect of surcharge loads becomes less prominent with an increase in H. Accordingly, the piles are less effective in providing resistance to the higher self-weight induced by the increased H. Results suggest that, for high slopes (*i.e,* H ≥15 m), single row of reinforced concrete piles placed in the middle of the slope may not be adequate to provide considerable stabilization in cases with surcharge loads.

The difference between the factor of safety of stabilized slope (F_s) and factor of safety of original slope prior to stabilization (F_{s0}) can be denoted by ΔF_s values. ΔF_s values are useful to quantify the improvement in F_s obtained by pile stabilization. Figure 4.13 demonstrates S/D ratio versus ΔF_s for a range of slope geometries analyzed in pile-stabilized slope cases. Figure 4.13a and Figure 4.13b is presented for pile-stabilized slope cases with H values in the 8-20 m range and 25-30 m range, respectively.

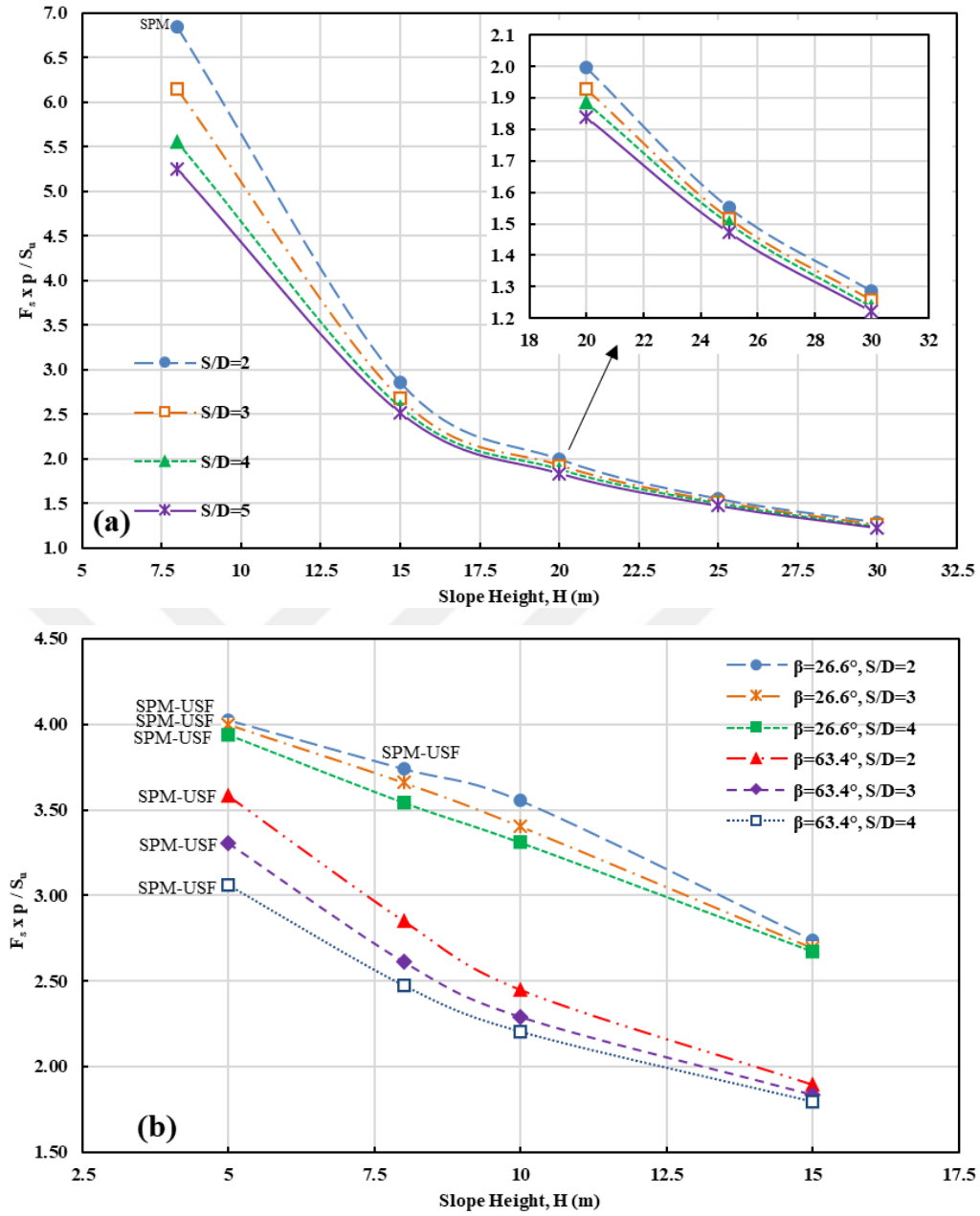


Figure 4.12. Normalized F_s (F_s x p / S_u) with respect to a range of H values and S/D ratios: (a) pile-stabilized slope cases with β=45°, (b) pile-stabilized loaded slope cases with β=26.6° and β=63.4°.

Results indicate that stabilization using piles perform exceptionally well when H is 8 m, and for higher slopes, ΔF_s gradually reduces with the increase in β. Highest improvements (ΔF_s>0.55) were observed in cases where the prevalent pile behavior was SPM. For this reason, selection of smaller pile diameters may be more economic depending on how much improvement is needed for a pile-stabilized slope project. Additionally, it was observed that

the effect of increase in H was more prominent than the increase in β. In this parametric study, the results of the analysis performed on high (*e.g.,* 25 m and 30 m) and steep (*e.g.,* β=56.3° and β=63.4°) slopes, showed that the single row of piles provide only marginal improvements. This also indicated the need for additional row of piles or other solutions to further increase the F_s in these cases.

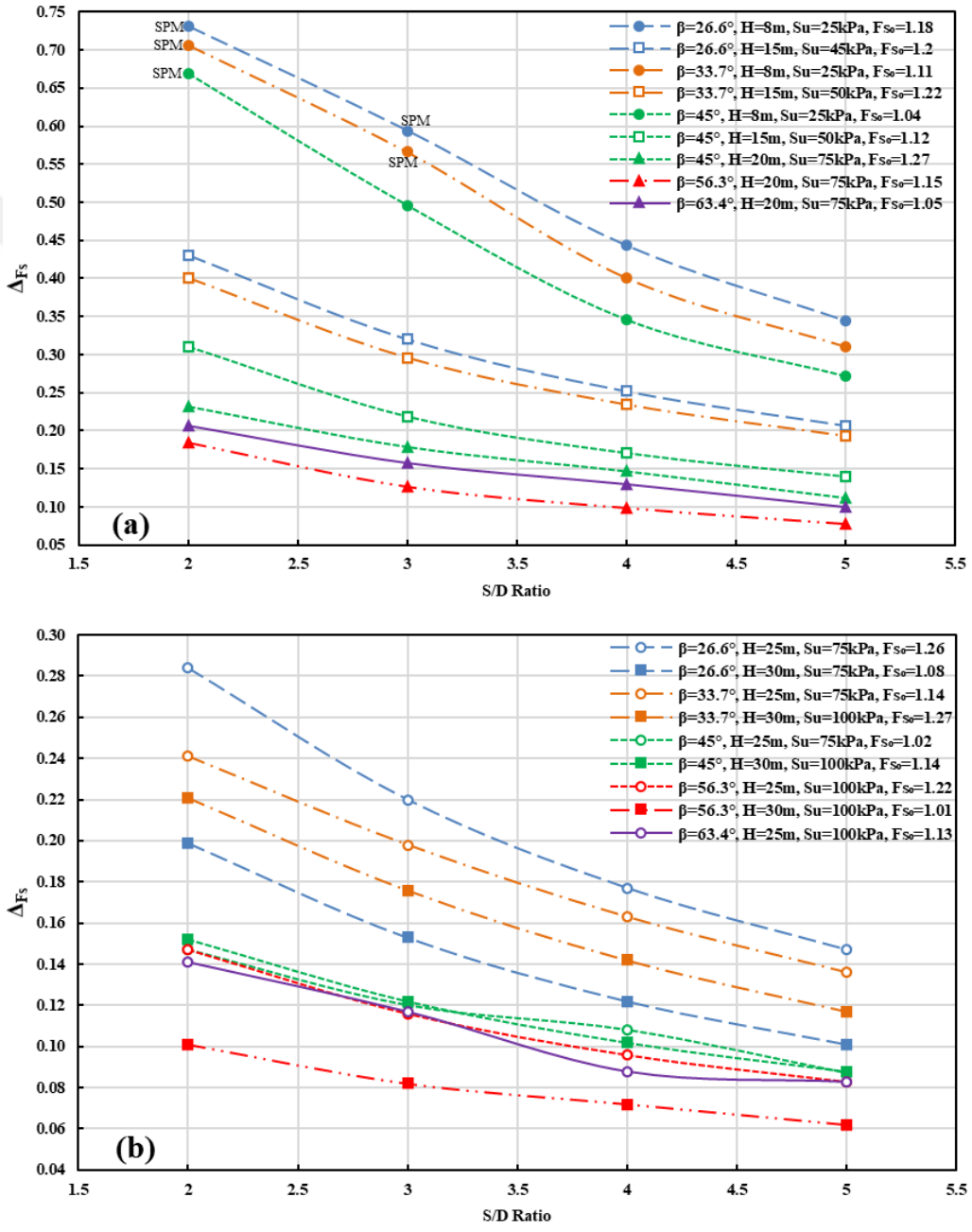


Figure 4.13. S/D ratio versus ΔF_s for a range of for pile-stabilized slope geometries with: (a) H=8-20 m range, (b) H=25-30 m range.

Figure 4.14 shows the S/D ratio versus ΔF_s for a range of slope geometries for pile-stabilized loaded slope cases. In loaded cases, ΔF_s values denote the difference between the factor of safety of stabilized slope (F_s) and factor of safety of loaded slope prior to stabilization (F_{sl}). In Figure 4.14a, results of H=5 m cases are presented. For these cases, SPM-USF was observed in all S/D ratios and β values. Results showed that there is an almost linear decrease in ΔF_s as the pile spacing increases. Additionally, ΔF_s values were found to be directly dependent on S_u of clays which was expected since the lateral resistance supplied by soil behind the piles are proportional to the strength of the soil. Highest improvement was observed in β=63.4° with the highest S_u, as these pile-stabilized steep slopes were significantly more rigid compared to other slopes due to their narrow width (*i.e.,* 2.5 m). Although increase in β creates an unfavorable condition for slopes with same H, higher ΔF_s values were obtained with the increase in β. The cause of this phenomenon was considered to be the geometry of the problem. With the increase in β, the distance between the piles and the surcharge load decreases when the piles are located at the mid height of the slope. These results also suggest that placing the piles closer to the surcharge load in pile-stabilized slopes could be more advantageous. F_{sl} values are also presented in the figure for each case. As can be seen in the slope with β=56.3°, when F_{sl} values were very close to failure conditions (*i.e.,* $F_{sl} \cong 1$), effect of pile spacing was more pronounced and the use of closer pile spacing values seems to be required to obtain adequate stabilization. In Figures 4.14b, 4.15a and 4.15b, results obtained for the remaining H values are presented. For these cases, LPM was dominant in most of the cases with the exceptions noted in the figures. Reduction in ΔF_s was clearly visible with the increase H and it was observed that ΔF_s values reduce even below 0.06 in H=15 m slopes with β=26.6° which shows that single row of piles provides almost negligible improvement to F_s. However, for steeper slopes with the same height and higher S_u values, piles seem to perform reasonably well when local surcharge loads are present.

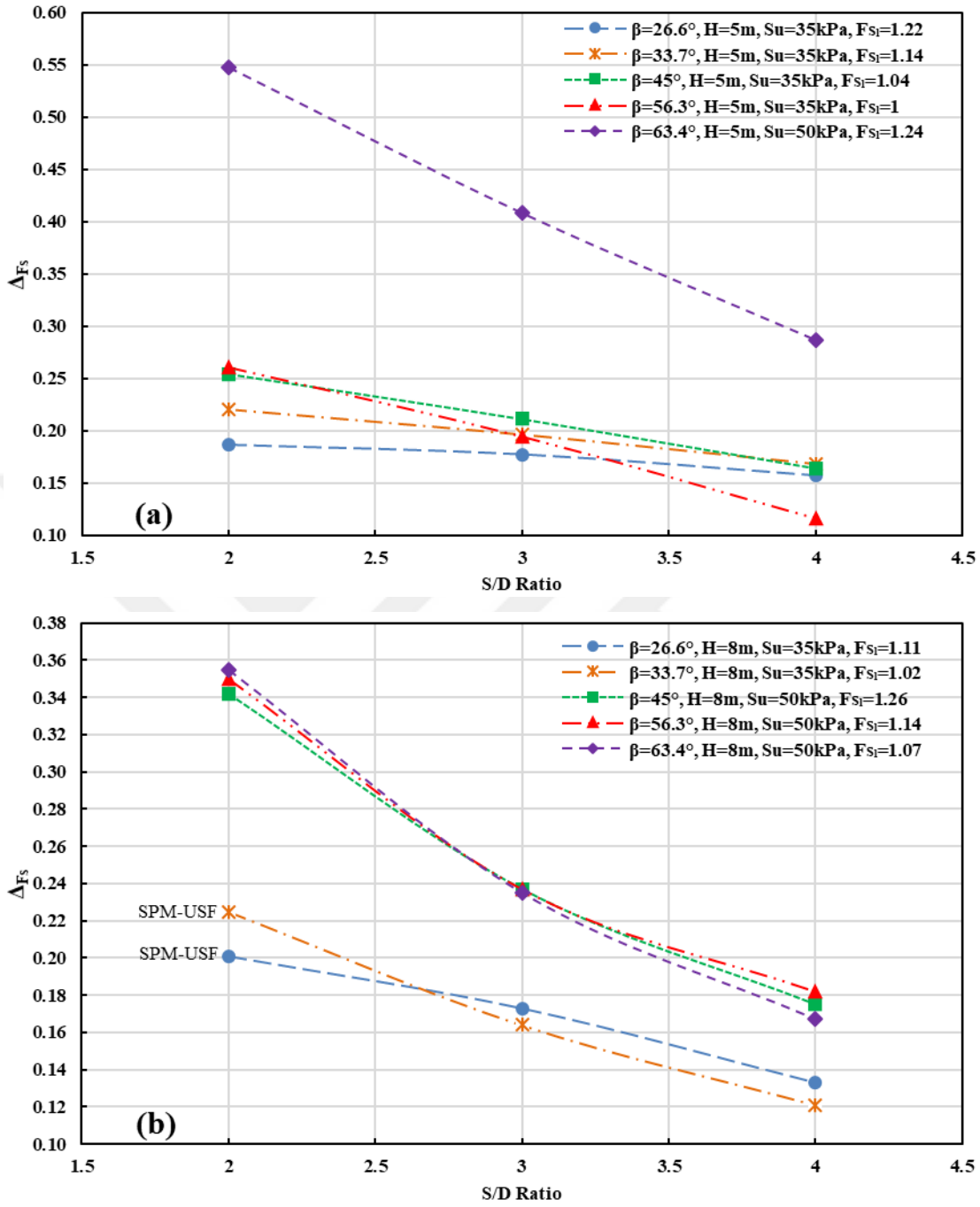


Figure 4.14. S/D ratio versus ΔF_s for pile-stabilized loaded slope cases with a range of β values: (a) H=5 m, (b) H=8 m.

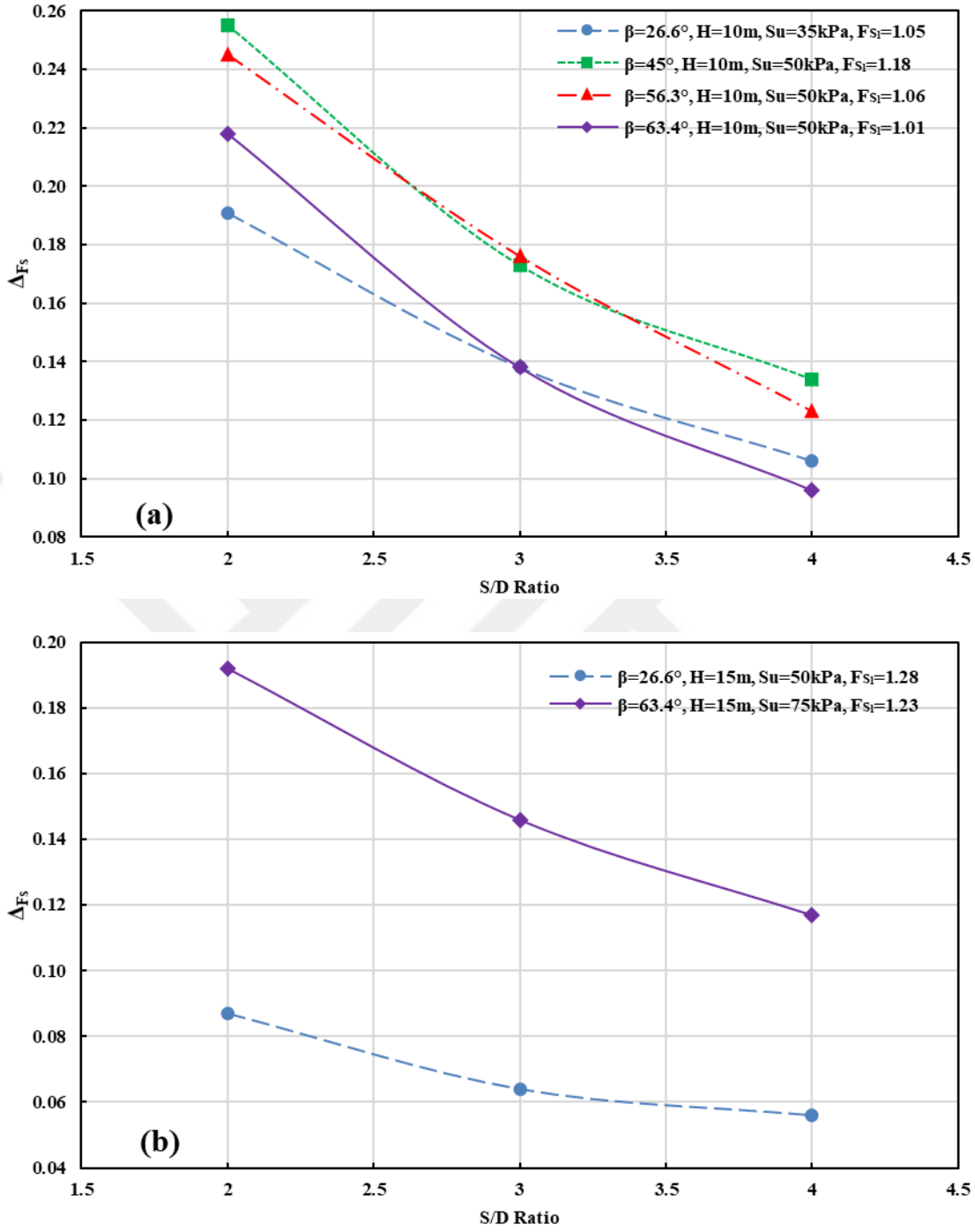


Figure 4.15. S/D ratio versus ΔF_s for pile-stabilized loaded slope cases with a range of β values: (a) H=10 m, (b) H=15 m.

According to Kourkoulis *et al.* (2011), presence of soil arching can be evaluated by determining the ratio of soil displacement between two piles to the displacement of the piled heads. When this ratio remains within the 1 to 2 range, the displacement of both the pile and the soil between the piles are quite similar. Consequently, the pile-slope system can be deemed working together and efficiently with respect to soil arching. Incremental displacements of various pile-stabilized slope cases are demonstrated in Figures 4.16 through 4.20. These figures were used to illustrate the progressive soil movement at failure conditions. Figures 4.16 through 4.20 represent various slope geometries that present increasingly unfavorable conditions (starting from first figure to last), in terms of increase in H and/or β values. In essence, Figures 4.16 through Figures 4.20 correspond to the most and least favorable geometric conditions among those presented, respectively. For each geometry, four (4) pile configurations with S/D ratios in the 2-5 range are presented. As can be seen from these figures, movement of piles and soil around the piles were very similar for cases with S/D=2, which strongly implies the presence of strong soil arching for this pile spacing, independent from the geometry. Soil arching decreased with an increase in *i)* slope height, *ii)* slope angle and most notably, *iii)* pile spacing. In most of the cases the pile heads experienced the highest lateral displacements. This shows that the piles are loaded due to the slope stabilization effect and the 3D load transfer mechanism in the pile-slope system works successfully. Additionally, the loaded soil area in the down-slope section behind the piles were observed to shrink as the slope geometry and pile spacing conditions become more unfavorable. Results support the trends observed ΔF_s values in Figures 4.13.

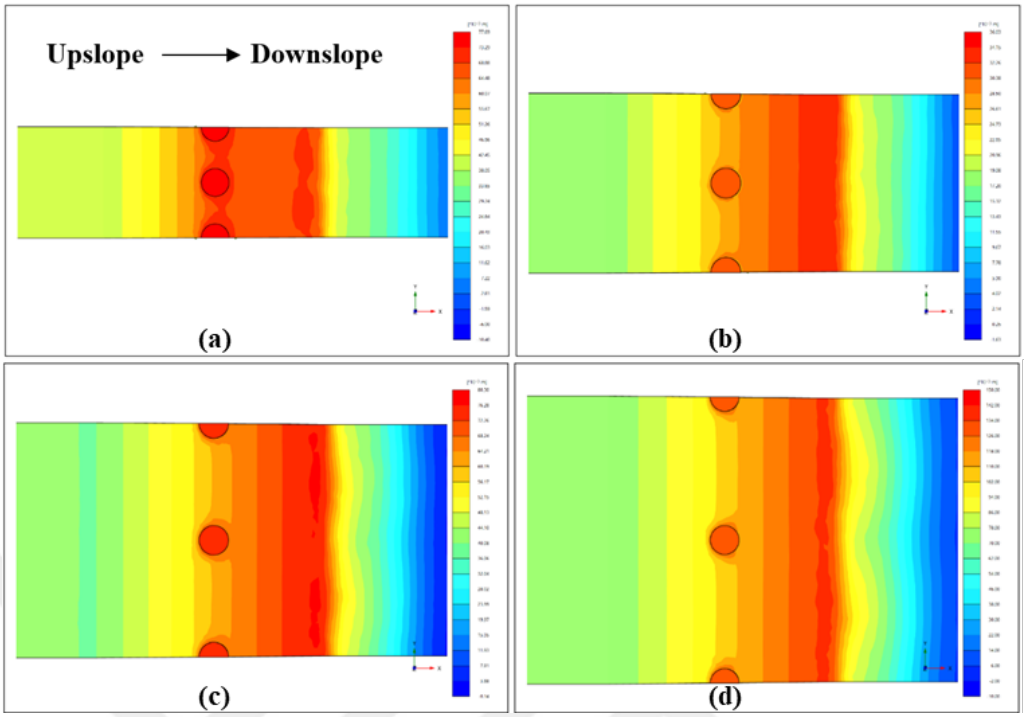


Figure 4.16. Incremental displacements (plan view) from safety analysis of pile-stabilized slope cases with β=33.7°, H=8 m, S_u=25 kPa: (a) S/D=2, (b) S/D=3, (c) S/D=4, (d) S/D=5.

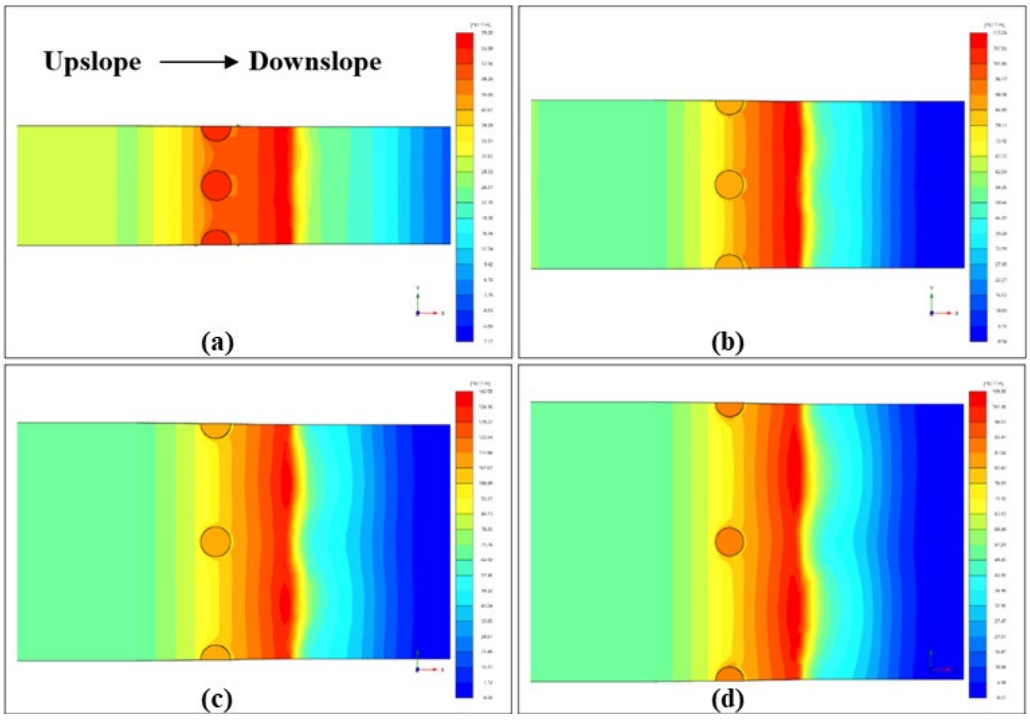


Figure 4.17. Incremental displacements (plan view) from safety analysis of pile-stabilized slope cases with β=45°, H=8 m, S_u=25 kPa: (a) S/D=2, (b) S/D=3, (c) S/D=4, (d) S/D=5.

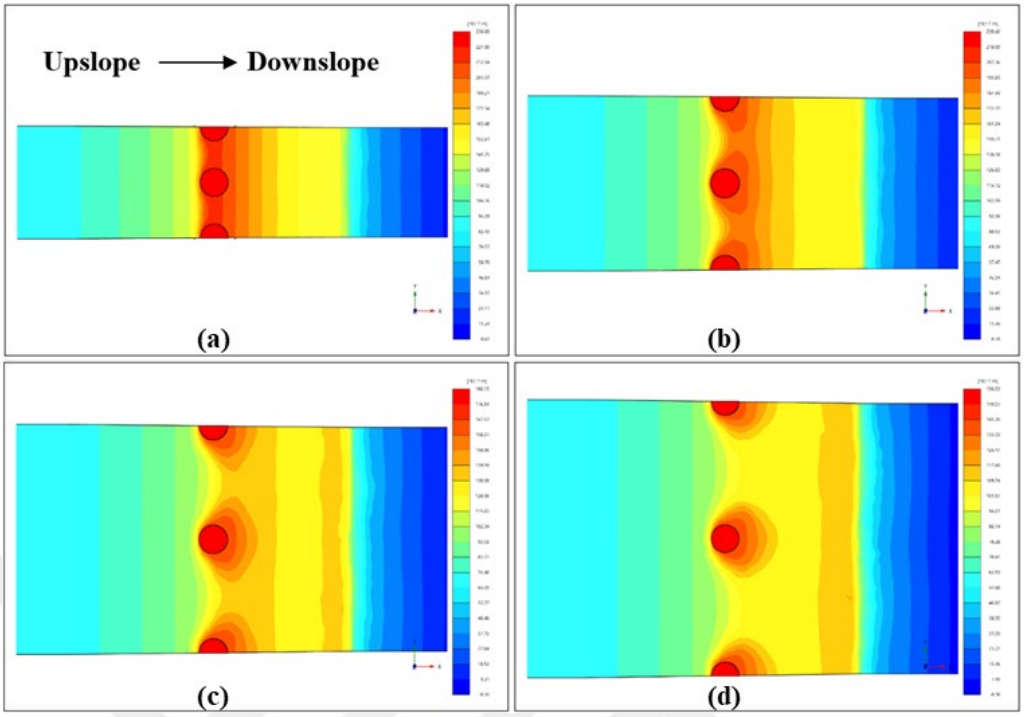


Figure 4.18. Incremental displacements (plan view) from safety analysis of pile-stabilized slope cases β=45°, H=15 m, S_u=50 kPa: (a) S/D=2, (b) S/D=3, (c) S/D=4, (d) S/D=5.

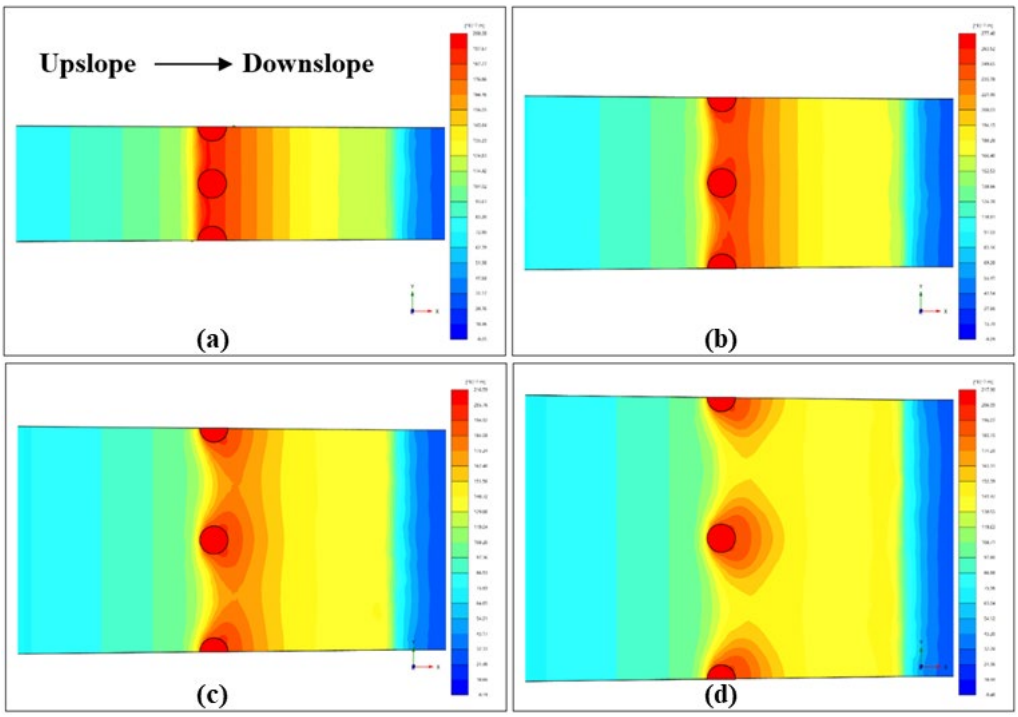


Figure 4.19. Incremental displacements (plan view) from safety analysis of pile-stabilized slope cases with β=45°, H=20 m, S_u=75 kPa: (a) S/D=2, (b) S/D=3, (c) S/D=4, (d) S/D=5.

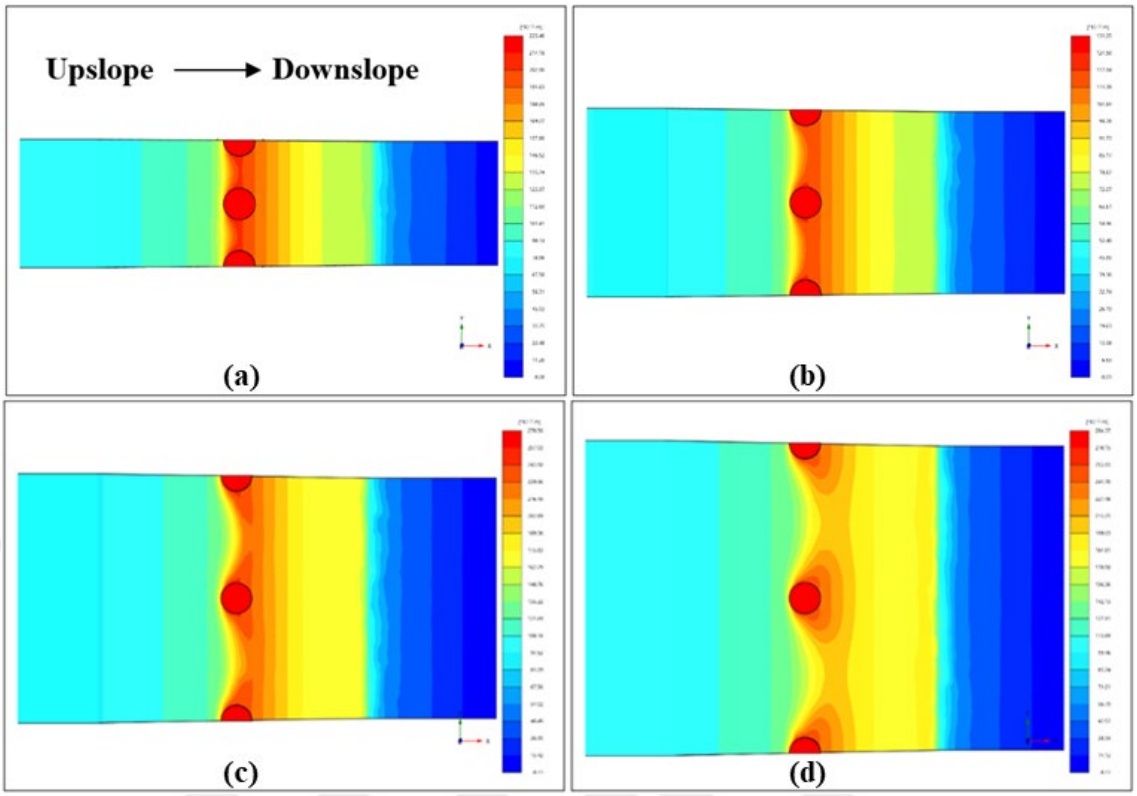
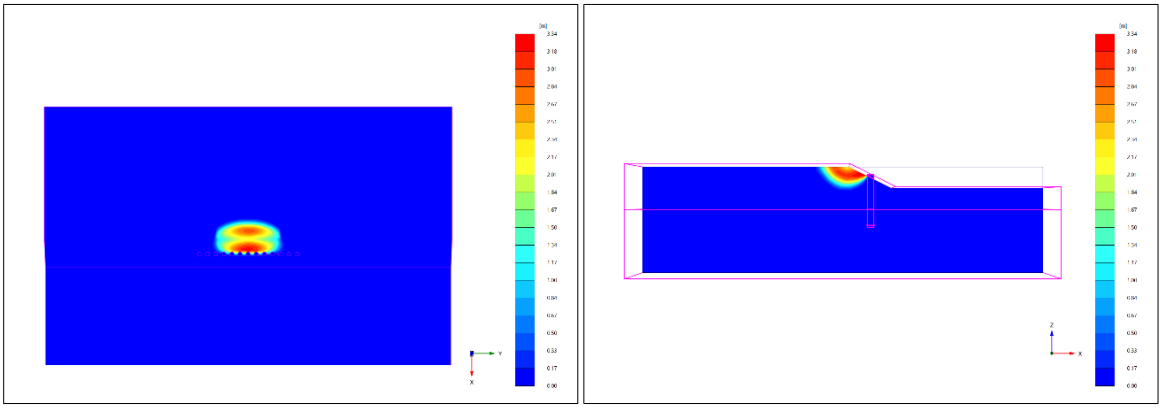


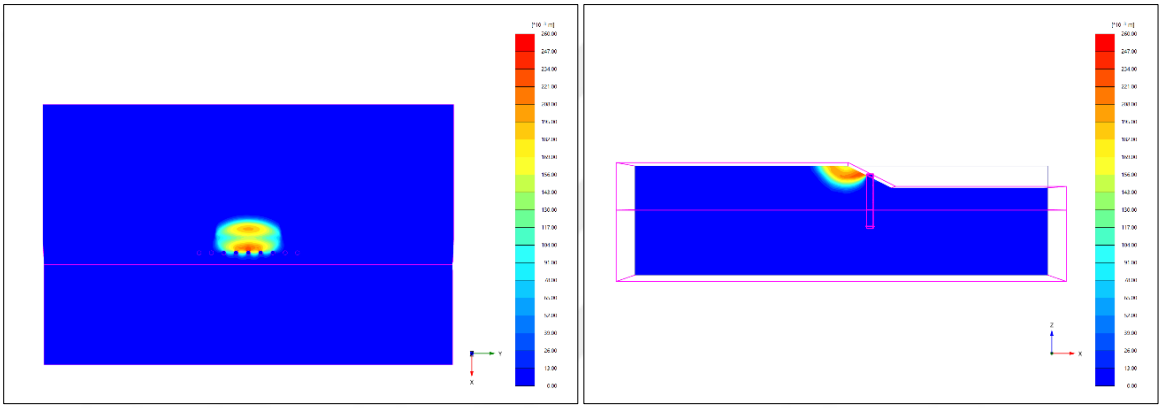
Figure 4.20. Incremental displacements (plan view) from safety analysis of pile-stabilized slope cases with β=56.3°, H=20 m, S_u=75 kPa (a) S/D=2, (b) S/D=3, (c) S/D=4, (d) S/D=5.

Plan and cross-section views of incremental displacements of various pile-stabilized loaded slope cases are shown in Figures 4.21 through 4.23. Similar to those presented for unloaded slope cases, Figures 4.21 through 4.23 represent various slope geometries that present increasingly unfavorable conditions (starting from first figure to last), in terms of increase in H and/or β values. Results were similar to the results obtained from cases without loading with the exception of depth of failure plane and pile group behavior. Generally, in the cases with low H values (*i.e.,* H≤8 m), SPM-USF behavior was observed, and movement of pile heads were relatively little compared to the soil in the up-slope section. In the cases with high slopes, LPM-DSF behavior was observed, and the movement of pile heads were similar compared to the soil surrounding the piles. For most of the cases investigated, cross-sections of the of the failure shapes were similar to each other, however, significant differences were observed in the axis along the depth of extrusion due to pile spacing effects. This highlights the importance of performing 3D analysis to better understand the 3D failure mechanisms and soil arching phenomenon. With the increase in pile spacing, a gradual

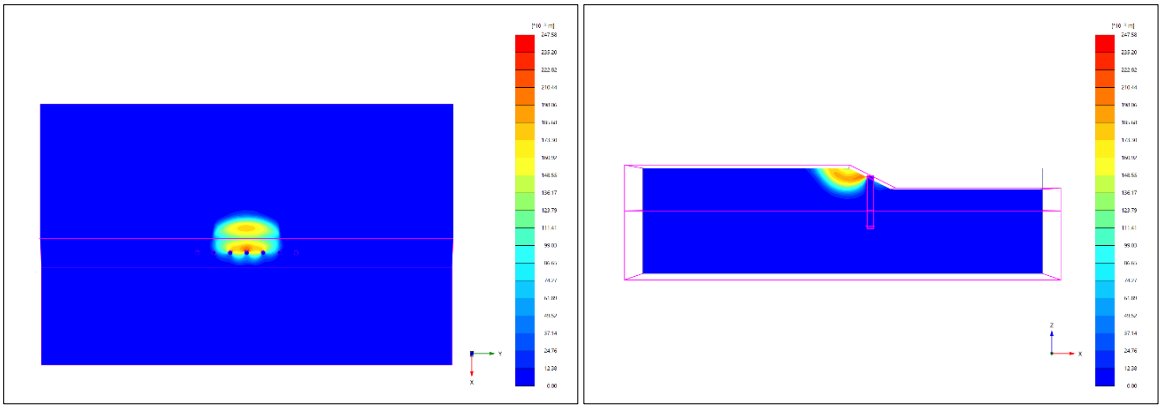
increase was observed in the relative movement of soil compared to the movement of pile heads. Also, piles placed in the outmost ends of the pile row were considered to be unexploited in some of the analyzed cases since very little relative movement was present in these pile heads. Even in the slope cases with β=63.4° and H=15 m shown in Figures 4.23a through 4.23c, in which the failure shape is wider than the pile row coverage length, outmost piles experienced very small lateral movement compared to piles close to the middle of the pile row. To better illustrate the pile group behavior along the coverage length of the pile row, bending moment distribution along pile depth of slope cases with β=26.6°and H=5 m and the slope case with β=63.4° and H=15 m are given in Figure 4.24 and 4.25, respectively. Figures 4.24a and 4.25a show bending moment distributions at the loading phase. The piles were loaded below their structural capacity and a gradual increase in pile bending moments from outmost pile to center pile was observed for both cases analyzed. Figures 4.24b and 4.25b show bending moment distributions of the piles in safety analysis. In these figures, USF was more critical in the slope case with β=26.6° and H=5 m since the piles were subjected to loads below their structural capacity. In the USF case, pile group behavior was similar to that of the loading phase and only magnitudes of the bending moments were increased. However, in the slope case with β=63.4°and H=15 m, DSF was prevalent, and the piles were loaded until they failed structurally. For the DSF case, all of the piles had very similar bending moment distribution. This is due to the fact that the observed failure shape was similar to that of plane strain conditions for the slope case with β=26.6°and H=15 m (*see* Figure 4.11b).



(a)

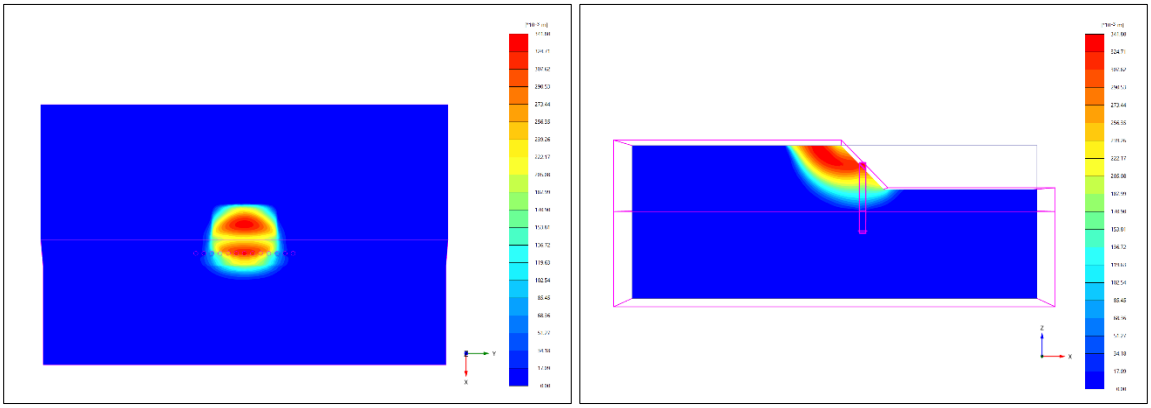


(b)

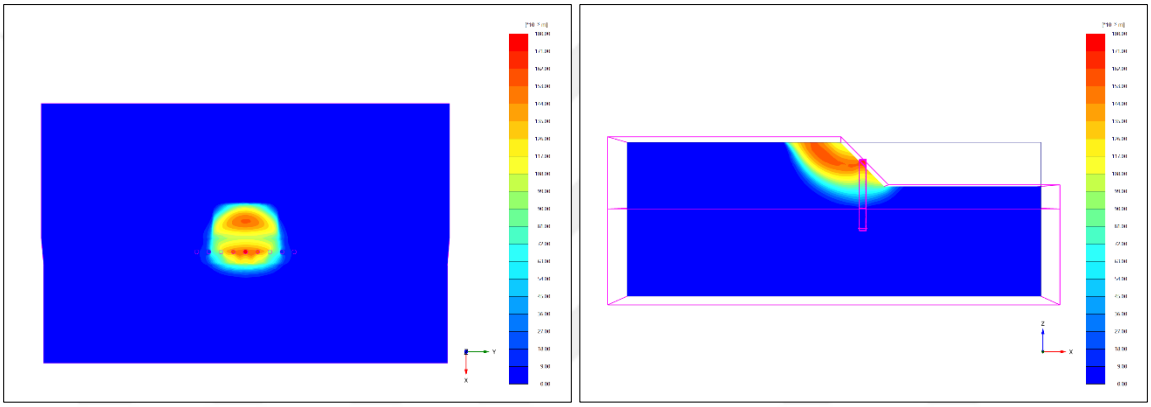


(c)

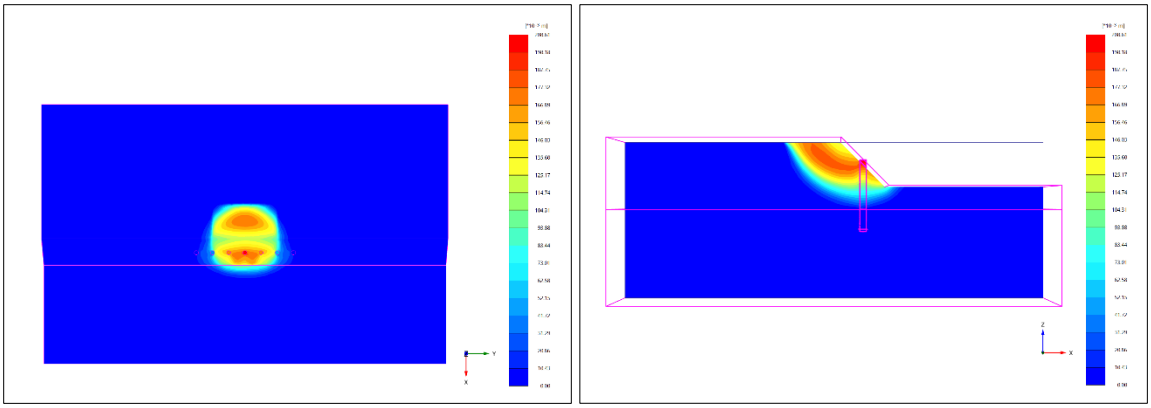
Figure 4.21. Incremental displacements shown on plan and cross section views from the safety analysis for the pile-stabilized loaded slope cases with β=26.6°, H=5 m, S_u=35 kPa: (a) S/D=2, (b) S/D=3, (c) S/D=4.



(a)

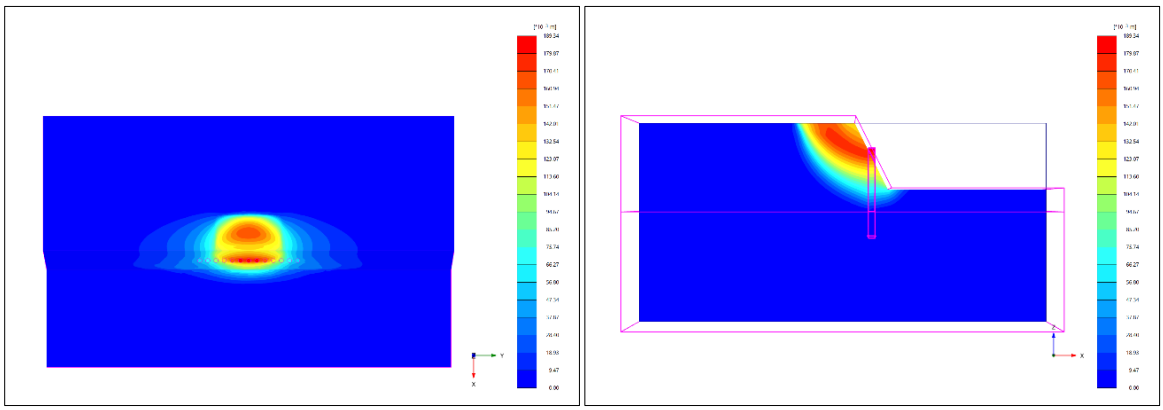


(b)

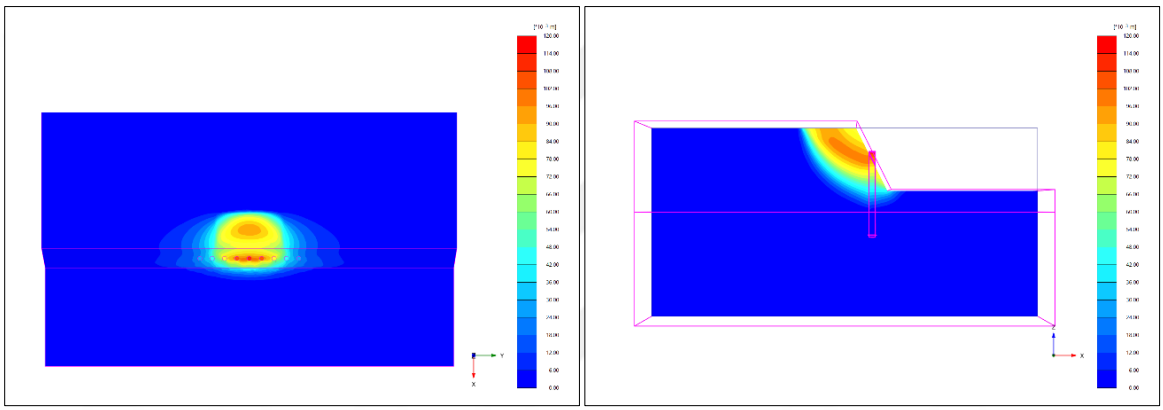


(c)

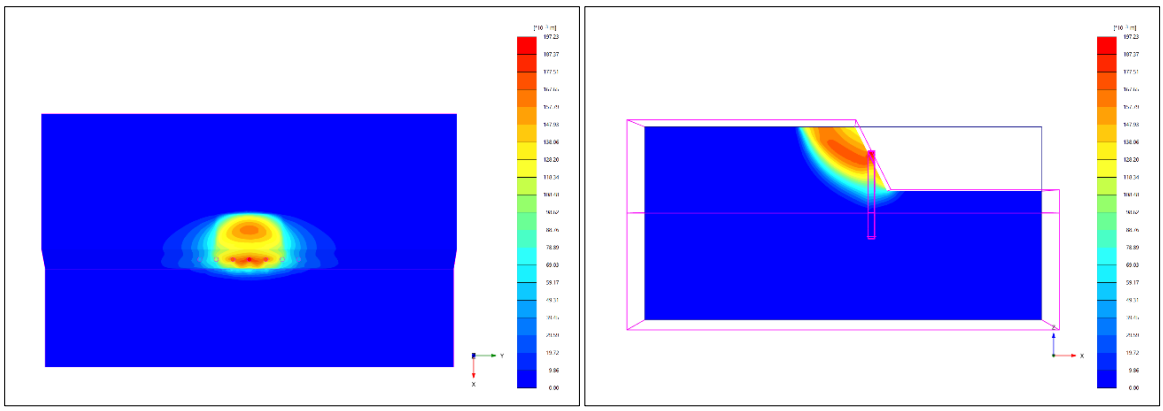
Figure 4.22. Incremental displacements shown on plan and cross section views from the safety analysis for the pile-stabilized loaded slope cases with β=45°, H=10 m, S_u=50 kPa: (a) S/D=2, (b) S/D=3, (c) S/D=4.



(a)



(b)



(c)

Figure 4.23. Incremental displacements shown on plan and cross section views from the safety analysis for the pile-stabilized loaded slope cases with β=63.4°, H=15 m, S_u=75 kPa: (a) S/D=2, (b) S/D=3, (c) S/D=4.

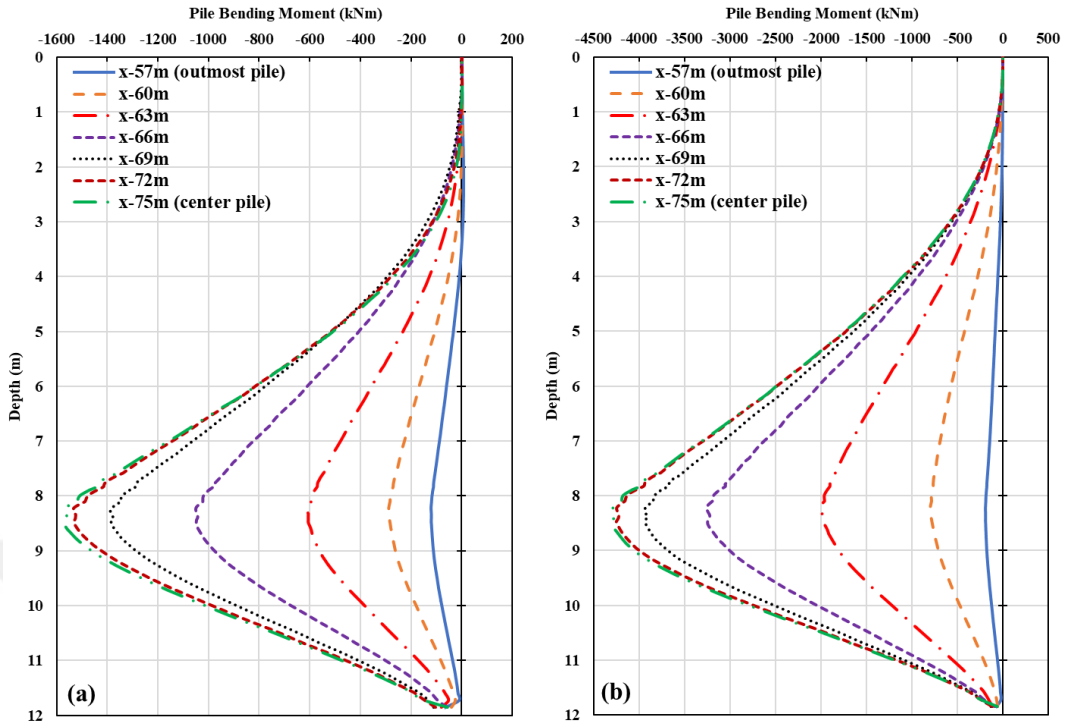


Figure 4.24. Pile bending moments versus the depth for pile-stabilized loaded slope case with β=26.6°, H=5 m, S_u=35 kPa, S/D=2: (a) deformation analysis, (b) safety analysis.

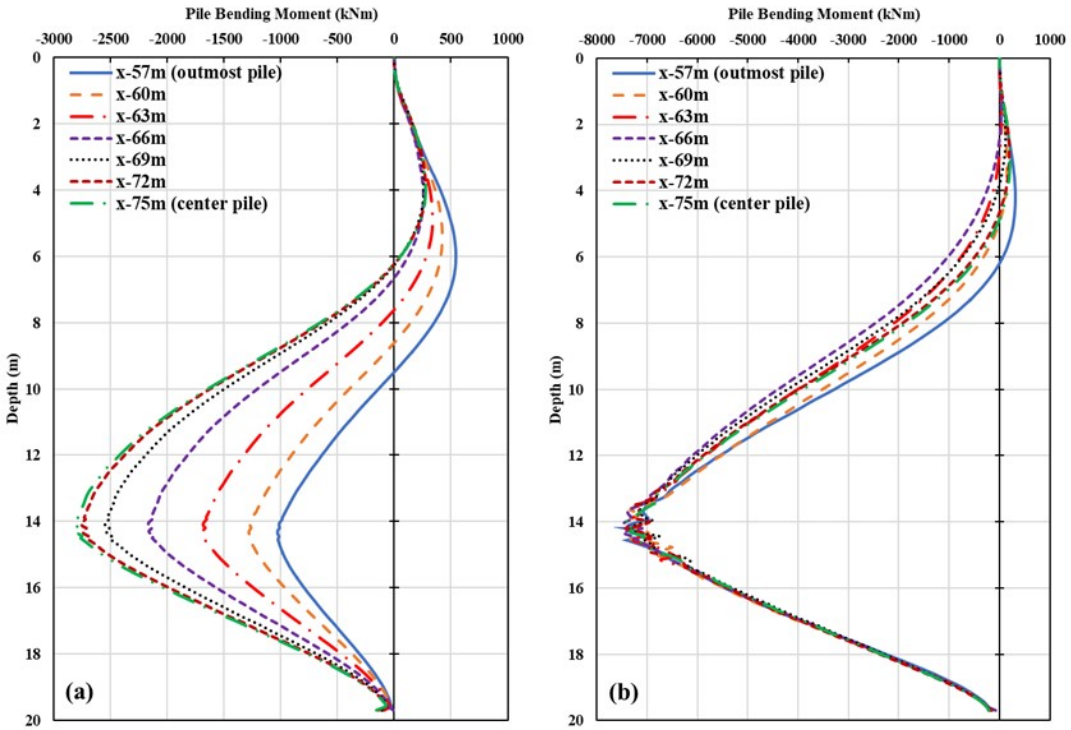


Figure 4.25. Pile bending moments versus the depth for pile-stabilized loaded slope case with β=63.4°, H=15 m, S_u=75 kPa, S/D=2: (a) deformation analysis, (b) safety analysis.

To demonstrate the effects of pile spacing on the pile behavior, the pile bending moment distribution along the pile depth for the slope case with β=45° and H=8 m is shown in Figures 4.26 and 4.27 considering S/D ratios of 2 and 4, respectively. Figure 4.26a and 4.27a show bending moment distributions at the loading phase (*i.e.*, deformation analysis). With the increase in S/D ratio, pile bending moments also increase. However, the overall behavior of piles placed on the same locations (*i.e.,* piles located in x=57 m, x=63 m, x=69 m and x=75 m points along the 150 m extrusion depth of the model) seem to be very similar in both pile spacings. Figure 4.26b and 4.27b show bending moment distributions at the safety analysis. According to Figure 4.26b and 4.27b, piles closed to the middle of the pile row reached structural failure in both cases and max bending moments of the outmost piles were not affected by the S/D ratio. The observed phenomenon was attributed to the fact that the piles situated near the center of the pile row were subjected to the most adverse loading conditions, leading to their primary structural failure. Upon the failure of these central piles, a subsequent slope failure becomes imminent, occurring before the outmost piles experience substantial loading, thereby resulting in their underutilization. These results also suggest that coverage length of 1.5 times of the surcharge length could be a conservative approach for shallow slopes. Moreover, alternative solutions such as using multiple rows of piles or adaptation of a pile cap beam may be required to utilize the outmost piles.

For pile-stabilized loaded slope cases, maximum bending moment (M_{max}) values obtained from S/D ratios of 3 and 4 were divided by maximum bending moment values obtained from cases with S/D ratio of 2 (M_{Max} / $M_{Max\text{-}S/D=2}$) to quantify the effect of spacing on maximum pile bending moments. Results are shown in Figures 4.28 and 4.29 for a range of slope geometries. As seen in figures, when S/D ratio was increased from 2 to 3, the increase in M_{max} was in the 16.5% - 28.3% range. Similarly, when S/D ratio increased from 2 to 4, the increase in M_{max} was in the 25.5% - 51.1% range. M_{Max} / $M_{Max\text{-}S/D=2}$ values were observed to be increasing with *i)* decrease in slope height, *ii)* increase in slope angle and *iii)* decrease in S_u. Highest differences were observed in cases where F_{sl} values were near 1 (*i.e.,* loaded slopes that were barely stable before pile stabilization). Similar approach was utilized for maximum lateral pile head displacements (y_{Max} / $y_{Max\text{-}S/D=2}$) and the results are presented in Figures 4.30 and 4.31. As seen in figures, when S/D ratio increased from 2 to 3, increase in y_{max} was in the 4.5% - 22% range and when the S/D ratio was increased from 2 to 4, the increase in y_{max} was in the 8.8% - 39.2% range.

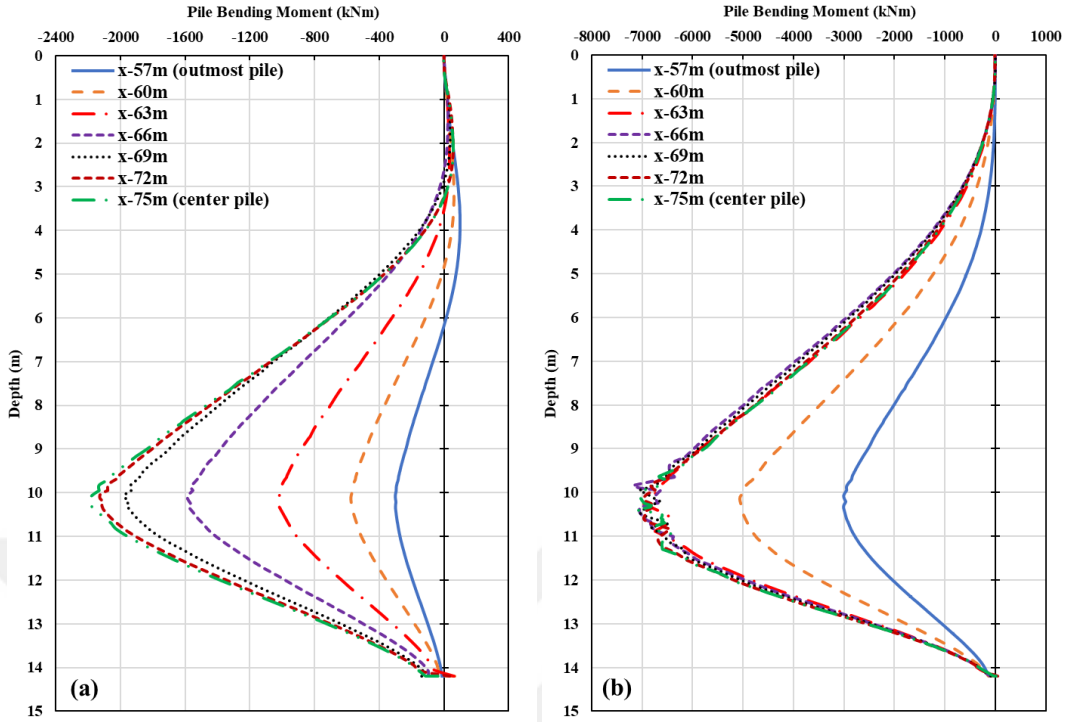


Figure 4.26. Pile bending moments versus the depth for pile-stabilized loaded slope case with β=45°, H=8 m, S_u= 50 kPa S/D=2: (a) deformation analysis, (b) safety analysis.

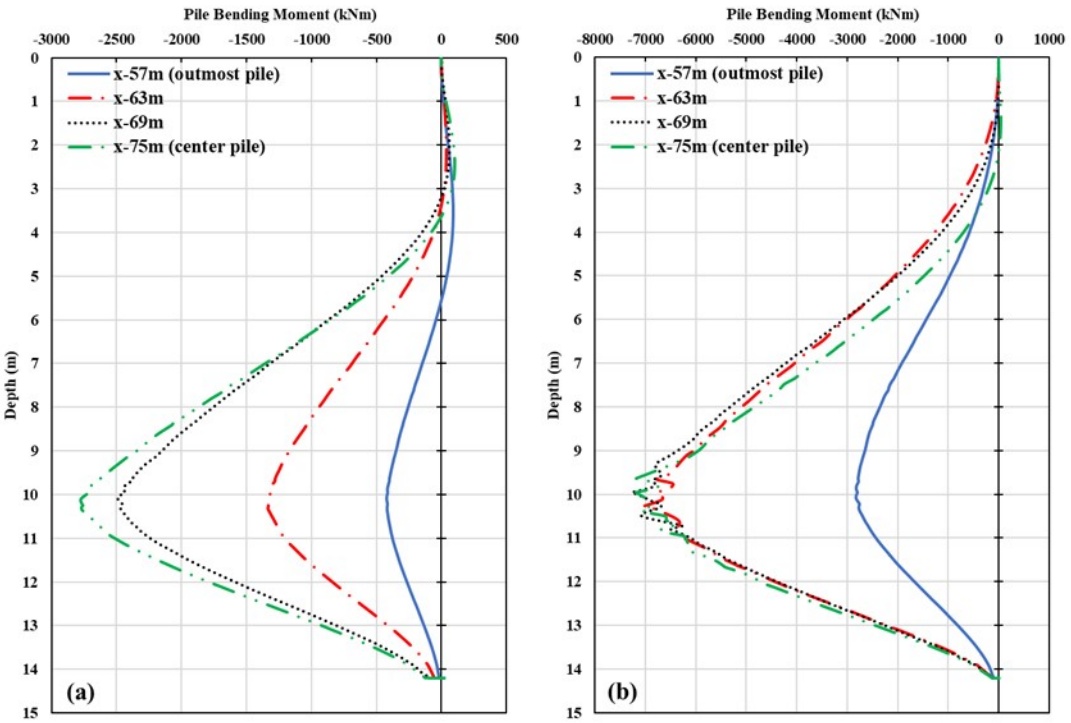


Figure 4.27. Pile bending moments versus the depth for pile-stabilized loaded slope case with β=45°, H=8 m, S_u= 50 kPa S/D=4: (a) deformation analysis, (b) safety analysis.

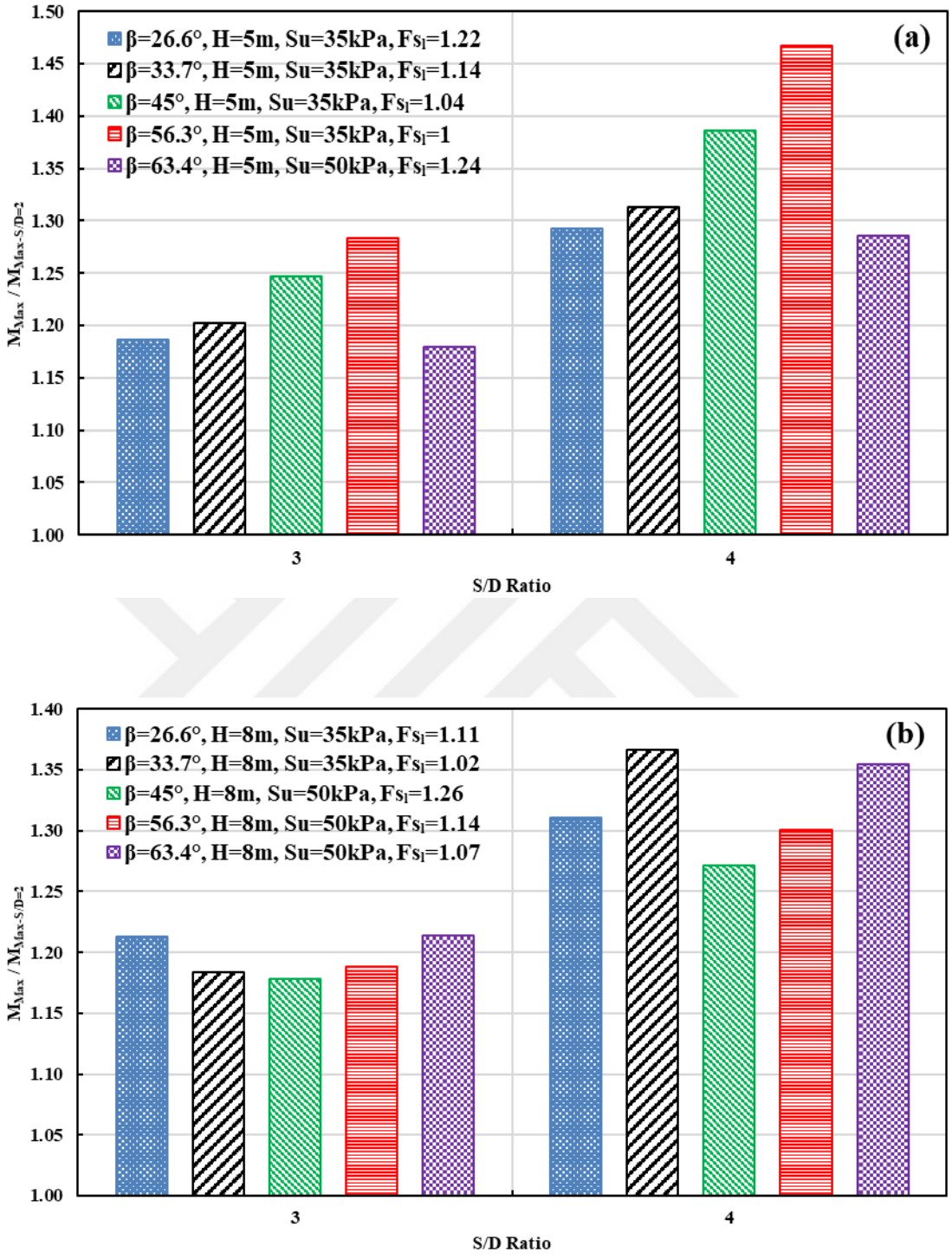


Figure 4.28. S/D ratio versus M_{Max} / $M_{Max\text{-}S/D=2}$ for pile-stabilized loaded slope cases with a range of β values: (a) H=5 m, (b) H=8 m.

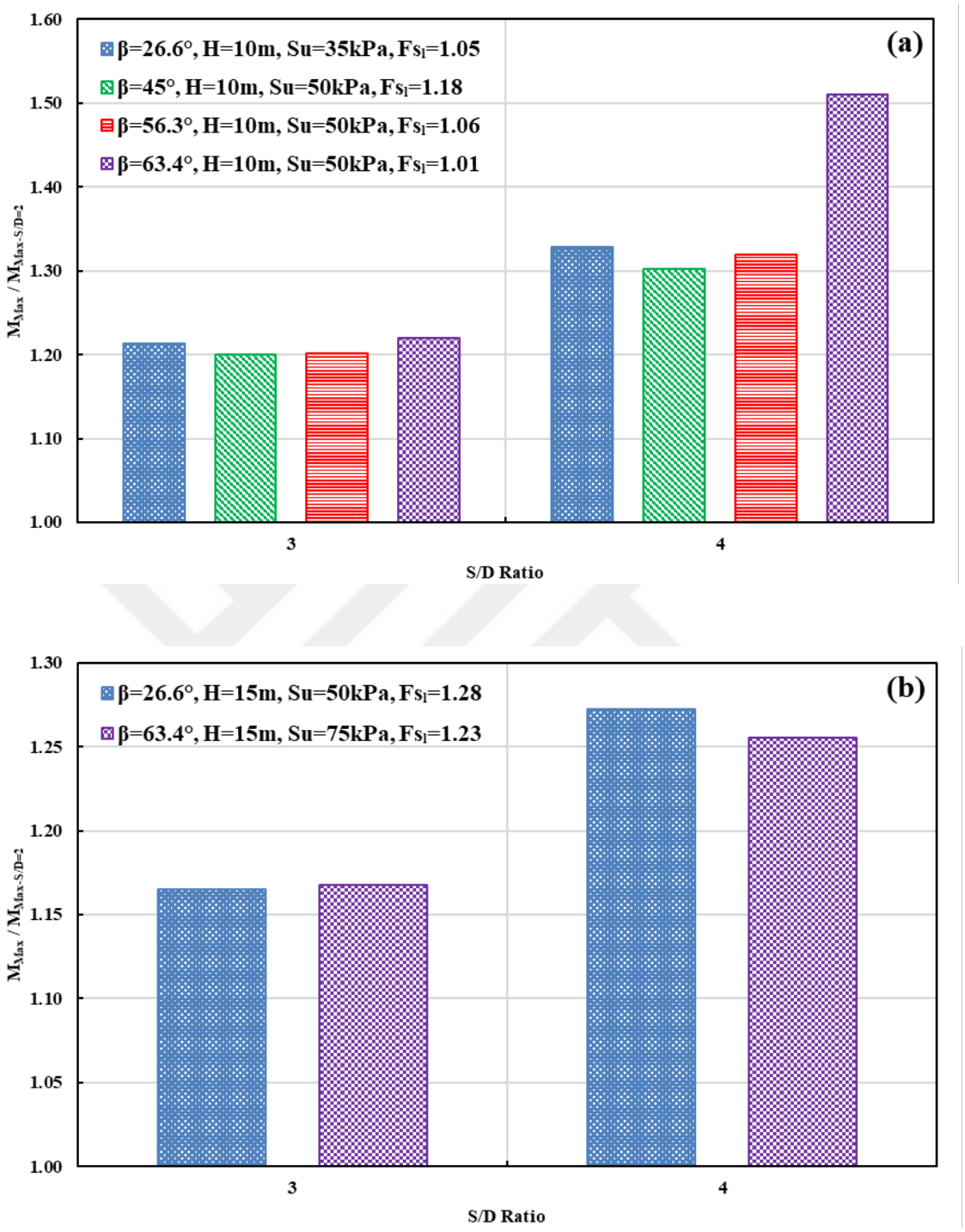


Figure 4.29. S/D ratio versus M_{Max} / $M_{Max\text{-}S/D=2}$ for pile-stabilized loaded slope cases with range of β values: (a) H=10 m, (b) H=15 m.

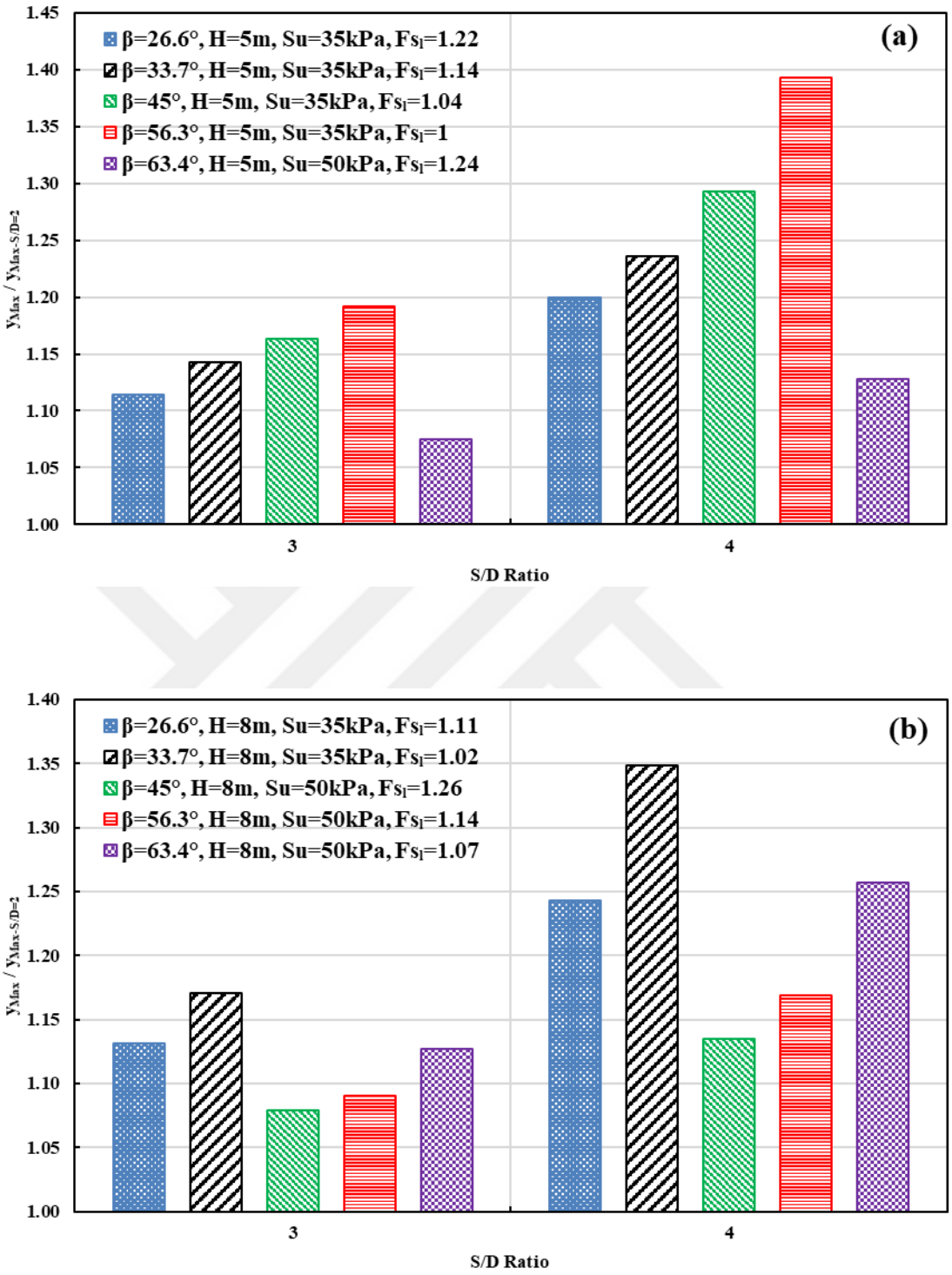


Figure 4.30. S/D ratio versus y_{Max} / $y_{Max\text{-}S/D=2}$ for pile-stabilized loaded slope cases with a range of β values: (a) H=5 m, (b) H=8 m.

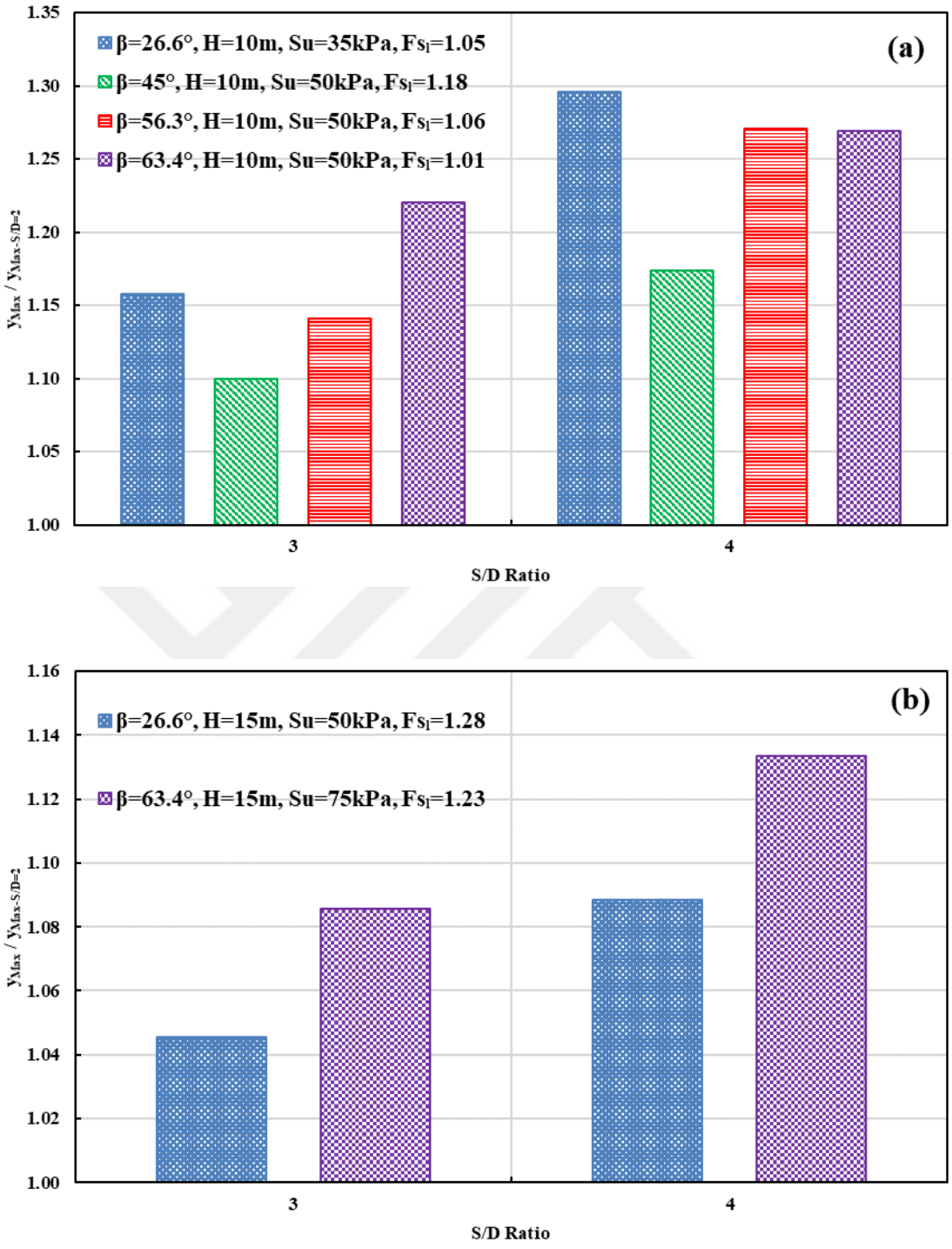


Figure 4.31. S/D ratio versus y_{Max} / $y_{Max-S/D=2}$ for pile-stabilized loaded slope cases with a range of β values: (a) H=10 m, (b) H=15 m.

4.7. Effect of Pile Cap Beam on Results

Deformation analysis at the loading phase and safety analysis results for various S/D ratios and pile head conditions are summarized in Table 4.3 and 4.4, respectively. As it can be seen from these tables, adaptation of a pile cap beam resulted in an increase in the F_s values, decrease in the pile head displacements, and decrease in the pile bending moments for all S/D ratios investigated in this research study. A maximum decrease of about 31% was observed in maximum bending moments and a maximum decrease of about 37% was observed in maximum pile head displacements with the inclusion of pile cap beams. These reductions are significant improvements. In terms of F_s, pile cap beam solution was observed to be more efficient in cases when S/D=3 and 4 compared to that of S/D=2. As illustrated in the case with S/D=3 presented in Figure 4.32, there seems to be a shift in pile bending moment distribution due to the pile cap beam leading to more favorable internal forces along the piles. Apparent failure mechanisms of cases with free and constrained pile head conditions are shown in Figure 4.33 for cases with S/D=4. As seen in the figure, pile cap beam facilitates a relatively even distribution of loads exerted onto each pile in the row compared to piles with free head condition. The pile cap enables the loading/utilization of the outmost piles that leads to an even distribution loads. Plan views of incremental displacements from safety analysis are shown in Figure 4.34 for various S/D ratios. Figure 4.34 clearly shows that the displacements were confined more effectively in cases with pile cap beam and thereby more favorable failure mechanisms were obtained in these cases compared to the pile cases with free head condition. For the case with S/D ratio of 2, failure mechanism changed from LPM-DSF to SPM-USF due to the inclusion of pile cap beam. In the cases with S/D ratio of 3 and 4, width of the failure shape reached to the limits of the area covered by the pile row.

Table 4.3. Results of deformation analysis at the loading phase for various S/D ratios and pile head conditions.

S/D Ratio	**Max Bending Moment (kNm)**			**Max Pile Head Displacement, U_x (cm)**		
	Free Head	Constrained Head	% Decrease	Free Head	Constrained Head	% Decrease
2	4243	2939	31%	12.3	8.3	33%
3	5097	3648	28%	14.0	9.3	34%
4	5600	3928	30%	15.6	9.9	37%

Table 4.4. Results of safety analysis for different S/D ratios and pile head conditions.

S/D Ratio	Factor of Safety, F_s		
	Free Head	Constrained Head	% Increase
2	1.30	1.36	4.4%
3	1.23	1.33	7.6%
4	1.18	1.27	7.5%

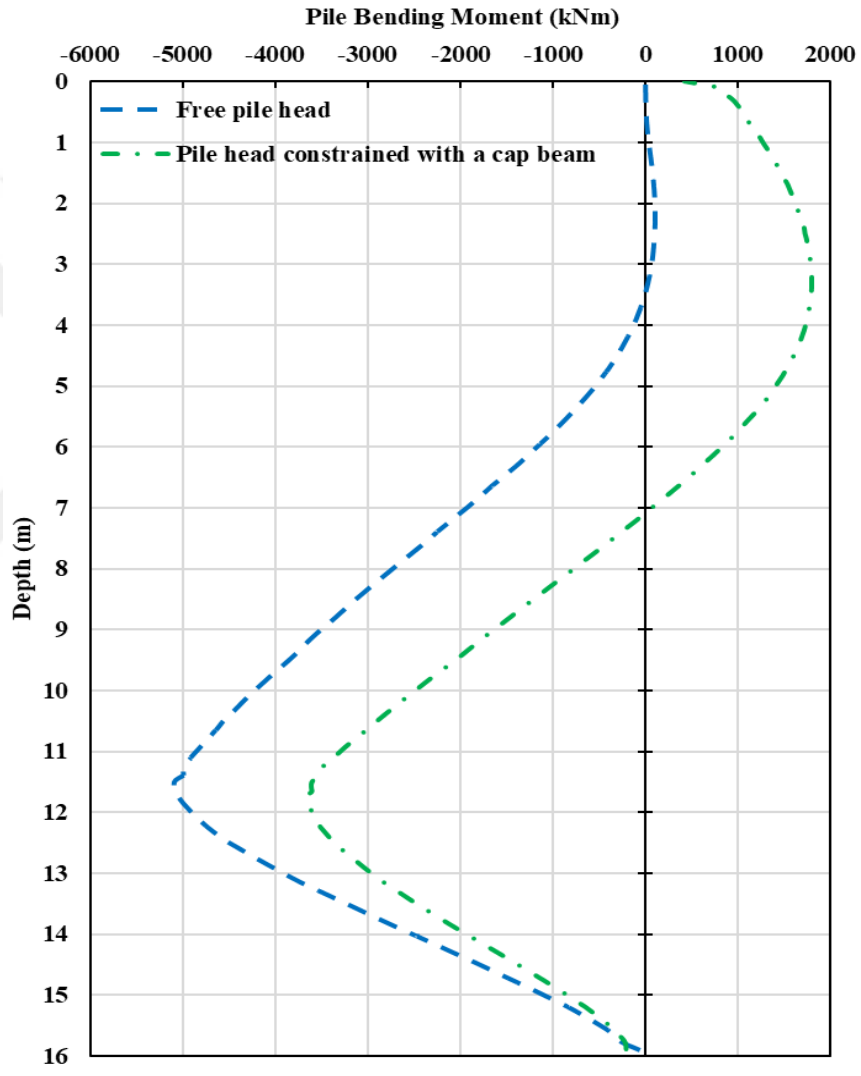


Figure 4.32. Pile bending moment along depth for pile-stabilized loaded slope case with β=56.3°, H=10 m, S_u=50 kPa, S/D=3

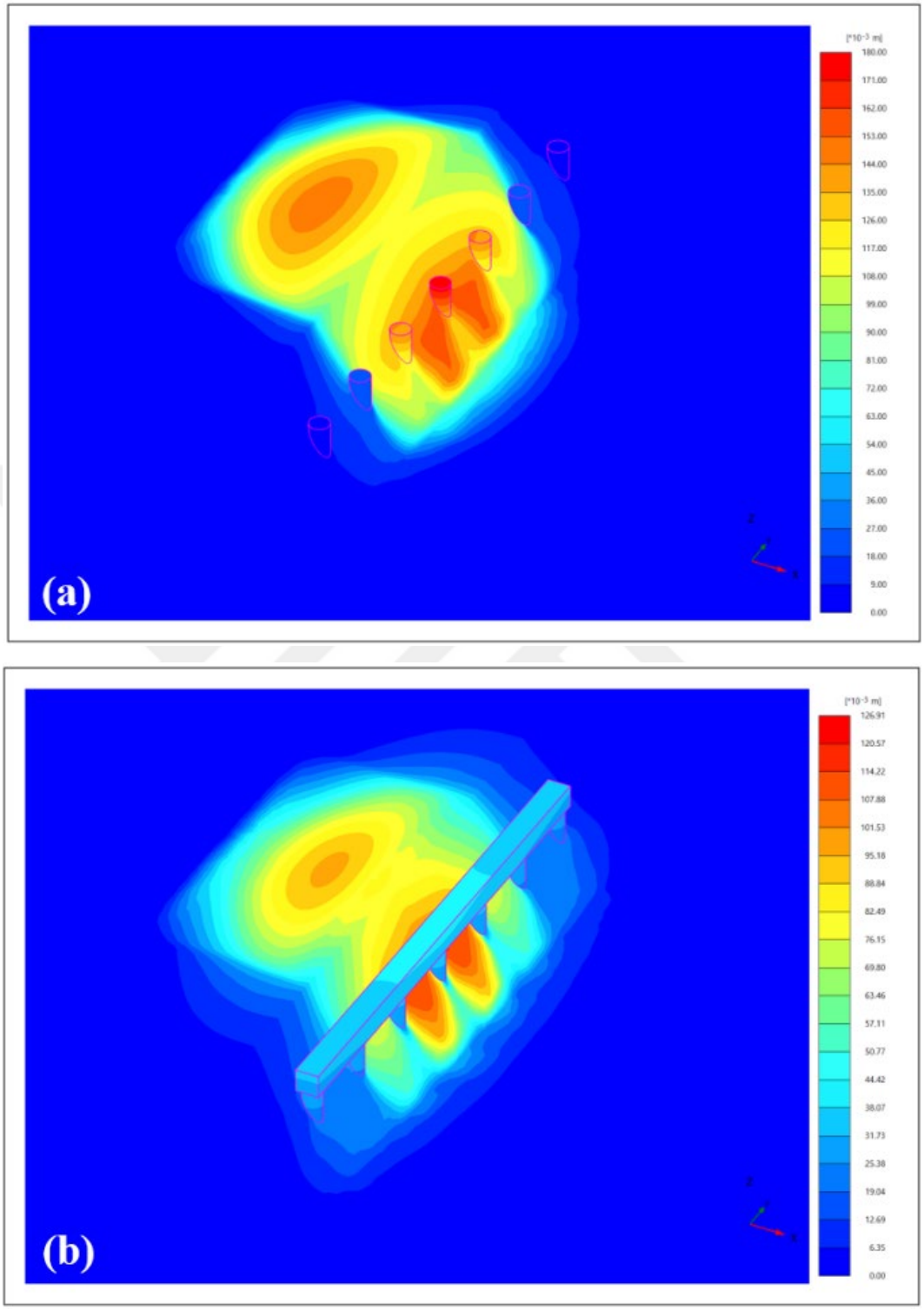


Figure 4.33. Incremental displacements from safety analysis for pile-stabilized loaded slope case with β=56.3°, H=10 m, S_u=50 kPa, S/D=4 with piles in: (a) free head condition, (b) constrained head condition.

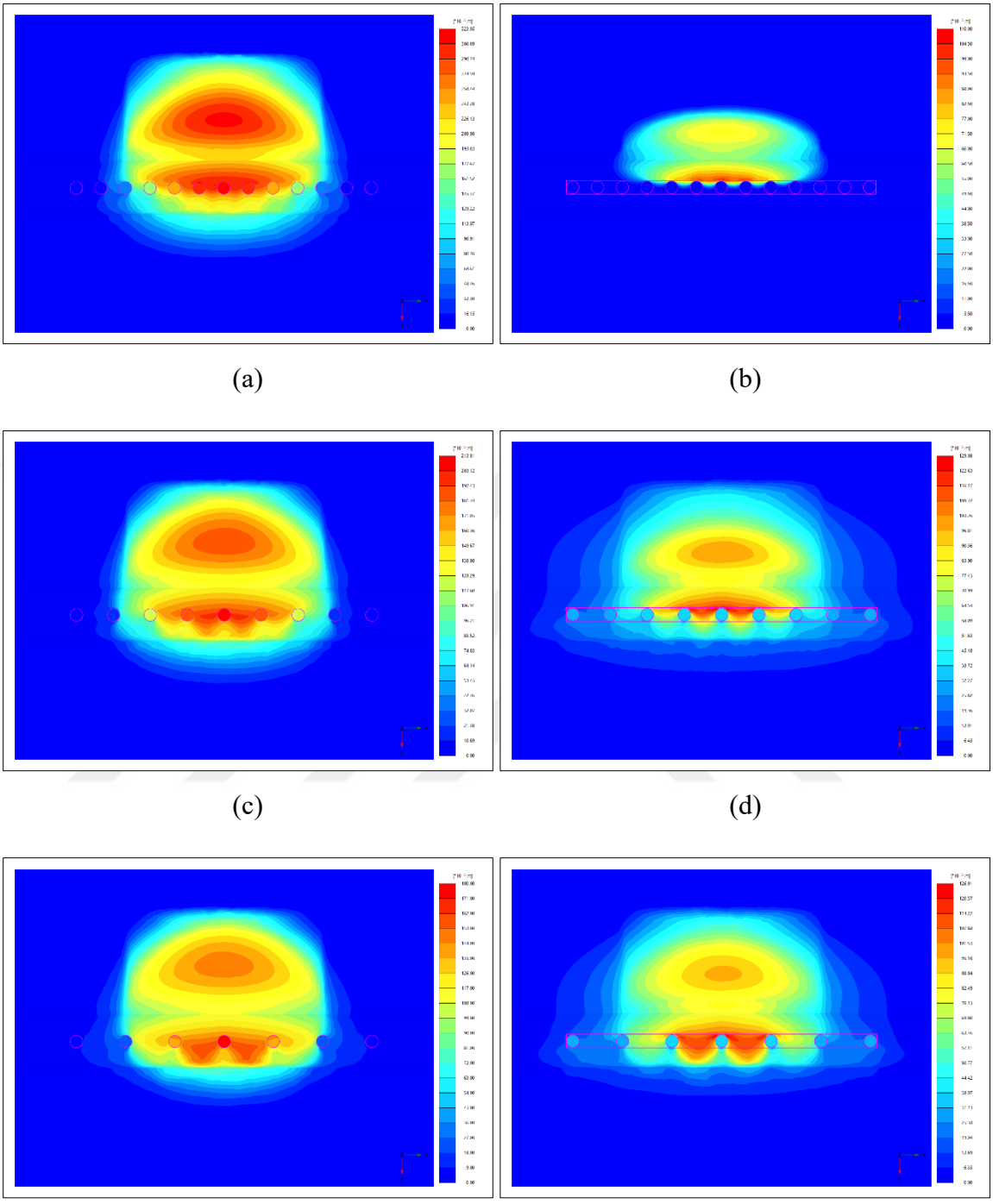


Figure 4.34. Incremental displacements from safety analysis of pile-stabilized loaded slope cases with β=56.3°, H=10 m, S_u=50 kPa: (a) S/D=2 with free head condition, (b) S/D=2 with constrained head condition, (c) S/D=3 with free head condition, (d) S/D=3 with constrained head condition, (e) S/D=4 with free head condition, (f) S/D=4 with constrained head condition.

5. CONCLUSION AND RECOMMENDATIONS

The short-term stability and the behavior of pile-stabilized clayey slopes were investigated in this study considering various soil properties, loading conditions, slope geometries, pile material behavior, pile head conditions and pile spacings. The piles were socketed into a dense sand layer and a surcharge load was applied near the slope crest. The failure mechanisms of the natural and loaded slopes, deformations under surcharge loads, F_s of the slopes and pile internal forces are investigated. Based on the results of 3D FEM analysis of pile-stabilized slopes, following conclusions were drawn:

- The results indicate that the assumption of linear-elastic pile material behavior overestimate the structural capacity of piles in safety analysis. This can result in unreasonably high F_s values for the pile-stabilized slopes, especially when the surcharge loads are high enough to load the piles near their structural capacity. The use of elasto-plastic pile models has the ability to better simulate pile behavior in both deformation and safety analysis, leading to more reliable F_s values for pile-stabilized slopes.
- Deep seated failure shapes were observed in all considered pile-stabilized slope cases without surcharge loads regardless of whether the internal pile forces approached the structural capacity of the piles or not. Rotational pile movement was observed in cases where structural capacity of the piles was not reached. In cases of failures controlled by the structural capacity of piles, a plastic hinge developed at the interface between stable (sandy) and unstable (clayey) layers.
- For the pile-stabilized loaded slope cases, when the piles were not loaded to their structural capacity, upper slope failures were observed. When the failure was dominated by the structural capacity of the piles, deep-seated failure mechanisms were observed.
- As slope height and slope angle increase, normalized F_s values decrease due to less favorable slope geometries, as can be anticipated. Among these two factors, the increases in slope height have a more pronounced impact on normalized F_s values compared to an increase in the slope angle.

- For high and gentle loaded slopes ($H \geq 15$ m and $\beta \leq 33.7$), the failure shape is defined by the slope's own weight rather than the surcharge loads. This means that the improvement in F_s due to local pile stabilization is constrained by the initial F_s of the slope before any surcharge loading is exerted and/or pile stabilization occurred. In other cases, the length of the zone improved by piles, that is equal to 1.5 times of the surcharge length was sufficient to achieve considerable stabilization.
- The results of the analysis performed on high ($H \geq 25$ m) and steep ($\beta \geq 56.3°$) natural (unloaded) slopes, showed that the single row of piles provide only marginal improvements. This also indicated the need for additional row of piles or other stabilization solutions to further increase the F_s in these cases.
- Improvement in F_s caused by pile stabilization decreases with the increase in spacing and the effect of S/D ratio reduces with the increase in slope heights for the cases with and without surcharge loads. The results suggest that, for high and gentle slopes ($H \geq 15$ m and $\beta \leq 33.7$), single row of reinforced concrete piles may not be enough to provide considerable stabilization when local surcharge loads are present.
- The most significant improvements in F_s ($\Delta F_s > 0.55$) were found in cases where SPM was prevalent. In cases, when minimal improvements are required in F_s, opting for pile diameters smaller than 1.5 m, which could lead to LPM, could be a more cost-effective choice for shallow slopes.
- When the F_s of a slope reduces to a value below 1 due to surcharge loads, significant displacements occur. In such cases, our preliminary analysis results indicated that stabilizing the slope with piles is not an efficient solution. Additionally, the initial F_s is very influential on the results even when the initial F_s prior to pile stabilization is above but near 1. In that case, all effects related to pile spacing are amplified due to higher displacements caused by the surcharge loading.
- Placing the piles closer to the surcharge load in pile-stabilized loaded slopes could provide higher stabilization (*i.e.,* improvement in F_s).
- The effects of soil arching decrease as: *i)* the slope height increases, *ii)* the slope angle increases, and most importantly *iii)* the pile spacing increases. These results highlighted the importance and requirement of 3D analysis when pile stabilized slopes with or without surcharge loads are considered. As soil arching can only be appropriately simulated in a 3D analysis, leading to more accurate estimation of deformations and F_s.

- For loaded slopes, it was observed that piles located closest to the center were exposed to the most adverse loading conditions. In some cases, this resulted in their structural failure. As these central piles fail, a subsequent slope failure occurs before any significant loading affects the outmost piles which leads to inefficient use of the outmost piles.
- Adaptation of a pile cap was discovered to be effective in increasing F_s values, decreasing pile head displacements, decreasing pile internal forces, and facilitating a relatively even distribution of loads exerted onto the piles in the row by utilizing the outmost piles.

Future research on pile-stabilized slopes should focus on exploring the influence of other pile related parameters, such as pile diameter, socket length, and more intricate pile placements such as frame and staggered configurations. Furthermore, it is necessary to conduct more detailed investigations for the modeling and stabilizing effects of pile cap beams. Finally, long-term stability analyses should be conducted to investigate the effects of the parameters examined under short-term conditions in this study.

REFERENCES

Abramson, L. W., T. S. Lee, S. Sharma, and G.M. Boyce, 1996, *Slope stability and stabilization methods*, John Wiley and Sons, New Jersey, USA.

Ashour, M., and H. Ardalan, 2012, "Analysis of pile stabilized slopes based on soil–pile interaction", *Computers and Geotechnics,* Vol. 39, pp. 85–97.

Ausilio, E., E. Conte, and G. Dente, 2001, "Stability analysis of slopes reinforced with piles", *Computers and Geotechnics*, Vol. 28, No. 8, pp. 591–611.

Baker, R., 2003, "A second look at Taylor's stability chart", *Journal of Geotechnical and Geoenvironmental Engineering*, Vol. 129, No. 12, pp. 1102–1108.

Bodour, W. A., and R. Y. Liang, 2010, "Field Study of Drilled Shafts Behavior during Surcharge Load Induced Slope Movement", *Geo-Florida 2010 Conference*, Florida, USA.

Brinkgreve, R. B. J., S. Kumarswamy, W. M. Swolfs, F. Fonseca, N. Ragi Manoj, L. Zampich, and N. Zalamea, 2021, *PLAXIS 3D 2021 Manual*. PLAXIS bv, Delft, Netherlands.

Broms, B. B., 1964, "Lateral resistance of piles in cohesive soils", *Journal of the Soil Mechanics and Foundations Division*, Vol. 90, No. 2, pp. 27–63.

Cai, F., and K. Ugai, 2000, "Numerical Analysis of the Stability of a Slope Reinforced with Piles", *Soils and Foundations*, Vol. 40, No. 1, pp. 73–84.

Chen, C., and G. R. Martin, 2002, "Soil–structure interaction for landslide stabilizing piles", *Computers and Geotechnics*, Vol. 29, No. 5, pp. 363–386.

Cheng, Y. M., T. Länsivaara, and W. B. Wei, 2007, "Two-dimensional slope stability analysis by limit equilibrium and strength reduction methods", *Computers and Geotechnics*, Vol. 34, No. 3, pp. 137–150.

Chow, Y. K., 1996, "Analysis of piles used for slope stabilization", *International Journal for Numerical and Analytical Methods in Geomechanics*, Vol. 20, No. 9, pp. 635–646.

Dawson, E., F. Motamed, S. Nesarajah, and W. H. Roth, 2000, "Geotechnical Stability Analysis by Strength Reduction". *In Proceedings of the Geo-Denver 2000 Conference,* Denver, USA.

Duncan, J. M., 1996, "State of the art: Limit Equilibrium and Finite-Element Analysis of slopes", *Journal of Geotechnical Engineering*, Vol. 122, No. 7, pp. 577–596.

Ellis, E., I. Durrani, and D. Reddish, 2010, "Numerical modelling of discrete pile rows for slope stability and generic guidance for design", *Geotechnique*, Vol. 60, No. 3, pp. 85–195.

Ersoy, H., A. Kaya, Z. Angin, and S. Dağ, 2020, "2D and 3D numerical simulations of a reinforced landslide: A case study in NE Turkey", *Journal of Earth System Science*, Vol. 129, No. 1.

Fantera, L., S. Lirer, A. Desideri, and S. Rampello, 2022, "Efficiency of piles stabilizing slopes in Fine-Grained soils", *International Journal of Geomechanics*, Vol. 22, No. 9.

Gao, Y., Zhang, F., Gan, L., Li, D., Wu, Y., and Zhang, N., 2013, "Stability charts for 3D failures of homogeneous slopes", *Journal of Geotechnical and Geoenvironmental Engineering*, Vol. 139, No. 9, pp. 1528–1538.

Georgiadis, K., 2010, "Undrained bearing capacity of strip footings on slopes", *Journal of Geotechnical and Geoenvironmental Engineering*, Vol. 136, No. 5, pp. 677–685.

Gerolymos, N., O. Papakyriakopoulos, and R. B. J. Brinkgreve, 2014, "Macroelement Modeling of Piles in Cohesive Soil Subjected to Combined Lateral and Axial Loading". *Proceedings of the 8th European Conference on Numerical Methods in Geotechnical Engineering*, Delft, Netherlands, pp. 373–378.

González, Y. T., V. R. Schaefer, and D. DK. Rollins, 2020, "Statistical assessment of factor of safety for Pile-Reinforced slopes", *Journal of Geotechnical and Geoenvironmental Engineering*, Vol. 146, No. 9.

Gregory, G. H., 2011, "Stabilization of Deep Slope Failure with Drilled Shafts: Lake Ridge Parkway Station 248; Grand Prairie, TX", *In Proceedings of The Geo-Frontiers 2011 Conference,* Dallas, USA.

Griffiths, D. V., and P. Lane, 1999, "Slope stability analysis by finite elements", *Geotechnique*, Vol. 49, No. 3, pp. 387–403.

Hassiotis, S., J. Chameau, and M. Gunaratne, 1997, "Design Method for Stabilization of Slopes with Piles", *Journal of Geotechnical and Geoenvironmental Engineering*, Vol. 123, No. 4, pp. 314–323.

He, Y., H. Hazarika, N. Yasufuku, and Z. Han, 2015, "Evaluating the effect of slope angle on the distribution of the soil–pile pressure acting on stabilizing piles in sandy slopes", *Computers and Geotechnics*, Vol. 69, pp. 153–165.

Ito, T., and T. Matsui, 1975, "Methods to estimate lateral force acting on stabilizing piles", *Soils and Foundations*, Vol. 15, No. 4, pp. 43–59.

Ito, T., T. Matsui, and W. Hong, 1981, "Design Method for Stabilizing Piles against Landslide - One Row of Piles", *Soils and Foundations*, Vol. 21, No. 1, pp. 21–37.

Ito, T., T. Matsui, and W. Hong, 1982, "Extended Design Method for Multi-Row Stabilizing Piles against Landslide", *Soils and Foundations*, Vol. 22, No. 1, pp. 1–13.

Jeong, S., B. C. Kim, J. Won, and J. Lee, 2003, "Uncoupled analysis of stabilizing piles in weathered slopes", *Computers and Geotechnics*, Vol. 30, No. 8, pp. 671–682.

Jiang, J., X. Huang, X. Shu, N. Xiao, Q. Yan, and W. Xiong, 2022, "Application of a damage constitutive model to pile–slope stability analysis", *Frontiers in Materials*, Vol. 9.

Kahyaoğlu, M. R., G. İmançlı, G. Özden, and A.Ş. Kayalar, 2017, "Numerical simulations of landslide-stabilizing piles: a remediation project in Söke, Turkey", *Environmental Earth Sciences*, Vol. 76, No. 19.

Kanagasabai, S., J.A. Smethurst, and W. Powrie, 2011, "Three-dimensional numerical modelling of discrete piles used to stabilize landslides", *Canadian Geotechnical Journal*, Vol. 48, No. 9, pp. 1393–1411.

Kelesoglu, M. K., 2015, "The evaluation of three-dimensional effects on slope stability by the strength reduction method", *KSCE Journal of Civil Engineering*, Vol. 20, No. 1, pp. 229–242.

Khan, M. S., M. Nobahar, M. Stroud, S. Ferguson, and J. Ivoke, 2022, "Performance evaluation of a highway slope on expansive soil in Mississippi", *International Journal of Geomechanics*, Vol. 22, No. 1.

Kourkoulis, R., F. Gelagoti, I. Anastasopoulos, and G. Gazetas, 2011, "Slope Stabilizing Piles and Pile-Groups: Parametric study and design Insights", *Journal of Geotechnical and Geoenvironmental Engineering*, Vol. 137, No. 7, pp. 663–677.

Kourkoulis, R., F. Gelagoti, I. Anastasopoulos, and G. Gazetas, 2012, "Hybrid method for analysis and design of slope stabilizing piles", *Journal of Geotechnical and Geoenvironmental Engineering*, Vol. 138, No. 1, pp. 1–14.

Lechman, J. B., and D. V. Griffiths, 2000, "Analysis of the Progression of Failure of Earth Slopes by Finite Elements", *In Proceedings of the Geo-Denver 2000 Conference*, Denver, USA.

Lee, C., T. Hull, and H. G. Poulos, 1995, “Simplified pile-slope stability analysis”, *Computers and Geotechnics*, Vol. 17, No. 1, pp. 1–16.

Li, H., and Q. Du, 2021, “Stabilizing a post-landslide loess slope with anti-slide piles in Yan’an, China”, *Environmental Earth Sciences*, Vol. 80, No. 22.

Liang, R. Y., and M. M. Yamin, 2009, “Three-dimensional finite element study of arching behavior in slope/drilled shafts system”, *International Journal for Numerical and Analytical Methods in Geomechanics*, Vol. 34, pp. 1157–1168.

Liang, R. Y., and S. Zeng, 2002, “Numerical study of soil arching mechanism in drilled shafts for slope stabilization”, *Soils and Foundations*, Vol. 42, No. 2, pp. 83–92.

Liang, R. Y., A. E. Joorabchi, and L. Li, 2014, “Analysis and design method for slope stabilization using a row of drilled shafts”, *Journal of Geotechnical and Geoenvironmental Engineering*, Vol. 140, No. 5.

Liang, R., M. Yamin, and W. M. Al. Bodour, 2009, “Lesson from instrumented slope stabilization project using drilled shafts”, *In Proceedings of the International Foundation Congress and Equipment Expo,* pp. 103-110, Florida, USA.

Lim, K., Lyamin, A. V., Cassidy, M., and Li, A., 2016, “Three-Dimensional slope stability charts for frictional fill materials placed on purely cohesive clay”, *International Journal of Geomechanics,* Vol. 16, No. 2.

Lirer, S., 2012, “Landslide stabilizing piles: Experimental evidences and numerical interpretation”, *Engineering Geology*, Vol. 149–150, pp. 70–77.

Michałowski, R. L., 2002, “Stability charts for uniform slopes”, *Journal of Geotechnical and Geoenvironmental Engineering*, Vol. 128, No. 4, pp. 351–355.

Obrzud, R. and A. Truty, 2018, *The Hardening Soil Model – A Practical Guidebook*, Z_Soil.PC 100701 report, revised 21.10.2018, Zace Services Ltd., Préverenges, Switzerland.

Pantelidis, L., and D. V. Griffiths, 2015, "Footing on the crest of slope: slope stability or bearing capacity?", *In Proceedings of the Engineering Geology for Society and Territory Conference*, Vol. 2, pp. 1231–1234, Turin, Italy.

Pirone, M., and G. Urciuoli, 2018, "Analysis of slope-stabilising piles with the shear strength reduction technique", *Computers and Geotechnics*, Vol. 102, pp. 238–251.

Potyondy, J. G., 1961, "Skin Friction between Various Soils and Construction Materials", *Geotechnique*, Vol. 11, No. 4, pp. 339–353.

Poulos, H. G., 1995, "Design of reinforcing piles to increase slope stability", *Canadian Geotechnical Journal*, Vol. 32, No. 5, pp. 808–818.

Pradel, D., J. Garner, and A. O. L. Kwok, 2010, "Design of Drilled Shafts to Enhance Slope Stability", *In Proceedings of the 2010 Earth Retention Conference*, Washington, USA.

Rocscience Inc., 2023, *Slide 9.02 2D Limit Equilibrium Slope Stability Analysis Program Manuel*, Toronto, Canada.

Şengör, M. Y., M. U. Ergun, and N. Huvaj Sarıhan, 2013, "Landslide stabilization by piles: A case history", *18th International Conference on Soil Mechanics and Geotechnical Engineering,* pp. 2253-2256, Paris, France.

Shiau, J., R. S. Merifield, A. V. Lyamin, and S. W. Sloan, 2011, "Undrained stability of footings on slopes", *International Journal of Geomechanics*, Vol. 11, No. 5, pp. 381–390.

Sloan, S. W., 2013, "Geotechnical stability analysis", *Geotechnique*, Vol. 63, No. 7, pp. 531–571.

Smethurst, J., and W. Powrie, 2007, “Monitoring and analysis of the bending behaviour of discrete piles used to stabilise a railway embankment”, *Geotechnique*, Vol. 57. No. 8, pp. 663–677.

Tschuchnigg, F., H. F. Schweiger, and, S. Sloan, 2015, “Slope stability analysis by means of finite element limit analysis and finite element strength reduction techniques. Part I: Numerical studies considering non-associated plasticity”, *Computers and Geotechnics*, Vol. 70, pp. 169–177.

Viggiani, C., 1981, “Ultimate Lateral Load on Piles Used to Stabilize Landslides”. *In Proceedings of the 10th International Conference on Soil Mechanics and Foundation Engineering*, Vol. 3, pp. 555-560, Stockholm, Sweden.

Wang, L., T. Wang, Y. Hu, W. Liao, and J. Ji, 2023, “Reliability analysis of pile stabilized earth slopes using weighted uniform simulation method”, *Computers and Geotechnics*, Vol. 162.

Wei, W. B., and Y. M. Cheng, 2009, “Strength reduction analysis for slope reinforced with one row of piles”, *Computers and Geotechnics*, Vol. 36, No. 7, pp. 1176–1185.

Wei, W. B., Y. M. Cheng, and L. Li, 2009, “Three-dimensional slope failure analysis by the strength reduction and limit equilibrium methods”, *Computers and Geotechnics*, Vol. 36, No. 1–2, pp. 70–80.

Xue, D., T. Li, S. Zhang, C. Ma, M. Gao, and L. Ji, 2018, “Failure mechanism and stabilization of a basalt rock slide with weak layers”, *Engineering Geology*, Vol. 233, pp. 213–224.

Yamasaki, K., R. W. Strom, R. A. Gunsolus, and D. A. Vessely, 2013, “Long-Term performance of landslide shear piles”, *In Proceedings of The Geo-Congress 2013 Conference*, San Diego, USA.

Yang, S., X. Ren, and J. Zhang, 2011, “Study on embedded length of piles for slope reinforced with one row of piles”, *Journal of Rock Mechanics and Geotechnical Engineering*, Vol. 3, No. 2, pp. 167–178.

Yildirim, I., Z., 2019, “Solution of a slope stability problem resulting from the loading of a levee”. *In Proceedings of The IMO International 8th Geotechnical Symposium* (In Turkish), Istanbul, Türkiye.

Zhang, H., H. Xing, L. Liu, and Y. Luo, 2021, “Field test and numerical analysis on deformation response of H-Type antislide pile: case study of Longjiayan landslide, China”, *Natural Hazards Review*, Vol. 22, No. 4.

Zhang, K., P. Cao, Z. Liu, H. Hu, and D. Gong, 2011, “Simulation analysis on three-dimensional slope failure under different conditions”, *Transactions of Nonferrous Metals Society of China*, Vol. 21, No. 11, pp. 2490–2502.

Zhou, C., W. Shao, and C. Van Westen, 2014, “Comparing two methods to estimate lateral force acting on stabilizing piles for a landslide in the Three Gorges Reservoir, China”, *Engineering Geology*, Vol. 173, pp. 41–53.

Zuo, J., B. Wang, W. Li, S. Han, and J. Wang, 2023, “Rotational mechanism for stability analysis of slopes reinforced with piles”, *Computers and Geotechnics*, Vol. 162.